

УДК 539.171

ARE CENTAUROS EXOTIC SIGNALS OF THE QUARK-GLUON PLASMA?

E. Gladysz-Dziaduś

Institute of Nuclear Physics, Cracow, Poland

INTRODUCTION	564
CENTAURO RELATED PHENOMENA IN CHACALTAYA AND PAMIR CHAMBERS	575
CENTAURO SPECIES STATISTICS	609
CENTAURO EXPLANATIONS	615
SEARCH FOR CENTAUROS IN ACCELERATOR EXPERIMENTS	641
CASTOR: A DETECTOR FOR CENTAURO AND STRANGE OBJECT RESEARCH	647
CENTAURO AND/OR STRANGELET SIMULATIONS	655
SUMMARY	670
REFERENCES	670

УДК 539.171

ARE CENTAUROS EXOTIC SIGNALS OF THE QUARK-GLUON PLASMA?

E. Gladysz-Dziadus

Institute of Nuclear Physics, Cracow, Poland

The exotic cosmic-ray events are reviewed with special emphasis on the connection between their hadron-rich composition and their strong penetrability in matter. Theoretical attempts to explain the Centauro-like phenomena are summarized. Results of accelerator experiments looking for Centauro-related objects are described and discussed. The discussion is completed with the overview of the current and future collider (RHIC and LHC) experiments which are expected to produce and detect such exotic objects in the laboratory. In particular, the CASTOR detector, dedicated to Centauro and strange objects research in heavy-ion collisions at LHC energies, is presented. Simulations of the passage of Centauros and strangelets through the deep CASTOR calorimeter are shown.

Рассматриваются экзотические события в космических лучах, подчеркивается связь между богатством их адронного состава и свойством сильно проникать в материю. Проводится обзор теоретических попыток объяснить события типа кентавр. Описываются и обсуждаются результаты экспериментов на ускорителях, проводимых в поисках объектов типа кентавр. Обсуждение завершается обзором текущих и планирующихся экспериментов на ускорителях (RHIC и LHC), в которых, как ожидается, удастся воспроизвести и детектировать подобные экзотические объекты в лаборатории. В частности, рассказывается о детекторе CASTOR, предназначенном для исследования кентавр- и странных объектов в столкновениях тяжелых ионов при энергиях LHC. Представлены схемы прохождения кентавроподобных и странных частиц через глубинный калориметр ускорителя CFSTOR.

INTRODUCTION

The main purpose of this work is to indicate and discuss some *unconventional signatures of the quark-gluon plasma*. The idea arised from the analysis of super-high energy cosmic ray events detected in emulsion chambers exposed at the mountain altitudes. These data reveal many unexpected features which could be understood by means of the quark-gluon plasma picture, and hence they could be the new and unexplored so far field of the signs of that new state of matter. The new accelerator experiments should not neglect the chance of enriching the studied signals by incorporating the unusual phenomena observed in cosmic ray experiments to the investigated ones, despite of many uncertainties and even their mysterious aspects.

The title of this work is rather symbolic. Centauro is a creature being in one half of a man and in the other half of a horse, both parts don't fit one to the

other. It is strange and mysterious, we are not sure if and how could it match to the real word? Moreover, we are not sure whether it exists at all. But we talk and think about it. Centauro is a good symbol of our current knowledge about the cosmic-ray exotic events.

In this paper, the experimental situation concerning the Centauro events and other related phenomena is reviewed with intention to emphasize a weakly known relation between Centauro species and the so-called strongly penetrating component. The work bases both on the quite recent publications and on the very old ones, sometimes forgotten preprints or conference proceedings. The volume of available information regarding this subject is extremely large, so I am sorry if something essential was omitted.

The first purpose of this work was to answer the following question: were the Centauro related phenomena really observed or is it some kind of *fata morgana*? Each reader should answer by himself. My personal opinion is that despite many experimental uncertainties, some mess in the data and difficulties in their interpretation, we really observe something new, what is outside the extrapolation of our present knowledge. The future accelerator experiments (RHIC, LHC) should take advantage of using these hints in their investigations.

The second question addressed was: where and how to look for these phenomena? The compositeness of the answer arises from the fact that many different aspects, such as: the naked experimental characteristics obtained from cosmic ray experiments, the so far negative results of accelerator searches and also the theoretical speculations, all of them should be taken into account. In connection with it, the past, present and future accelerator Centauro searches are presented, and several different models are described. Among numerous attempts to explain Centauros, some models which could be tested in accelerator experiments and in particular those based on the quark-gluon plasma idea were chosen to this review.

Most attention is given to the scenario of the Centauro strange quark-matter fireball. Its production in nucleus–nucleus collisions and a subsequent evolution could possibly result in the strangelet(s) formation, in the strangeness distillation process. The passage of strangelets through a deep emulsion chamber (calorimeter) should give the specific energy deposition pattern which could be a very spectacular quark-gluon plasma signature. This signal is independent of the strangelet charge (it allows one to detect also strangelets with $Z = 0$) and promises to detect both long- and short-lived strangelets, in contrary to other experimentally used signatures, based mainly on Z/A ratio and sensitive only to stable strangelets.

Both experimental Centauro characteristics and model predictions indicate the forward rapidity region as the most favourable place for production and detection of such anomalous phenomena. This is very essential statement in the context of the current and future experiments, mostly concentrated on the exploration of the midrapidity region. This point is also strongly forced in the paper, claiming the

CASTOR detector (developed as the CMS experiment subsystem) as the good tool for new physics studies.

Quark-Gluon Plasma and Its Signatures. The understanding of the equation of state of nuclear, hadronic and partonic matter is an interdisciplinary interest to particle physics, nuclear physics, astrophysics and cosmology. It is also the main motivation for studying relativistic heavy ion collisions which are primarily searching for the so-called quark-gluon plasma (QGP). A quark-gluon plasma is a state in which quarks and gluons, the fundamental constituents of matter, are no longer confined within the dimensions of the nucleon, but are free to move around over a volume in which a high enough temperature and/or density prevails. The plasma exhibits the so-called «chiral symmetry» which in normal nuclear matter is spontaneously broken, resulting in effective quark masses which are much larger than the actual masses. A quark-hadron phase transition is believed to have occurred at about ten microseconds after the Big Bang when the Universe was at a temperature of approximately 150 to 200 MeV. The QGP may also exist in the cores of dense stars at high baryon densities. The critical energy density for the quark-gluon plasma formation is predicted to be $\sim 1 \text{ GeV}/\text{fm}^3$, or seven times the energy density of normal nuclear matter. The compilation of heavy-ion studies, looking for the quark-gluon plasma state, can be found for example in [1, 2]. More detailed reviews of theoretical and experimental topics of the quark matter are presented in [3–6].

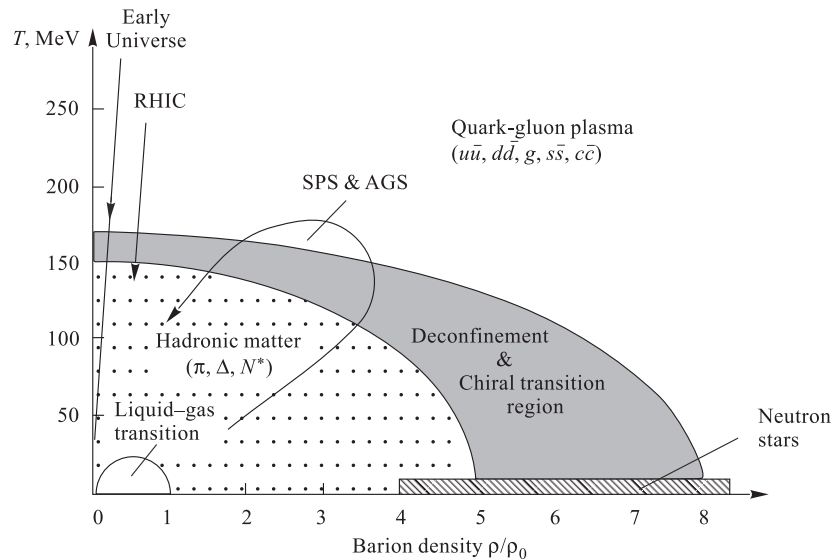


Fig. 1. Schematic phase diagram of nuclear matter [1]

Displayed in Fig. 1 is a schematic phase diagram of nuclear matter, showing the behaviour of nuclear matter as a function of temperature and density (or pressure). Conventional nuclear physics concerns low temperatures and near to normal nuclear-matter density. This region is presently accessible in heavy ion studies at the SPS accelerator at CERN and at the AGS accelerator at Brookhaven National Laboratory. These collisions may partially cover the transition region into the quark-gluon plasma regime. The Relativistic Heavy Ion Collider (RHIC) at Brookhaven has just started, and the LHC at CERN scheduled for 2006 should reach temperatures and densities close to that of the early Universe.

As the QGP phase is rather complicated transient state, many interesting or even unexpected phenomena could be observed during its formation, expansion, cooling, and hadronization. There are many predictions for possible signatures of QGP formation and of partial restoration of chiral symmetry, grouped into several classes. Among them the following topics are frequently proposed to investigate:

- *Thermodynamic variables.* This point includes a study of energy and entropy densities: ε , s , and a pressure p of the interacting system. These thermodynamical quantities T , s , and ε can be identified with the average transverse momentum of produced particles $\langle p_T \rangle$, the hadron rapidity density dN/dy , and the transverse energy density dE_T/dy , respectively. They are proposed to be investigated as a function of the temperature T and the baryochemical potential μ_b . If a phase transition to QGP occurs, a rapid rise in the effective number of degrees of freedom (expressed by ε/T^4 or s/T^3) is expected to be observed over a small range of T .

Measurements of the cross sections for the production of various types of particles as a function of transverse momentum and rapidity can test thermalization and space-time evolution of the system. Rapidity distributions of the more abundantly-produced light particles, such as pions and kaons should provide important information on the dynamics of the collision process.

- *Fluctuations.* Thermodynamical instabilities during the phase transition could lead to large fluctuations. Critical fluctuations, appearing in energy density, entropy density, multiplicity, particle ratios, etc., should be looked for in individual events, as a function of p_T , rapidity, azimuthal angles, etc. The fluctuations depend on the nature of the phase transition. For the multiplicity fluctuations, predictions range from enhanced multiplicity fluctuations connected to the production of QGP droplets and nucleation processes in a first order phase transition, to a strong suppression of fluctuations as a consequence of rapid freeze-out just after the phase transition. The sources of dynamical fluctuations could be also the disoriented chiral condensates or jets.

- *Electromagnetic signals.* The only way to see the quarks directly is to detect the electromagnetic radiation which they emit. Real and virtual photons in the form of lepton pairs are an ideal probe of the early stages of the interaction, since they escape the interaction region without subsequent interaction or modification

due to the final state of the interaction. They can probe the interior of the quark-gluon plasma during its hottest and earliest phase. Unfortunately there are also many other processes which can produce photons, which are primarily electromagnetic decays of hadrons and resonances and direct hard photons from QCD Compton scattering or lepton pairs from Drell–Yan process. Thus the main problem is how to separate the yields for electromagnetic probes, which are rather small relative to background processes.

- *Quarkonium suppression.* J/ψ are made of c and \bar{c} quarks. They are rare because charm quarks are very heavy and can only be produced at the very first stages immediately after the collision, while the constituents of the two nuclei still have their full energy. The suppression of J/ψ production in a quark-gluon plasma occurs because a $c\bar{c}$ pair formed by the fusion of two gluons cannot bind inside the quark-gluon phase. The confining strong force, which would normally bind the newly created charm quarks within a small, but finite time (formation time) into a J/ψ , is screened in the QGP by deconfined quarks and gluons. If the screening radius (Debye radius), which is inversely proportional to the density of colour charges and therefore to the energy density, is smaller than the size of the J/ψ ($\simeq 0.5$ fm), a bound state cannot be formed. The charm quarks dissolve and separate in space to later appear after hadronization as two mesons with open charm.

Less tightly bound excited states of the $c\bar{c}$ system, such as ψ' and χ_c , are more easily dissociated and will be suppressed even more than the J/ψ . Similar arguments can be made also for the heavier $\Upsilon, \Upsilon', \Upsilon''(b\bar{b})$ systems).

- *Strangeness (heavy flavour) enhancement.* An enhancement in the production of strange particles resulting from chemical equilibrium of a system of quarks and gluons was one of the first predictions for a signature of QGP formation. In «chemical» equilibrium, the abundances of particle species (hadrons/quarks) are governed by Boltzmann factors, i. e., essentially by temperature, respective masses and chemical potential. Compared with hadronic processes, the production of strange quarks is favoured in a QGP because there the mass of the strange quark is reduced from ~ 500 to ~ 150 MeV (chiral symmetry restoration), i. e., a value comparable with the critical temperature. In addition, in a baryon-rich region the creation of light u and d quarks is hindered by the large number of valence quarks already present in the colliding nuclei (Pauli blocking), leading to a large chemical potential for these quarks in favour of s and \bar{s} production. Especially multistrange baryons and antibaryons are predicted to be strongly enhanced. The more speculative aspect is connected with the possible existence of exotic matter, i. e., the droplets of strange quark-matter. Also an enhancement of charm can be expected.

- *Disoriented Chiral Condensate.* DCC is a coherent excitation of the pion field corresponding to a local misalignment of the chiral order parameter. According to this speculative hypothesis the pieces of strong interacting vacuum

with a rotated chiral order parameter might be produced in high-energy particle collisions. Such domains would decay into neutral and charged pions, favouring pion ratios N_{π^0}/N_{π} substantially different from 1/3. The formation of DCC should lead to large fluctuations in the ratio of neutral to charged pion yields at low p_T , and consequently to fluctuations in $\langle p_T \rangle$ of charged particles.

- *High p_T probes of QCD.* The colour structure of QCD matter can be studied by its effects on the propagation of high- p_T partons in highly excited matter and a quark-gluon plasma. The characteristics of the fragmentation products of hard scattering can provide information on the matter through which the hard scattered parton propagates.

Highlights from Accelerator Experiments. The experimental programmes in relativistic heavy ions using the BNL-AGS and CERN-SPS started in 1986. At BNL ion beams of silicon and gold, accelerated to momenta of 14 and 11 GeV/c per nucleon respectively, have been utilized in approximately 10 fixed-target experiments. About 15 heavy-ion experiments at CERN studied heavy-ion interactions, utilizing beams of oxygen at 60 and 200 GeV/c per nucleon, sulphur at 200 GeV/c per nucleon and Pb at 160 GeV/c per nucleon. The experiments were all optimized for measuring different signals which might indicate if and how a quark-gluon plasma was formed. Some of them optimized their detectors for one rare signal, while others developed multipurpose detectors which were sensitive to multiple signals. Many interesting effects, concerning mainly the equilibration of hadronic matter, chiral symmetry restoration and deconfinement, which generally support the QGP hypothesis, have been observed in the AGS and SPS experiments. The long awaited first results from the RHIC are now also available indicating very interesting physics.

- First of all, it seems that the conditions required for the QGP formation have been reached. For instance, a large degree of stopping, resulting in the transfer of a large amount of energy from the relative motion into other degrees of freedom, was observed in central collisions of the heaviest systems at the AGS and SPS (e.g., NA49, NA44, E866, E877 experiments). At SPS, this creates the high energy densities ($\varepsilon \sim 1.5\text{--}2.0 \text{ GeV}/\text{fm}^3$) beyond those predicted for production of a quark-gluon plasma. The early, very dense state (fireball) has an energy density of $\sim 3\text{--}4 \text{ GeV}/\text{fm}^3$ what corresponds to a temperature of about 240 MeV. The first estimates from RHIC [7], obtained by using the Bjorken formula with the thermalization time $\tau = 1 \text{ fm}/c$, give an energy density of $4.6 \text{ GeV}/\text{fm}^3$, which is 60% larger than measured at the CERN-SPS. In addition, it is suspected that the density can be substantially higher due to the shorter thermalization time in the higher parton density environment, and some estimates give an energy density even in the range $23.0\text{--}50 \text{ GeV}/\text{fm}^3$.

- The data do not contradict the picture in which the created quark-gluon plasma cools down and becomes more dilute. At an energy density of $\sim 1 \text{ GeV}/\text{fm}^3$ (and a temperature of $\sim 170\text{--}180 \text{ MeV}$), the quarks and glu-

ons condensate into hadrons, and the final abundances of the different types of particles are fixed. At an energy density of around $50 \text{ MeV}/\text{fm}^3$ (and a temperature of $\sim 100\text{--}200 \text{ MeV}$), the hadrons stop interacting completely and the fireball freezes out. Thermal and chemical equilibrium models are generally able to reproduce the particle abundances and particle spectra measured in central collisions, once the strong influence of the collective nuclear flow is taken into account. As a result, the parameters which best fit the particle ratios and particle spectra were found: the temperature at chemical equilibrium $T = 160\text{--}175$ ($120\text{--}140$) MeV, the baryochemical potential $\mu_b = 200\text{--}270$ (540), and the strangeness saturation factor $\gamma_s = 0.6\text{--}1.0$ for SPS (AGS) energies. The preliminary results of analysis of particle ratios [7], from all four RHIC experiments, show reasonable agreement with a baryon chemical potential $\mu_b \simeq 45\text{--}55 \text{ MeV}$ and a chemical freeze-out temperature $T \simeq 160\text{--}180 \text{ MeV}$, which is not significantly different from the temperature measured at the CERN-SPS. The value of baryon chemical potential estimated from RHIC experiments is much lower than that obtained from the CERN SPS, showing a closer but not yet complete approach to a baryon free regime at RHIC. The first measurements of the elliptic flow at RHIC indicate excellent agreement with a hydrodynamical model up to $p_T \simeq 1.5 \text{ GeV}$ (STAR), what may indicate a large degree of thermalization in the early stages, validating the assumption of hydrodynamical expansion. Thus, there is evidence for chemical and thermal equilibrium from the accelerator experiments results, although the issue of strangeness saturation (i. e., if $\gamma_s = 1$), which is required for deconfinement is still to be settled (NA44 and NA49 experiments find only partial chemical equilibrium for strange particles).

- An important aspect of «chemical equilibrium» is the observed enhancement of strange particles. One can ask how many strange quarks and anti-quarks are formed relative to the newly produced up and down quarks and antiquarks. For proton–proton and electron–positron collisions, the fraction of extra strange quarks made is ~ 0.2 . But for the nucleus–nucleus collisions, the fraction is twice as high, i. e., it is seen «global strangeness enhancement by a factor of two» (NA49). Multistrange hadrons are enhanced more strongly (WA97, NA49, NA50) up to a factor of 15 for the Ω hyperon and its antiparticle (WA97).

- An increase in the pion-to-baryon ratio from approximately 1 to about 7, when going from the AGS to the SPS energies indicates the rise in entropy density.

- Measurements of charmonium production exhibit a suppression of the yield of both the J/ψ and the ψ' relative to Drell–Yan pair production for central collisions of Pb + Pb at the SPS (NA50, NA38 Collaborations). The yield of the ψ' relative to Drell–Yan is also observed to be suppressed for central collisions of the lighter S + Pb system, whereas the J/ψ is not. These results follow the expected pattern that the Debye screening will initially affect the ψ'

before the J/ψ and suggest that the deconfinement regime has been reached at the SPS.

- So far, no apparent signal from direct photons radiated by quarks in QGP is found. For S + Au collisions, WA80 and NA45 established that not more than 5% of the observed photons are emitted directly. For Pb + Pb collisions, WA98 has reported indications for a significant direct photon contribution. Preliminary data from NA45 are consistent with this finding, but so far not statistically significant. NA50 has seen an excess by about a factor of 2 in the dimuon spectrum in the mass region between ϕ and J/ψ vector mesons. On the other hand, the data (NA45) show that in S + Au and Pb + Au collisions the expected peak from ρ vector meson is completely smeared out. Simultaneously, electron pairs (virtual photons) measurements exhibit an enhancement at low to intermediate pair masses (in the mass region between the mass of two pions and 1.5 GeV/c, i.e., around the ρ meson) relative to pairs expected from hadronic decays for central collisions of the heavier systems (S + Au and Pb + Au) at the SPS (CERES/NA45, HELIOS-3 Collaboration). This effect is investigated by using different theoretical approaches and ideas such as $\pi\pi$ annihilation, a decreased ρ mass due to partial chiral symmetry restoration and other effects. The ρ is of particular interest as it has a short lifetime compared to the interaction times and it decays very quickly in the presence of the medium (whether QGP or hadronic). Thus it should exhibit signs of possible chiral restoration if there is a reduction of the ρ -meson mass. The clear excess in the mass spectrum of e^+e^- bears the questions: is it thermal radiation from a hot source or rather does it indicate in-medium effects for vector meson resonances? In the latter case, it could be a signal of the onset of chiral symmetry restoration as matter becomes denser.

- To the list of interesting phenomena, the suppression of transverse momentum spectra at $p_T > 3$ GeV/c, announced preliminary by the PHENIX experiment [8] at RHIC, should be added. It could be evidence for an energy loss of gluon minijets, the so-called «jet-quenching» mechanism in high density matter with dense colored sources [9]. This is in contrast to data at SPS energies, where WA98 found no evidence for quenching in Pb + Pb collisions but a factor of two Cronin enhancement.

Summarizing, the results of relativistic heavy ion experiments are quite intriguing. The data from any one experiment are not enough to give the full picture, but the combined results from all experiments rather agree and fit. The attempts to explain all of them simultaneously, using established particle interactions have failed, but, on the other hand, many of the observations are consistent with the predicted signatures of a quark-gluon plasma. At a special seminar on 10 February 2000, spokespersons from the experiments on CERN's Heavy Ion programme stated that the collected data from seven CERN experiments (NA44, NA45, NA49, NA50, NA52, WA97, NA57, and WA98) give

compelling evidence that a new state of matter has been created although this evidence is so far «indirect» [10]. The first measurements from the RHIC were the results on global observables such as: charged particle multiplicity, transverse energy and elliptic flow. They all show nontrivial collective behaviour. The multiplicity characteristics are tried to be understood by means of models including the mechanisms of parton saturation [11] or string percolation [12].

Experimental Hints from Unusual Cosmic Ray Events. Cosmic-ray induced reactions can be satisfactorily described in terms of standard ideas below the energy of about 1000 TeV. Above this threshold the global behaviour of cosmic-ray families is hardly explained by smoothly extrapolating the hadron multiple production characteristics which were learnt through CERN collider energies. The families of hadrons and photons, mainly observed by mountain cosmic ray laboratories, exhibit many surprising features such as: rapid attenuation in the atmosphere, multicore structure with unexpectedly high alignment level, large lateral spread, extremely high energy concentration in the forward angular region (halo), etc. The observed flux value of cosmic ray families is smaller than expected. According to [13] experimental intensity of families at the Pamir is $I(\sum E_\gamma \geq 100 \text{ TeV}) \simeq 0.35 \text{ m}^{-2} \cdot \text{y}^{-1} \cdot \text{sr}^{-1}$. The simulated data, based on different simulation codes, give 3 ~ 4 times higher intensity than observations. In addition, the spectra of high energy showers in families are in younger stage of the shower development, what indicates that majority of observed families originate from main interaction slightly above the observed levels. At energies $10^{15} - 10^{17}$ eV, the wide spectrum of exotic events hardly explained by the known mechanisms appears.

The global characteristics of gamma-hadron families are affected by the primary cosmic ray chemical composition and show a high sensitivity to a hadronic interaction model used in the interpretation. Thus, in principle, the problem seems to reduce to a question of whether the data signal a change in the composition of cosmic ray primaries at these energies, or whether they signal a change in the hadronic interactions. Some unusual features of cosmic-ray events could be, in part, understood by the use of a Fe-dominant composition in the primary flux. However, the recent results from Chacaltaya and Tien-Shan («Hadron» Experiment) installations operating simultaneously the emulsion chamber and the air shower array also indicate that discrepancy between the predicted (based on conventional models) and observed family flux cannot be reconciled by the heavy-dominant composition of the primary cosmic rays [14, 15]. Moreover, experimental results concerning the composition of primary cosmic ray spectrum seem to exclude this explanation. In fact, the primary flux composition in the energy region above 10^{14} eV can only be obtained by using indirect methods of ground-based detectors looking at showers initiated by the interaction of primary nuclei in the upper atmosphere. Hence, there are substan-

tial uncertainties on the primary cosmic ray composition in this energy region. As a heavy dominant composition does not have convincing observational support [16], it seems that *the introduction of some new mechanism, or a global change of the characteristics of hadronic interactions at around 10^{16} eV, especially in the most forward angular region is necessary* to explain the experimental data.

In this work various anomalies such as: exotic events called Centauros, Mini-Centauros, Chirons, etc., were reviewed. These events have many common features, and they are very frequently connected with the so-called long-flying (penetrating) component. There are strong indications that they are connected one to the other, and they have a common origin.

In fact, the strongly penetrating component has two faces. At first, it has been observed in the apparatus in the form of strongly penetrating single cascades, clusters of showers or the so-called «halo». This phenomenon manifests itself by the characteristic energy pattern revealed in shower development in the deep chambers (calorimeters) indicating a slow attenuation and many maxima structure (see Sec. 1). The second aspect is connected with the anomalously strong penetrability of some objects during the passage through the atmosphere. In principle, both items can be connected one to the other and could be different faces of the same phenomenon.

The mentioned here anomalies are not rare occurrence but they manifest themselves at the 5% level or above. There are many theoretical attempts to explain the observed anomalies, among them the quark-gluon plasma scenario is the very promising one.

As the wide spectrum of exotic events seen in cosmic ray experiments is observed at *forward rapidities*, thus this region seems to be a potential place for the new physics. Unfortunately, the physics in the very forward rapidity region in ultrarelativistic nucleus–nucleus collisions has not been rigorously addressed by theory so far. The main reason is the difficulty of the calculations in an environment of finite baryochemical potential. There are, however, some phenomenological and QCD-inspired attempts to predict new phenomena or to explain unusual phenomena already seen. It is expected that this region will contain only a small fraction of the totally produced particles and at the same time the vast majority of the available total energy with the baryon density reaching here the maximum. Figures 2 show the pseudorapidity distributions of multiplicity and energy, obtained in simulations (HIJING generator) of 50 central Pb + Pb collisions at LHC energies $\sqrt{s} = 5.5$ TeV [17]. There are shown separately distributions of electromagnetic and hadronic component, and the acceptance of the CASTOR detector (see Sec. 5) is marked. Figure 3 shows distributions of the baryon number predicted by VENUS and HIJING for the same reactions.

Such environment offers the possibility for the appearance of novel, surprising phenomena. In particular, strangelets, the small droplets of strange quark matter,

are predicted to be formed from the Quark Gluon Plasma, predominantly in a high baryochemical potential environment. Production of heavy flavour [18, 19] and super-heavy particles, if they exist, may also be seen at very forward rapidities. For instance, the new heavy vector bosons V^+ , V^- , V^0 with masses up to 6 TeV are theoretically predicted [20]. Another phenomenon which is attracting a lot of theoretical investigation is colour superconductivity at finite baryon density [21]. At relatively low temperature, the baryon rich environment may lead to the formation of Deconfined Quark Matter (DQM) in the core of neutron stars [22]. Also the understanding of cosmic ray exotic phenomena in terms of hadronization of DQM in an extremely high baryon density environment has been proposed [23–25].

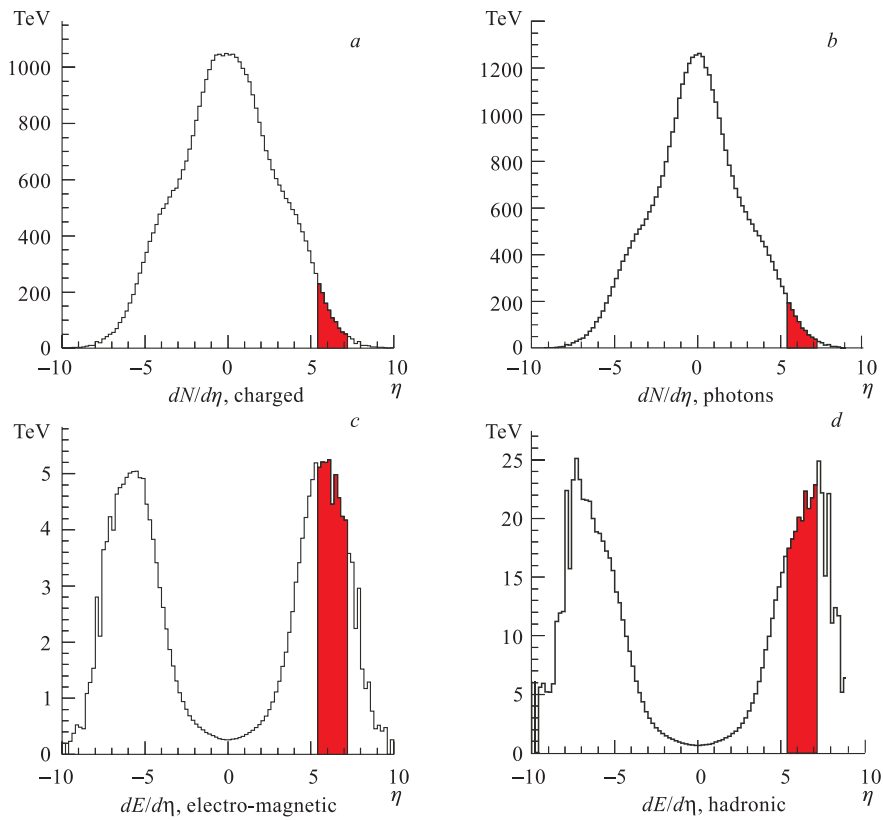


Fig. 2. Average pseudorapidity distribution of particle multiplicities and energy flow. 50 central Pb + Pb collisions at energy $\sqrt{s} = 5.5 A \cdot \text{TeV}$ were generated by HIJING. CASTOR geometrical acceptance is indicated [17]

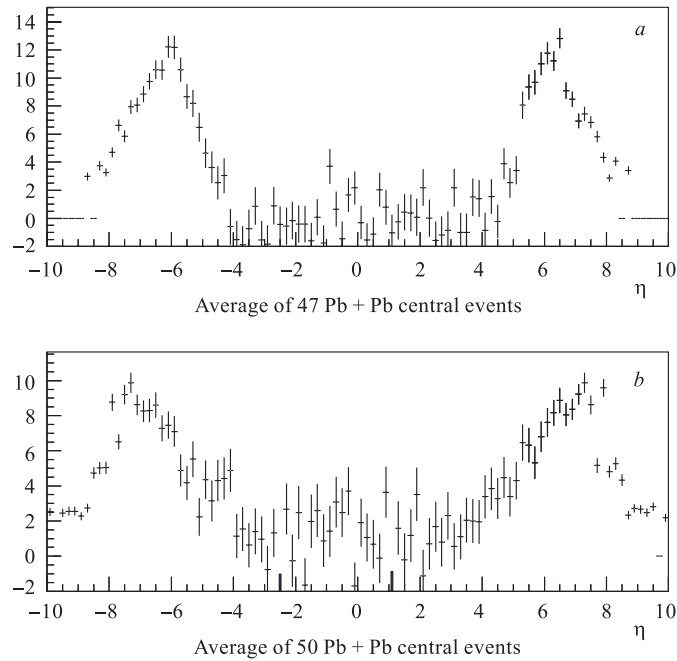


Fig. 3. Baryon number distribution for central Pb + Pb collisions at energy $\sqrt{s} = 5.5 A \cdot \text{TeV}$ generated by VENUS (a) and HIJING (b)

All these phenomena should be searched for and studied. Unfortunately, most of the present and future nucleus–nucleus experiments are concentrated on exploration of the poor baryon region and doing the «midrapidity physics». In this work the importance of the CASTOR project, as the unique experimental design to explore this interesting region at very high energies planned to be reached at the LHC nucleus–nucleus collisions will be emphasized.

1. CENTAURO RELATED PHENOMENA IN CHACALTAYA AND PAMIR CHAMBERS

The Centauro related phenomena have been discovered and analyzed in emulsion chamber experiments investigating cosmic ray interactions at the high mountain laboratories at Mt. Chacaltaya (5200 m above sea level and Pamirs (~ 4300 or 4900 m above sea level).

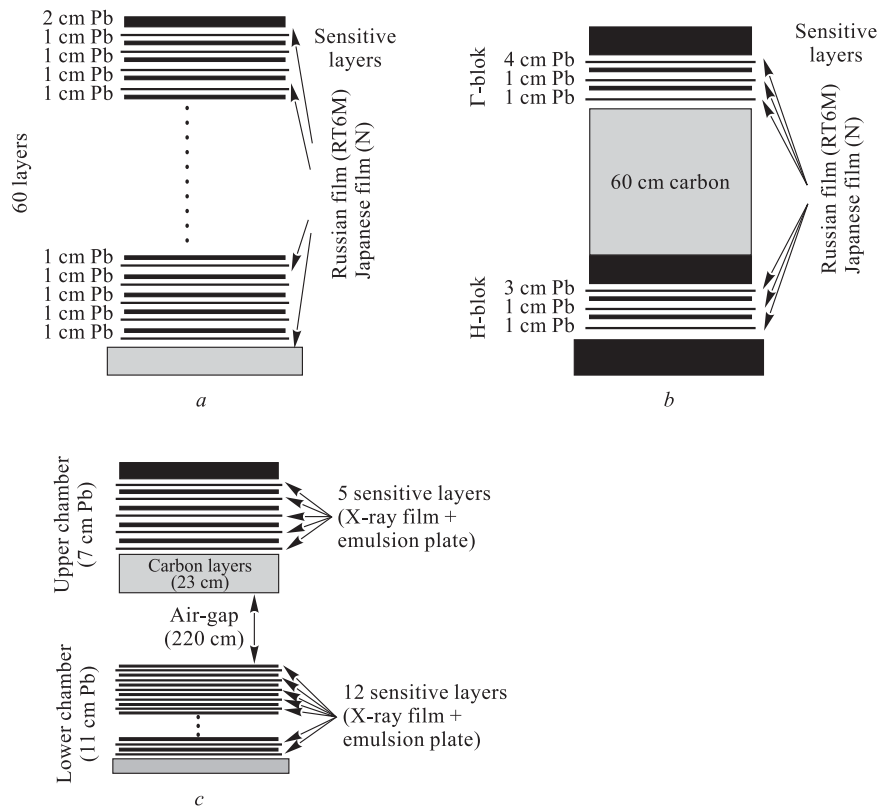


Fig. 4. Schemes of typical emulsion chambers [26]: a) Pamir thick Pb chamber; b) Pamir carbon chamber; c) Chacaltaya chamber No. 21

In principle the detectors used in these experiments are similar. They consist of three parts: upper and lower chambers, and the carbon target between them. The upper part called the gamma block detects mainly the electromagnetic component. In the lower chamber there are registered mainly hadrons. Both the upper and the lower chambers are sandwiches of the lead absorber and the sensitive layers which are mostly X-ray films, sometimes emulsion plates. Chambers have rather big areas, of the order of several tens m^2 , and are exposed for a long time periods, of about one year.

However, the direct comparison and interpretation of the experimental data is difficult because of some differences in the depth and construction of the chambers. Figure 4 shows the schemes of Chacaltaya two-storey chamber, a traditional

style carbon chamber employed in Pamir experiments and also a schematic view of a homogeneous thick lead chamber (60 or 110/120 cm thick lead). The typical Pamir carbon chambers consist of two (or three) parts: a gamma-block of 5 or 6 cm Pb thick and one (or two) hadron(H)-blocks each consisting of carbon layer of 60 cm thick and 5 cm of Pb. The thickness of a standard Pamir-type carbon chamber amounts to $\sim 1.7 \lambda_{\text{geo}}^*$, what assures the detection efficiency to be over $\sim 60\text{--}70\%$. Thicker carbon-type chambers (consisting of four hadron blocks) have been also used sometimes. The homogenous lead chambers are simply sandwiches of Pb absorber layers (the upper layer has usually 2 cm Pb and the consecutive ones have 1 cm Pb) and the sensitive material being mainly the X-ray films. The detection efficiency of the thickest Pb chambers is $\sim 80\text{--}90\%$. Typical two-storey Chacaltaya chamber consists of the upper chamber of 6–10 cm Pb thick, the target layer 20–30 cm of carbon, the air gap (e. g., 150 cm) and the lower chamber of 6–15 cm Pb thick. Some chambers (as for example Chacaltaya chambers No. 19–22) were covered by several nuclear emulsion layers over all area of both the upper and the lower chamber. It enables a careful study (under the microscope) of the shower structures. It is essential in classification of the showers (an identification of the photonic and hadronic cascades) and in the study of the strongly penetrating component. Typical detected event, called here family, is generated in a collision of a cosmic-ray particle (mostly p or π) with air nuclei at the distance of about 500–1000 m above the apparatus. The collision mean free path of cosmic ray hadrons is about 1200 m and mean free path for pair creation by γ quanta is about 770 m of the atmosphere at the top of Chacaltaya ($\lambda_{n\text{-air}}^{\text{int}} = 75 \text{ g/cm}^2$, $\lambda_{p\text{-air}}^{\text{int}} = 110 \text{ g/cm}^2$, 1 c. u. = 37.7 g/cm^2). Keeping in mind these numbers, we see that particles born in a typical act of interaction must traverse about $0.5\text{--}1 \lambda^{\text{int}}$ (≈ 2 c. u.) of matter, before reaching the detector. Thus the families born at large distances above the chamber are not «clean» events but they are affected by electromagnetic-nuclear cascade processes in the atmosphere.

Normal events contain about 30% of π^0 mesons. Since each π^0 decays into 2γ , there is produced roughly one γ for each charged particle in the primary interaction. As the products of the interaction descend towards the chamber, the fraction of their electronic and photonic content increases through the shower formation, so that a «usual» family (hadrons, gammas, and electrons with the common origin) seen in the upper detector is always several times larger than its continuation into the lower detector. In «normal» families, from the energy range $\Sigma E_\gamma = 100\text{--}1000 \text{ TeV}$, the hadronic component constitutes $\leq 30\%$ of the total visible energy. Thus, a big surprise were the events with the contrary situation. Since the upper half of these events did not allow one to predict their lower part, such events were named «Centauros».

* λ_{geo} is the geometrical collision mean free path of ordinary cosmic-ray baryons.

At present, rather big statistics of cosmic-ray families with visible energy greater than 100 TeV from Chacaltaya and Pamir-joint experiments exists [13,26]. The experimental material, suitable for investigation of the above mentioned exotic phenomena, was collected by the Brasil–Japan Chacaltaya Collaboration, starting from the 1970s, when the Centauro I was found. Since 1980, the joint experiment has been conducted at the Pamir, by the Pamir and Chacaltaya groups after Nakhodka Symposium, and a part of the material from the standard type carbon Pamir chambers has been reanalyzed in the same manner as in Chacaltaya experiment, with the point of view of exotic phenomena. In 1991, a joint analysis, undertaken by Moscow State University and Japan groups using the homogenous thick lead chambers, has been also started. 477 events with the visible energy $\Sigma E_{\text{vis}} \geq 100$ TeV, coming from the total exposure of $\approx 1548 \text{ m}^2 \cdot \text{y}$, are reported in [13] where unusual characteristics of high-energy cosmic-ray families were studied with CORSIKA simulation code.

Partial analyses, concerning selected subjects, have been done sometimes using higher statistics. In addition some extremely interesting events have been found also in other types of thick chambers (as well as homogenous lead chambers and carbon type chambers consisting of several hadron blocks), see Subsec. 1.1.2. The detailed analysis of 17 super-high energy families ($\Sigma E_{\text{vis}} \geq 700$ TeV) coming from Pamir thick lead chambers is presented in [26].

The present experimental results obtained by Chacaltaya and Pamir Collaboration show that hadron rich families occupy more than 20 % of the whole statistics and indicate the existence of several types Centauro species, characterized by:

- abnormal hadron dominance (both in multiplicity and in energy content);
- rather low total (hadron) multiplicity, in comparison with that expected for nucleus–nucleus collisions at that energy range;
- transverse momentum of produced particles much higher than that observed in «normal» interactions ($p_T \approx 1.7$ GeV/c for Centauros and 10–15 GeV/c for Chirons, assuming the gamma inelasticity coefficient $K_\gamma \approx 0.2$);
- isotropic η distribution.

They can be divided into several groups, such as:

1. Centauros of original type;
2. Mini-Centauros;
3. Chirons;
4. Geminions.

1.1. Centauros of Original Type. 1.1.1. «Classical» Chacaltaya Centauros.

History. Centauro, which is mainly characterized by large imbalance between the hadronic and photonic component, has been a puzzle for so many years. The first Centauro [27] was found many years ago, in 1972, in the two-storey Chacaltaya chamber No. 15. It is the most spectacular and indisputable event of this kind. The triangulation measurement (by angular divergence) of shower direction was feasible for the event and it allowed one to estimate the interaction height to

be 50 ± 15 m above the chamber. It is relatively small distance and this is the reason that the event is clean, i. e., it didn't suffer from the electromagnetic and nuclear cascade in the atmospheric layer above the apparatus. The scheme of the event is shown in Fig. 5. In the upper chamber, there were observed 7 cascades, identified as one atmospheric e/γ and 6 Pb-jets. In the lower part of the detector 43 observed cascades have been classified as 7 Pb-upper-jets, 29 C-jets and 7 Pb-lower-jets.

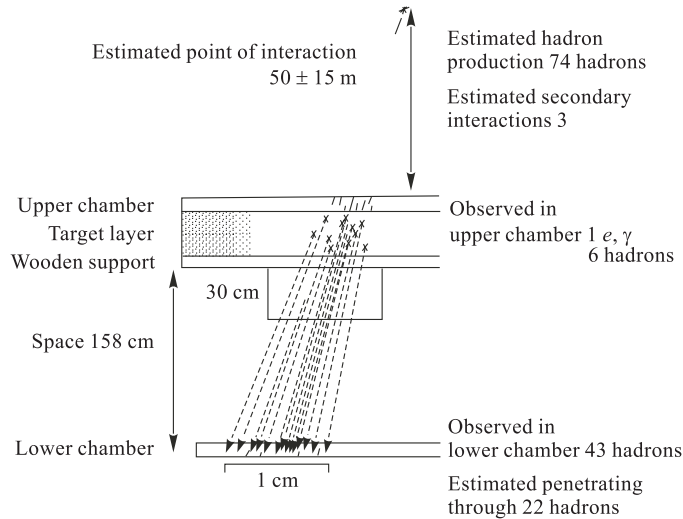


Fig. 5. Illustration of Centauro I [29]

A «normal» family seen in the upper detector is always several times larger than its continuation in the lower detector. So, the Centauro I event, with the contrary situation, was a very big surprise. The suspicion that the event might have happened during a short period of assembling or removing the chamber was eliminated because the upper detectors were always mounted before the lower ones and the lower detector is always the first to be removed.

After introducing corrections for the hadron detection efficiency and secondary particles generated in the atmospheric interactions above the chamber (A-jets), the Centauro I can be considered as the event with the total interaction energy $\Sigma E_\gamma = 330$ TeV, in which only one electromagnetic (e/γ) particle and 74 hadrons have been produced. The estimated interaction height allowed one

to calculate the transverse momenta of produced secondary hadrons. The visible part of the average p_T value is $\langle p_T^\gamma \rangle = 0.35 \pm 0.4$ GeV/c. It results in the average transverse momentum of a produced hadron $\langle p_T \rangle = 1.75$ GeV/c, taking the gamma-inelasticity factor $\langle K_\gamma \rangle = 0.2^*$.

It is very exciting that in 1997, during the International Cosmic Ray Conference, held in Durban in South Africa, the next clean Centauro event has been reported [28]. Since the finding of the first event Centauro I, a systematic search for such surprising families has been made in the successive exposure of the Chacaltaya chambers and a little later also in the Pamir chambers. The next four events, found in Chacaltaya chambers, in several years after the discovery of the Centauro I, have been analyzed and described in detail in [29]. These well-known events are called «classical Centauros».

Multiplicities and Energies. The main characteristics of the «classical Centauros» are presented in Table 1. There are shown multiplicities (above the energy threshold) and energies of both electromagnetic and hadronic components concerning three stages of analysis of the events. The observed multiplicities (upper part of the table) are the mixture of the particles born in the parent interaction and these generated in secondary atmospheric interactions. Hadronic multiplicities are uncorrected for the chamber detection efficiency. There is shown also a class of cascades detected in the upper chamber, labeled as «unidentified», which in principle could have both electromagnetic and hadronic origin. The fraction of the observed hadronic energy to the total visible energy of the event named $Q_h = \Sigma E_h^\gamma / \Sigma E_{\text{tot}}$ was also calculated. This parameter is now widely used in the analysis of the imbalance between hadronic and electromagnetic components of cosmic ray events.

The medium part of the table contains the above-mentioned characteristics, corrected for the hadron detection efficiency. Also separation of electromagnetic and hadronic cascades from the «unidentified» group, by means of statistical procedure, was done. These corrections can be made by using the experimental distribution of the depths of interaction points in the chamber (C-jets, Pb-upper-jets and Pb-lower-jets) and one can estimate the number of arriving hadrons and gammas at the top of the chamber. Knowing both the number of hadrons arriving at the top of the chamber and the interaction height, it is possible to estimate the multiplicity of hadrons produced in the parent Centauro interaction and also the number of secondary atmospheric nuclear interactions (A-jets) during their passage to the chamber and in a consequence the number of gamma rays

*Such value of K_γ factor is usually quoted for nucleons and used by Japan–Brasil Collaboration, basing on assumption that the hadrons born in the Centauro interaction are nucleons. A little higher value, $K_\gamma \simeq 0.4$, is being preferred for pions. In that case, preferred by DCC followers, $\langle p_T \rangle \simeq 0.875 \pm 0.375$ GeV.

Table 1. Characteristics of Chacaltaya Centauros

Chacaltaya Centauros					
Centauro No. Chamber No.	I 15	II 17	III 17	IV 17	V 16
Observed in the chamber					
N_γ	1	—	—	—	—
N_{unid}	—	5	26	61	34
N_h	49	32	37	38	31
ΣE_h^γ , TeV	222	179	169	144	167
ΣE_{tot} , TeV	231	203	270	286	285
Q_h	0.96	0.88	0.63	0.50	0.59 0.72*
Estimated at the top of chamber					
N_h	71	66	63	58	45
ΣE_h^γ , TeV	321	369	287	220	242
N_γ	1	0	17	51	31
ΣE_γ , TeV	9	0	66	119	108
Estimated in Centauro interaction					
N_h	74	71	76	90	63
ΣE_h^γ , TeV	330	370	350	340	350
N_γ	0	0	0	4	0
H , m	50	80	230	500	400
$N_{A-\text{jets}}$	3	5	13	32	18
* Value obtained after re-analysis of the event [30]. It is the lower limit as the highest energy hadron was excluded.					

produced in the parent Centauro interaction. As is seen in the lower part of Table 1, the number of gammas or electrons estimated to be produced in the Centauro interaction is practically zero, so the number of neutral pions or other rapid-gamma-decaying hadrons must be negligibly small. The details of such analysis are presented for example in [31], where Centauro IV as a typical case of the event with not too small production height has been studied.

Centauro Production Heights. Unfortunately, measurements of the heights of interaction points, through the shower geometry, were possible only for a few exotic events [32–34] found in Chacaltaya chambers, among them for Centauro I and later for Centauro IV and Centauro VII. The production heights for majority of other events were estimated comparing their respective lateral spreads with that of Centauro I and assuming the same average p_T for produced hadrons. The

production heights are mostly higher than that for Centauro I, so it is natural that the events, suffering from nuclear-electromagnetic cascade in the atmosphere, contain stronger admixture of atmospheric gammas and electrons.

Other Centauro Properties

- Centauros are observed in the very high energy region. The energy threshold for their production is about 1000 TeV. As the average observed energy (for 5 Chacaltaya Centauros) is 348 TeV, the total incident energy was estimated to be 1740 TeV, assuming the value of inelasticity coefficient $K_\gamma = 0.2$.

- Pseudorapidity distributions of Centauro species (Centauros, Mini-Centauros and Chirons) are consistent with a nearly Gaussian distribution [35], centered at $\langle \eta_{\text{Cent}} \rangle_{\text{lab}}^{\text{exp}} = 9.9 \pm 0.2$ for Centauros. Generally, experimental characteristics support a formation and a subsequent isotropic decay of a fireball with the hadron multiplicity $N_h = 100 \pm 20$ and the mass $M_{\text{Cent}} \simeq 180 \pm 60$ GeV, where the error is mainly due to the uncertainty in the p_T value. The Centauro features based on the fireball model are described in Subsec.3.4.2 and are shown in Tables 2 and 11.

- Centauro origin and the kinematical region in which the phenomenon is observed are still the matter of debate. These questions are addressed in detail in Sec.3 concerning Centauro models and in Sec.4 regarding the accelerator searches of the exotic phenomena. Both these questions, however, cannot be

Table 2. Average characteristics of 5 Chacaltaya Centauros assuming nucleon–nucleon or nucleus–nucleus collisions

Hadron multiplicity $\langle N_h \rangle$	64–90, $\langle 75 \rangle$
γ multiplicity	0
Average total incident energy, TeV	$\langle E \rangle \geq 1740$
Pseudorapidity of emitted baryons	$\langle \eta_{\text{lab}} \rangle = 9.9 \pm 0.2$
Width of pseudorapidity distribution	$\langle \Delta \eta \rangle \simeq 1 \pm 0.2$
Average transverse momentum, GeV/c	$\langle p_T \rangle = 1.75 \pm 0.7$
Assuming nucleus–nucleus collision [23, 24]	
Total interaction energy in «60 + 14» c. m., TeV	$\sqrt{s} \geq 6.8$
Total interaction energy in $N-N$ c. m., TeV	$\sqrt{s_{N-N}} \geq 0.23$
Incident projectile rapidity	$y_{\text{lab}}^{\text{proj}} \simeq 11$ $y_{\text{c. m.}}^{\text{proj}} \simeq 4.8$
Assuming nucleon–nucleon collision	
Total interaction energy in $N-N$ c. m., TeV	$\sqrt{s_{N-N}} \geq 1.8$
Incident projectile rapidity	$y_{\text{lab}}^{\text{proj}} \simeq 15.1$ $y_{\text{c. m.}}^{\text{proj}} \simeq 7.5$

answered on the basis of only experimental data. Some additional assumptions and model speculations are necessary. It should also be noted that both these questions are connected one to the other and the answer is important for the planning of the new collider experiments. Table 2 illustrates the problem.

In Table 2 are shown energies, pseudorapidities, and maximal projectile pseudorapidities, calculated both in the laboratory and in the centre-of-mass system, for two different scenarios of the collision: formation of Centauros in either nucleon–nucleon or nucleus–nucleus collision, and assuming the projectile being the medium primary cosmic ray nuclei with a mass ~ 60 and the target with a mass ~ 14 , being a medium atmospheric air nucleus. It is clear that answering the question, whether Centauros are produced at the midrapidity or rather in the projectile fragmentation region and where in the new colliders should we expect them, depends on the kind of a target and a projectile, which are unknown objects in these experiments. It is seen that assuming nucleon–nucleon collision we can expect Centauros produced somewhere between the central and the fragmentation rapidity region. In this case, the threshold for Centauro formation is close to the Fermilab collider energies. On the other hand, if Centauros are produced in nucleus–nucleus collisions they should be looked for in the projectile fragmentation region. The question of the possible Centauro formation in the new collider experiments (at RHIC and LHC) will be considered later.

1.1.2. Other Centauro and Centauro-Like Events. Besides the «classical Chacaltaya Centauros», a quite reasonable statistics of Centauro-like (or hadron rich) events has been collected both by Chacaltaya and by Pamir experiments. Unfortunately, in contrast to the undisputable Centauro I, some of these events were born at rather large distances from the apparatus, thus they possess the significant fraction of electromagnetic component, which probably has been generated in the nuclear and electromagnetic cascade processes, in the atmospheric layer above the chamber. Besides that, the serious difficulties were met during the measurements and analysis of some exotic super-families (with the very high visible energy, $E_{\text{vis}} \geq 500$ TeV) which are very frequently accompanied by the so-called «halo». These are the reasons that some events could not be analyzed in detail and they are not so spectacular as the Centauro I. Here they are named *Centauro-like events*. They are not so well known as «classical» Centauros although they carry a big amount of exciting experimental information. Here will be listed and described examples of the most interesting Centauro-like (or hadron-rich) events.

Centauro-New (C22-Sxxx-1019) [14, 28]. The second clean Centauro event was reported in 1997 at the 25th International Cosmic Ray Conference in Durban. The event was found in the Chacaltaya two-storey chamber No. 22, consisting of the upper chamber (7 cm Pb), target layer (30 cm CH₂), air space (237 cm), and the lower chamber (11 cm Pb), i. e., of the total thickness $\sim 0.49\lambda_{\text{int}}$. It is the family of 31 showers (13 with energy exceeding 1 TeV) of the total observed energy 57.4 TeV (or 51.2 TeV when the energy threshold of 1 TeV is used). No

showers in the upper chamber have been found. According to [28], there is no trivial reason for the fact that no showers are observed in the upper chamber (the lower chamber was constructed only after the upper chamber was completed). Hence, the event is considered as clean Centauro (or Mini-Centauro regarding its relatively small energy), without presence of γ rays. It is the second, besides the Centauro I, event of this type.

Centauro VI [36–38]. The event No. C20-107S-089I was observed in the Chacaltaya two-storey emulsion chamber No.20. The measurements were restricted to X-ray film observation because the emulsion plates were not in fully satisfactory condition. The observed results, i. e., the domination of hadrons in the high energy region and the exponential $E \cdot R$ distribution* can be interpreted under the hypothesis of Centauro interaction. Assumption of the same average transverse momentum of secondary hadrons as that measured for Centauro I ($\langle p_T(\gamma) \rangle \sim 0.35$ GeV/c) leads to the production height of about 800 m. The estimated multiplicities and energies of photonic and hadronic components (for showers with visible energy greater than 4 TeV) at the top of the chamber are: $N_\gamma = 15$, $\Sigma E_\gamma = 95.2$ TeV, $N_h = 40$, $\Sigma E_h^\gamma = 900$ TeV. The estimated number and energy of hadrons at the interaction point are: $N_h = 80$, $\Sigma E_h^\gamma = 1500$ TeV [38].

Centauro VII [32, 36, 37]. The event No. C21-87S-75I [32, 37] named Centauro VII was the first Centauro with halo. Fortunately, the observed halo has not been developed so well and the energetic showers were distinguishable even on the X-ray film. It has been found in the Chacaltaya two-storey chamber No. 21, consisting of the upper chamber (7 cm Pb) and the lower one (11 cm Pb) with the carbon target (23 cm pitch) and the air gap (2 m) between them. In this event, the detailed study of the shower core structure in nuclear emulsion plates was done. Also the decascading procedure was used to study the longitudinal and lateral characteristics of the event. The family has an extremely large visible energy ($\Sigma E_{\text{vis}} \approx 5600 + 500$ TeV (halo) [32]). The interaction height, estimated by triangulation measurements [32], is about 2000–3000 m above the chamber. Such value of the production height results in the average transverse momentum value consistent with the Centauro-type events. The event is undisputably the hadron-rich family with Q_h value of the same order as for «classical» Centauros: $Q_h = 0.46$ for $E_{\text{th}} = 2$ TeV increasing to $Q_h \approx 0.8$ when assuming the most unfavourable case that all halo energy is of electromagnetic origin and when the analysis is limited to the most energetic cascades, with energies higher than 20 TeV (what seems to be justified by the large production height).

The family is in an old stage of development due to the long distance atmospheric propagation, judging from the existence of a large number of lower

* E is an energy and R is a distance of a particle from the energy weighted family centre.

energy degraded gamma-rays. However, the family contains, in the central region, several very high energy showers, higher than or close to 100 TeV. Those are confined within the radius smaller than several centimeters from the centre of the family. All of them started the shower development from the upper chamber and were penetrating deeply into the lower chamber, far beyond the expectation from simple electromagnetic cascades. Their transition curves are shown in Fig. 6.

This family is sometimes claimed to be the *Chiron-type* interaction because of very large lateral spread of hadrons [37] (the spread of high energy hadrons with $E(\gamma) \geq 40$ TeV is as large as $\langle E(\gamma)R \rangle \simeq 1300$ GeV · m) and the existence of the *strongly penetrating component*, revealing typical *minicluster* configuration. The majority of very high energy penetrating cascades, given in Fig. 6, show a typical *minicluster* structure. Re-analysis of the event [30] confirmed its exotic character and showed that characteristics of the hadronic secondaries are compatible with assumption of one emitting fire-ball.

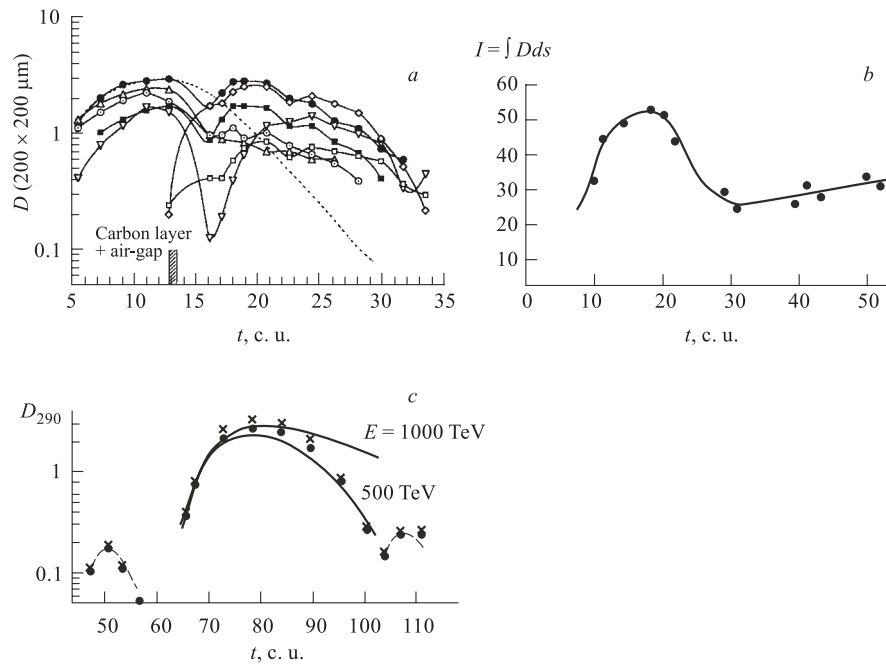


Fig. 6. *a)* Examples of penetrating component in Centauro-like events found in carbon chambers. Transition curves present the darkness D on the X-ray films with the depth in radiation units in the chamber. *b)* Penetrating black core in family Tatyana [44]. *c)* For family Elena [41] calculated curves for γ quanta are shown. Black dots are experimental points without methodological corrections, crosses are corrected experimental points

Centauro «Pamir» [37,39,40]. Centauro event, marked in [37] as G178H178 or P3'-C2-B178 in [39,40], was found in the carbon-type chamber No.2 of P-3', consisting of the standard gamma block (6 cm Pb) followed by the carbon target (60 cm C) and the hadron block (5 cm Pb), from USSR–Japan joint exposure at the Pamir. The event shows every feature of a Centauro, i. e., the energy is mainly released into the hadron-induced showers and the average lateral visible-energy spread is much higher for the hadron induced showers than for the γ -ray induced ones. For the hadron induced showers both spectra: the fractional visible energy and the lateral visible energy spread, can be well reproduced by exponential functions. The height of the interaction was estimated to be $H = 700 \pm 100$ m, from the lateral visible energy spread of hadrons with $\Sigma E_h^\gamma \geq 4$ TeV and by using the same as for Centauro I $\langle p_T(\gamma) \rangle$ value. Estimated numbers and energies of electromagnetic and hadronic component at the top of the chamber are: $N_\gamma = 55$, $\Sigma E_\gamma = 372.5$ TeV, $N_h = 45$, $\Sigma E_h^\gamma = 700$ TeV. The multiplicity and energy of hadrons estimated at the original interaction is $N_h = 77 \pm 16$ and $\Sigma E_h^\gamma = 1000$ TeV [38], respectively (for showers with the visible energy greater than 2.3 TeV).

Elena [41]. Elena is a superfamily with a total measured energy ~ 1700 TeV, detected in the Pamir deep lead chamber of a total thickness of 60 cm, what corresponds to $\sim 3\lambda_{\text{int}}$. It has given a rather rare opportunity to observe the transition of particles produced in such high energy interaction through the deep chamber. The majority of superfamilies were detected in relatively thin chambers ($\leq 1.5\lambda_{\text{int}}$) what makes impossible the detailed investigation of hadron characteristics.

This event reveals the features of Centauro-type families, such as the wide energy weighted lateral distribution and the large fraction of the family energy transferred to hadrons. $Q_h = 0.7 \pm 0.07$, when corrected for hadron detection efficiency, what locates the family well beyond the region of usual fluctuations on the N_h vs. Q_h diagram. Soft spectrum of γ rays indicates that the family is «old». The height of the initial interaction point was determined, assuming that $\langle p_T(\gamma) \rangle$ of hadrons is 0.35 GeV/c. It gives the height ~ 1500 – 2000 m above the chamber. A similar analysis as that done for «classical» Centauros, i. e., evaluation of the number of hadrons generated in the primary interaction and the number of their interactions in the air above the chamber, does not contradict the scenario of the development of a Centauro-type event occurring at large height above the apparatus.

The total number of detected hadrons is 31 and among them 4 hadrons undergo in the chamber several interactions. Especially interesting is the «leading» hadron. It was located at a distance of 7.5 mm from the family energy weighted centre and it was not accompanied by any γ rays at a distance closer than 1 mm. It started its development rather deeply inside the chamber and escaped through its bottom after passing 35 cm of Pb (~ 65 c.u.). Three separate maxima are

seen in the cascade longitudinal development (see Fig. 6). Dark spots produced on the X-ray films by electromagnetic showers induced by this hadron have large transverse dimensions, ~ 3 mm, and look like a «halo». The estimated energies and the points of origin of the showers producing each of the three «humps» have the following values: $E_1 = 9.8$ TeV, $t_1 = 39.7$ c. u., $E_2 = 500\text{--}1000$ TeV, $t_2 = 57$ c. u., $E_3 = 20$ TeV, $t_3 = 90$ c. u. The analysis presented in [41] showed that it is difficult to explain such shape of a transition curve, assuming the «normal» interaction of high energy leading hadron. For example, the probability of producing the observed ratio of released energies corresponding to the first two humps by a subsequent interactions of a hadron in usual nuclear-electromagnetic cascade in lead is as small as $\sim (1\text{--}4) \cdot 10^{-3}$.

C-K [42,43]. The family named here C-K was found in a deep lead chamber «Pamir 76/77», of a total thickness of 60 cm Pb. It has been measured and analyzed by the Cracow group. It has been classified as a Centauro-like event accompanied by the strongly penetrating component. It was the first hadron-rich event with so spectacular evidence for penetrating cascades. Fortunately, it was found in the homogenous type thick lead chamber which gives possibility

of the detailed study of the transition curve structures. Comparison of this family with classical Centauros is shown in Fig. 7. On the diagram of the number of hadrons N_h vs. the hadron energy fraction Q_h for Chacaltaya events [29,44], the event C-K has been marked by the star. For the Chacaltaya events, the hadronic part includes C-jets, Pb-lower-jets, and identified Pb-upper-jet, and A-jets identified as a shower cluster with association of a hadron in it. Since the effective thickness of the Chacaltaya chambers is about 1.5 nuclear mean free paths, and the «identified A-jets» cover only the A-jets with production heights less than ~ 100 meters, the «hadron energy sum» $\Sigma E_h^{(\gamma)}$ will give an under-estimate on an average. The C-K event has been registered in the deep lead chamber, so that the loss due to penetration is negligible. On the other hand, a relatively high threshold for hadrons in Pamir chambers (here it was assumed to be 2 TeV) as compared with the Chacaltaya detectors reduces the number of hadrons. Keeping in mind these two effects it seems that such comparison is roughly reasonable. The hadron-rich nature of the event is evident.

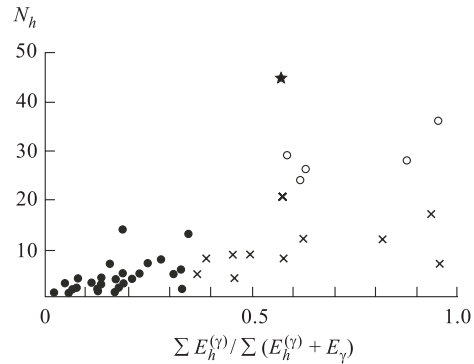


Fig. 7. Diagram of the number of hadrons and hadronic energy fraction: Chacaltaya events with the total visible energy greater than 100 TeV [44]: \circ — Centauro; \times — Mini-Centauro; \bullet — others; \star — C-K [42]

Table 3. Unusual cascades in Centauro-like event C-K

Cascade No.	Starts at		Finishes at		Penetrated c. u.	Number of maxima
	c. u.	Layer No.	c. u.	Layer No.		
197.08	11.8	5	120.7	Escape	108.9	11
748.01	48.3	23	120.7	Through Bottom	72.4	5

Among cascades belonging to the family, two cascades reveal unusual features. They were observed not far from the energy weighted centre of the family, in the very close distance one to the other. Both cascades demonstrated a multi-core structure. They started their development rather deeply inside the chamber and after passing a very thick layer of lead, escaped through the bottom of the chamber. The features of these cascades are summarized in Table 3. Their transition curves reveal surprising features. Both cascades have unexpectedly long range and many maxima character. The longer cascade, shown in Fig. 8, penetrated more than 109 cascade units, and 11 maxima at its transition curve appeared. The average distance between the neighbouring humps is very small, equals only 10.4 ± 4 c. u. These features are hardly explained by simulations. According to calculations [45], an average cascade initiated by a hadron with energy ~ 100 TeV can be detectable in such chamber only to the depth of 45.5 c. u. (for measurements with diaphragm of a radius of 50μ). Moreover, the many maxima

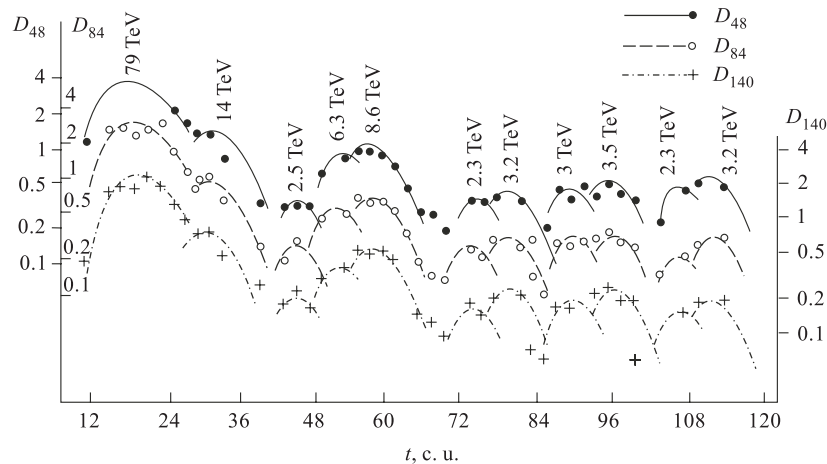


Fig. 8. Transition curves in X-ray film darkness D (measured in three diaphragms of a radius $R = 48, 84$ and 140μ) for cascade No. 197.08. Energy (in TeV units) liberated into the soft component is indicated at each hump (averaged over three estimated values) [42]

cascade curves are obtained in simulations very rarely. But even in that case, only very limited number of humps can be detected (two–three) and the average distance between them is much larger (23 ± 10 c.u.) than that observed here. Unexpectedly, both unusual cascades penetrate through the whole chamber practically without noticeable attenuation, and a weak growing rather than quenching of the cascades is observed. From this point of view they remind the long-lived cascades discovered by means of the Tien-Shan calorimeter [46].

P3'-C2-201 [37,40,47]. This candidate of Centauro type interaction of the highest energy range, occurring at very high altitude above the apparatus, marked as G201H201 in [37], was detected in the Pamir joint standard carbon type chamber P3'-C2. It has got a small blackened area (in the radius of about 2 mm on the X-ray film) in the centre of the family, being considered as the premature stage of the halo. It is composed of several very high energy showers strongly penetrating into the lower chamber. It is difficult to clearly resolve such a blackened area into individual shower-cores on X-ray film, and therefore this part was separately analyzed. The estimated height of the family turns to be ~ 2000 m above the chamber (from the lateral spread of the high energy hadrons and by assuming $\langle p_T(\gamma) \rangle \simeq 0.35$ GeV/c). Such value of the height gives the original multiplicity of hadrons of about 100.

Halina [37,48,49]. This event has been found among 7 high-energy hadron-gamma families of $\Sigma E_\gamma \geq 800$ TeV in a systematic study of carbon chambers of $\simeq 400$ m²·y exposure (the Polish part). It was detected in the Pamir-79/80 carbon chamber C42, consisting of the standard gamma block (of 6 cm Pb) and two hadron blocks (of 5 cm Pb) interlayered the carbon target (60 cm of carbon), i. e., the effective thickness of the chamber was $\sim 2.3 \lambda_{\text{geo}}$. It is a good design for investigation of a hadronic component, as the detection probability of hadrons in the chamber is larger than that of the standard type carbon chamber and it is close to 90%. It is no halo event despite its high energy.

This event reveals all exotic Centauro features:

- It has hadron-rich nature: the energy fraction of a hadronic component in the peripheral region $Q_h = 0.45$. About 30% of its energy is carried by 106 identified hadrons (with the visible energy greater than 2 TeV).
- Its longitudinal and lateral characteristics cannot be fully explained by usual hadron interactions, even when the contributions of heavy nuclei in primary particles are considered.
 - Extraordinary wide lateral spread both in gamma-rays and in hadrons results in the transverse momentum of produced particles $p_T \simeq 1$ GeV/c.
 - There are 6 showers which penetrate from the gamma-block to both hadron blocks.

Andromeda [50]. Andromeda was detected in the flat chamber CH-14 (11 cm Pb, 41% hadron detection efficiency) of the Chacaltaya experiment and it is known as the first and most famous example of the superfamily with the huge

halo of the radius of about 3.2 cm. Unfortunately, the chamber was not thick enough to study the full development of the halo transition curve and a hadron component of the event. Some authors [44] interpreted a halo in Andromeda as caused by a numerous bundle of high-energy atmospheric γ quanta. However, the observed decrease of the intensity of the halo transition curve with the depth in the chamber is less than that expected from a pure electron shower. Besides, the energy spectrum of hadrons is harder than that of electrons/ γ rays and generally its characteristics are found to be inconsistent with the hypothesis of a proton primary with pion multiple production under the scaling model. In [50] the event is claimed to be hadron rich. Estimates of the total energy of the photonic and hadronic component (after corrections for detection efficiency) show that the hadrons carry $\sim 47\%$ of the total energy.

Ursa Maior [37,50–52]. It was found in the two-storey Chacaltaya chamber CH-15 (64 % hadron detection efficiency). Similarly as Andromeda, it is a typical halo (with the multicore structure) super-family. The hadronic component occupies the substantial part of the whole energy (38 % after correction for efficiency and above the threshold of the shower spot detection). The study of correlations between hadrons and γ rays situated the family in the region of big values of the hadron number and hadron energy, and outside fluctuations expected from a scaling type model with the proton primary.

Mini-Andromeda III [37,51,52]. It was registered in Chacaltaya two-storey chamber CH-19 (59 % hadron detection efficiency). The wide halo (with the radius of about 2.2 cm) reveals the core structure. Similarly as in the previous events the chamber is too thin for a study of the full longitudinal halo development and the structures in the halo transition curve. But even at this limited length, the observed attenuation of the halo transition curve is weaker than that expected from a pure electromagnetic origin. In spite of the indications on the very high production altitude (wide lateral hadronic spread), this family is extremely rich in hadrons both in energy fraction and in number. The hadrons occupy $\sim 44\%$ of the total energy (above the threshold of shower spot).

Tatyana [44,53]. *Tatyana* is one of the highest energy events known in the world statistics, extremely interesting and difficult for measurements and analysis. The estimated visible energy of the event is about 11000 TeV, thus the total energy of the event was estimated to be about 15000 TeV. The super-family was detected in the Pamir 450-73/74 carbon type chamber. In contrary to the majority of other chambers, it is the extremely deep apparatus, consisting of the standard gamma block and four identical hadron blocks (each consisting of 20 cm carbon layer followed by 5 cm of Pb) what gives in total about $5 \lambda_{\text{int}}$ or 55 cascade units. It makes possible the direct study of the penetrating power of the family. The halo, occupying the central part of the event easily traversed the whole chamber, revealing the unexpectedly strong penetrating power. The blackness of the core does not show any sign of attenuation down to the bottom of the chamber, even a

Table 4. Centauro-like events

Event, Ref.	Collab., Chamber		N	E , TeV	Q_h	$\langle ER \rangle$, GeV·m	E_{halo} , TeV	E_{th} , TeV	Remarks
Cent. New [14, 28]	Brasil–Japan 2-storey	γ h	0 13	0 51.2	1			1	
Cent. VI [36, 37]	Brasil–Japan 2-storey	γ	56	361				4	
			157	644				2	
		h	28	390				4	
			68	496				2	
		tot		751 1140	0.52 0.44	735* 803*		4 2	
Cent. VII [32, 36, 37]	Brasil–Japan 2-storey	γ	547	2978				2	Centauro or Chiron Penetr. cascades and mini-clusters, halo
			265	2179				4	
		h	129	2486				2	
			74	2328				4	
		tot		5464 4506	0.46 0.52 0.8	842* 857*	500	2 4 20	
Cent. Pamir [37, 39, 40]	USSR–Japan Standard carbon	γ	15	95		67		4	
			120	298		28.6		1	
		h	22	444		244		4	
			37	476		173		1	
		tot		539	0.82 0.62	495*		4 1	
Elena [41]	Pamir Deep carbon	γ	78	600		360		4	Str. pen. leading cascade
		h	23	1100		885		4	
		tot		1700	0.65±0.05				
		h	22**	300**		475**		4	
C-K [42]	Pamir Deep Pb	γ	74	306		111		~ 1	Str. pen. cascades
		h	55	531		195			
				382***					
		tot			0.64				
		γ	27	198				4	
		h	22	446					
		297***							
		tot			0.69				

* Measured by showers of $E(\gamma) \geq 20$ TeV.
 ** Without leading cascade.
 *** Energy released only in the first peaks.

rise of the transition curve is observed (see Fig. 6). The absence of the attenuation of the core through the chamber indicates that the secondary particles are more penetrative than normal hadrons. Outside the core halo region, of a diameter ~ 1 cm, there are numerous showers. There were detected 224 γ quanta with $\Sigma E_\gamma \sim 3200$ TeV and 66 hadrons with $\Sigma E_h^\gamma \sim 1500$ TeV. Tatyana has been classified as the family with high energy of the hadronic component.

The main features of these and other Centauro-like/hadron-rich events are summarized in Tables 4 and 5. The hadron dominant character of families registered in Pamir-joint chambers series P3 and P2 was spectacularly presented on the correlation diagram (N_h vs. Q_h) in [40], also in comparison with classical Chacaltaya Centauros and some halo families such as Andromeda, Ursa Maior and U. M. III [55] (see also Fig. 18 in Subsec. 2.1).

Table 5. Hadron-rich events

Event, Ref.	Collab., Chamber		N	E , TeV	Q_h	$\langle ER \rangle$, GeV·m	E_{halo} , TeV	E_{th} , TeV	Remarks
P3'-C2-201 [37,47]	USSR-Japan Standard carbon	γ	132	1479	0.42	435*	400	4	Penetr. casc., premature halo
		h	43	1089				4	
		tot		2568				4	
Halina [37,48,49]	Pamir Deep carbon	γ	171	1630	0.37	883*		4	Penetr. casc.
			469	2468				2	
		h	65	936				4	
			106	1071				2	
		tot		2566				4	
		3540	2						
C141-G4836 H4784 [37,48]	Pamir Standard carbon	γ	157	1277	0.25	1071*	-	4	Hadron rich
			346	1807				2	
		h	31	415				4	
			50	482				2	
tot		1692	4						
		2289	2						
Andromeda [50]	Chacal. Flat Pb	γ	627	4488	$\sim 0.47^{**}$		~ 21000	1	
		h	110	1656				1	
		tot	268**	(4039)**					
Ursa Maior [37,50-52]	Chacal. 2-storey	γ	239	1074	$\sim 0.38^{**}$	498*	~ 980	2	Single cluster ~ 1080 TeV
			430	1344				1	
		h	38	508				2	
			54	532				1	
			(84)**	(830)**				1	
		tot		1582				0.32	

The ending of Table 5

Event, Ref.	Collab., Chamber		N	E , TeV	Q_h	$\langle ER \rangle$, GeV·m	E_{halo} , TeV	E_{th} , TeV	Remarks	
M. A. III [37, 51, 52]	Chacal. 2-storey	γ	192	1701					4	
			441	2370					2	
			537	2531					1	
			80	1070					4	
			112	1167					2	
			115	1172					1	
(195)**	(1986)**	$\sim 0.44^{**}$								
tot			2771	0.39	842*		4			
			3536	0.33	866	~ 5060	2			
Tatyana [53]	Pamir Thick carbon	γ	224	3200				~ 1	Periph. region Str. penetr. halo	
			h	66						1500
			tot							~ 11000
						~ 6000				
P2-C96-125 [37, 40, 54]	USSR– Japan Standard carbon	γ	40	288					Data for off halo part ($r \geq 1.2$ cm) 2 penetr. clusters	
			h	20						579
			tot							5437
P3'-C2-168 [37, 40]	USSR– Japan Standard carbon	γ	41	316						
			h	15						212
			tot							528
P3'-C5-505 [37, 55]	USSR– Japan Standard carbon	γ	98	705					Data for off halo ($r \geq 2.2$ cm) Penetr. halo	
			h	49						513
			tot							10400
P3'-C2-228 [40]	USSR– Japan Standard carbon	γ	30	246						
			h	18						236
			tot							483

* Measured by showers of $E(\gamma) \geq 20$ TeV.
 ** After correction for detection efficiency.

1.2. Mini-Centauros. Mini-Centauros are events of the same hadron dominant nature as Centauros, the difference being their smaller multiplicity. By the Brasil–Japan Collaboration, 15 atmospheric and 9 produced in the target layer Mini-Centauros were reported [29, 38]. Among 15 atmospheric families, there were two favourable cases where the heights of the interaction vertex have been determined through triangulation measurement of shower positions and directions [33]. In these events, the direct measurements of the transverse momenta of

hadronic showers were possible, giving $\langle p_T(\gamma) \rangle \simeq 0.35$ GeV/c. In searching for Mini-Centauros among C-jets, the criterion was imposed that any pair of showers which couple to form a particle of neutral pion rest mass within the experimental error, i. e., $90 \leq m_{i,j} \leq 200$ MeV, where $m_{i,j}$ is the invariant mass of the shower pair, was not found.

The main features of Mini-Centauro events are the following:

1. Hadron multiplicity $N_h \simeq 10-20$.
2. $\langle p_T(\gamma) \rangle$ value as large as for Centauros ($\langle p_T(\gamma) \rangle \simeq 0.35 \pm 0.10$ GeV/c).
3. Approximately gaussian pseudorapidity distribution.
4. Experimental characteristics in accordance with isotropic decay of the fireball with the mass $M_{fb} \simeq 35$ GeV and average multiplicity $\langle N_h \rangle = 15 \pm 3$.
5. Incident energy $\langle E_0 \rangle_{lab} \simeq 940$ (100) TeV for atmospheric (carbon target) Mini-Centauros. These values correspond to $\sqrt{s} = 1.3$ TeV (430 GeV) when assuming a nucleon incidence.
6. Average pseudorapidity in c. m. s system, assuming the proton incidence $\langle \eta \rangle = 3.7$ (they are produced in a little more forward region than Centauros).

The characteristics of individual Chacaltaya Mini-Centauros can be found in [29]. Similarly as Centauros they are sometimes accompanied by the strongly penetrating component. The detailed study of C-jets and Pb-jets from Chacaltaya Mini-Centauros (from chambers No. 17, 18, and 19) revealed the existence of penetrative miniclusters among them [56]. This analysis gave also some suggestions on the genetic relations among different types of exotic phenomena.

Families of similar type were reported also by Pamir Collaboration. By a systematic survey in the Pamir chamber in the exposure of ~ 100 m² · y [44, 57], six Mini-Centauro events were found among ~ 50 families observed in the Pamir carbon-chambers C18, C19, C24 in «Pamir 78/79» and C34 in «Pamir 79/80».

Table 6. Mini-Centauros in Pamir-joint chambers, examples

Event, Ref.	Collab., Chamber		N	E , TeV	Q_h	$\langle ER \rangle$, GeV·m	E_{th} , TeV
P3'-C2-223 [40]	USSR- Japan Standard carbon	γ	3	25	0.92	57	4
		h	5	302		172	4
		tot		327			4
G544H534 [37]	USSR- Japan Standard carbon	γ	18	187	0.65	309*	4
		h	11	339			4
		tot		526			4

*Measured by showers of $E(\gamma) \geq 20$ TeV.

Comparison with simulation calculations showed that these events are beyond the fluctuations in the atmospheric nuclear cascade process originating from normal type meson production (see Fig. 2 in [57]).

The examples of other than «classical» Chacaltaya Mini-Centauros are shown in Table 6.

1.3. Chirons. Chirons are hadron-rich species characterized by the following features:

1. The interaction energy close to that of Centauros and estimated to be ~ 1670 TeV.

2. Rather low hadron multiplicity $N_h \approx 10-20$. The characteristic feature is the existence of *clean hadronic cascades*, not clustered among electromagnetic cascades from atmospheric showering of γ 's in the atmosphere.

3. Extremely large lateral spread ($\langle E(\gamma)R \rangle = 10-20$ GeV \cdot m, hence $\langle p_T(\gamma) \rangle$ being 2-3 GeV/c, and $\langle p_T \rangle \approx 10-15$ GeV/c).

4. Pseudorapidity distribution of high energy showers in accordance with isotropic decay of the fireball with the mass $M_{\text{Chiron}} \simeq 180$ GeV and centered at $\eta_{\text{cms}} \simeq 2.3$ [29].

5. Frequent appearance of strongly penetrating single cores or the so-called miniclusters (i. e., clusters of particles with very small lateral spread corresponding to very low mutual transverse momentum $p_T(\gamma) \approx 10-20$ MeV/c). They are observed mainly in the centre of the family.

6. Existence of unusual hadronic component with the short interaction mean free path, as small as $\sim 1/3-1/2$ of the nucleon geometrical collision mean free path.

The study of C-jets and Pb-jets belonging to the Chiron-type families may indicate the existence of the chain of genetic relations [56] among such phenomena as Chiron, Centauro, Mini-Centauro, etc.

Similarly as «classical» Chacaltaya Centauros several clean Chiron families have been reported by Chacaltaya group [29]. The first event of this type, Chiron I (family 198S-154I) [26, 44], was found in 1979 in Chacaltaya chamber No. 19. Similarly as Centauro I, it is the clean family for which the altitude of interaction vertex was measured by triangulation method to be 330 ± 30 m above the chamber. This allowed one to measure transverse momenta of observed secondaries and resulting $\langle p_T(\gamma) \rangle \sim 1.42$ GeV/c. The total visible energy of the event was estimated to be ~ 400 TeV. The event shows extremely large transverse momenta of produced secondaries and no π^0 meson emission. Besides that it indicates the existence of penetrating shower clusters which show similar lateral spread with atmospheric cascades (\sim a few mm in diameter). The transition curves of high energy showers for both single-cores-upper and shower-clusters-upper start development just after entering into the upper chamber, like electromagnetic cascades, however on the other side, they show strong penetrating power, far over than that expected from the pure electromagnetic shower development, see

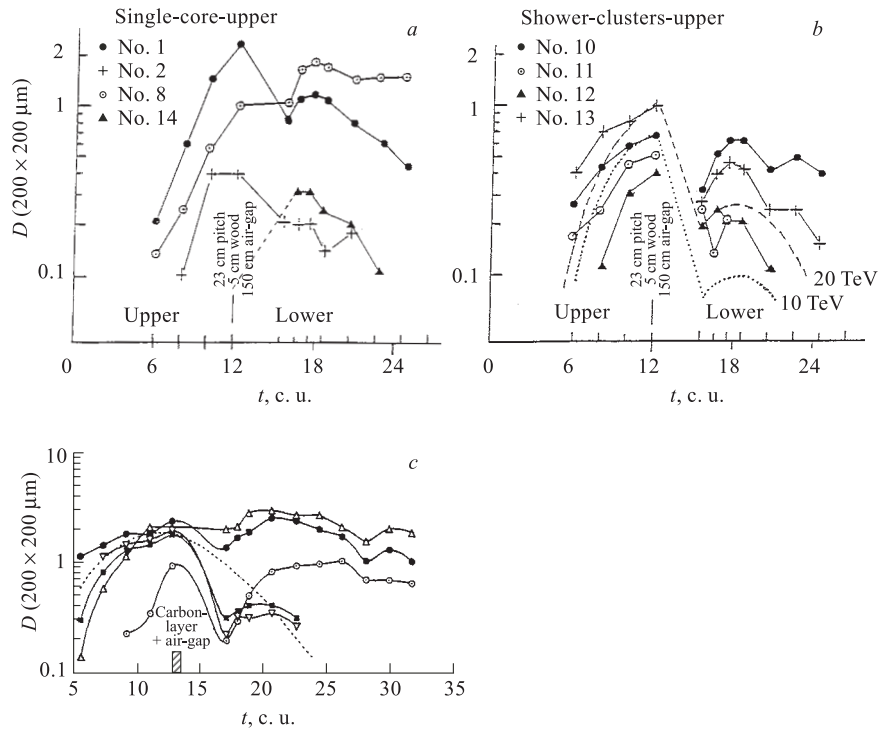


Fig. 9. Examples of penetrating component in Chiron-type families: *a, b*) Chiron I [26]; *c*) C22-113S-84I [37]. The transition curves are compared to those expected for electromagnetic cascades (shown by dotted and dashed lines)

Fig. 9. The showers are separated at such large distances to each other that none of the couple of showers which could be attributed to a π^0 meson decay were found. They have been tentatively named «miniclusters» to distinguish them from pure electromagnetic atmospheric cascades. Later, two other events were found for both of which the estimation of interaction heights was possible by the triangulation method [33, 34].

A systematic study of Chiron type interactions was extended to the strong penetrative families with wide lateral spread detected in other chambers. 30 Chiron-type events found in the systematic study of the Chacaltaya chamber No. 19 are described in detail in [33, 58]. Other events have been collected in the past several years and the analysis of 82 Chiron-type families (selected out from 120 families from Chacaltaya chambers No. 19, 20, and 22) is presented in [26, 59, 60]. 21 Chiron events among them were found. Four Chiron-type

Table 7. Chiron-type events, examples

Event, Ref.	Collab., Chamber		N	E , TeV	Q_h	$\langle ER \rangle$, GeV · m	E_{halo} , TeV	E_{th} , TeV	Remarks		
B154S-B133I [62]	Chacal. 2-storey	γ	132	818	0.39	140	—	—	Penetr. cascades and minicl.		
		h	24	528						323	
		tot		1346						—	
P3-C1-G48H57 [37,63]	USSR–Japan Standard carbon	γ	34	383	0.48	3141*	—	4	Penetr. clusters and cascades		
		h	5	347						—	4
		tot		730						—	4
113S-084I [37]	Chacal. 2-storey	γ	67	513	0.62	1362*	—	2	Penetr.		
		h	25	839						—	2
		tot		1352						—	—
P3-C4-G369H370 [37]	USSR–Japan Standard carbon	γ	107	1337	0.4	701*	—	4	Penetr. multi-cluster		
		h	26	898						—	4
		tot		2235						—	4

*Measured by showers of $E(\gamma) \geq 20$ TeV.

events, found among ~ 60 families with total observed energy greater than 100 TeV from Pamir exposure (~ 120 m²·y of carbon chambers and ~ 9 m²·y of thick lead chambers), have been reported in [61].

The examples of Chiron-type families, which have been found more recently, are presented in Table 7. These are:

Ch18-B154S-B133I [62]. The event was recorded in Chacaltaya chamber No. 18. Despite the large total visible energy (1346 TeV) the family has no halo. It has large lateral spread and it is much more rich in hadron component than usual events. Hadrons carry about 40 % of the total visible energy. The most striking feature of the family is the existence of two exotic hadrons within an extremely collimated cluster of showers located in its central part. One gives rise to a Pb-jet in lower chamber. It was found in the downstream of the shower observed in the upper chamber and consists of at least four cores, remaining a miniclusters. Their average visible transverse momentum is about 2 GeV/c (from measurements of the geometrical convergence between cores at different depths in the chamber). The other gives rise to a pizero-less C-jet (no pair of showers which couples into a π^0 produced in the target layer). Both jets are hardly explained as well as being of «usual» hadron or single « γ -ray» origin.

The event contains also several anomalously collimated bundles of showers which penetrate through the whole chamber and their observed darknesses in the

lower chamber are appreciably larger than those expected for pure electromagnetic shower (see figures in [62]).

P3-C1-G48H57 [37,63]. The event found in the Pamir-joint chamber C1 series P3 is the example of the quasi-clean family. The analysis of both longitudinal ($f = E/E_{\text{vis}}$) and lateral ($E(\gamma)R$) spectra shows that the majority of high-energy secondary particles arrive at the chamber directly. Provided that the interaction height is ~ 1 km (\simeq one collision mean free path) or less, the present event is the example of particle production with large transverse momenta, $\langle p_T(\gamma) \rangle$ of the order of 2–3 GeV/c or more. Multiplicity of the secondaries at the main interaction is ~ 10 –15. Among high energy showers there are the strongly penetrating ones which after starting development in the gamma block enter further into the lower chamber. Two penetrating clusters with a small lateral spread were also detected.

C22-113S-84I [37]. This is another example of the quasi-clean Chiron-type family found in the Chacaltaya chamber No.22. In Fig. 9, transition curves of high-energy showers are shown. They are far beyond the fluctuation of simple electromagnetic cascades, even though they start shower development in the upper chamber.

P3-C4-G369H370 [37]. It is the Chiron type family registered in the Pamir joint chamber C4 series P3, marked as P3'-C4-368 in [59]. Several penetrating miniclusters emitted with abnormally large p_T values were found among secondaries. The energy weighted spread of these clusters is small, $\langle E(\gamma)R \rangle \simeq 10$ –20 GeV · m, while the energy spread for the whole family, when it is measured by cluster energy, shows very large p_T emission, namely $p_T(\gamma) \simeq 2$ GeV/c or more ($\langle E(\gamma)R \rangle \simeq 2800$ GeV · m).

Since the time of the first finding of the exotic cosmic-ray interaction named «Centauro», it has been even-standing problem whether the produced secondaries from such an exotic events are «ordinary» hadrons or something new. In fact, *secondary hadrons from the Chiron-type interaction reveal very exotic characteristics:*

- *Single or multicore structure and two very different transverse momentum components.* About one half of hadronic cascades is single core structure while another half develop a multicore structure at the lateral spread of ~ 0.1 –1 mm, what can be connected with the intrinsic p_T of $10 \sim 20$ MeV/c. These narrowly collimated jets of cascades are called *miniclusters*. The ratio of $\langle E(\gamma)R \rangle$ of hadronic cascades in the Chiron families to the $\langle \langle E(\gamma)r \rangle \rangle$ in miniclusters is ~ 300 . This is a surprisingly large ratio, telling us that *secondaries in the parent interaction are produced with extra large p_T , or miniclusters are connected with very small transverse momenta phenomena, or both.*

- *Strongly penetrating power.* Majority of miniclusters cannot be of electromagnetic origin because of their *penetrating power*. About one half of *miniclusters* is strongly penetrative. Figures 9 and 10 show several examples of transition

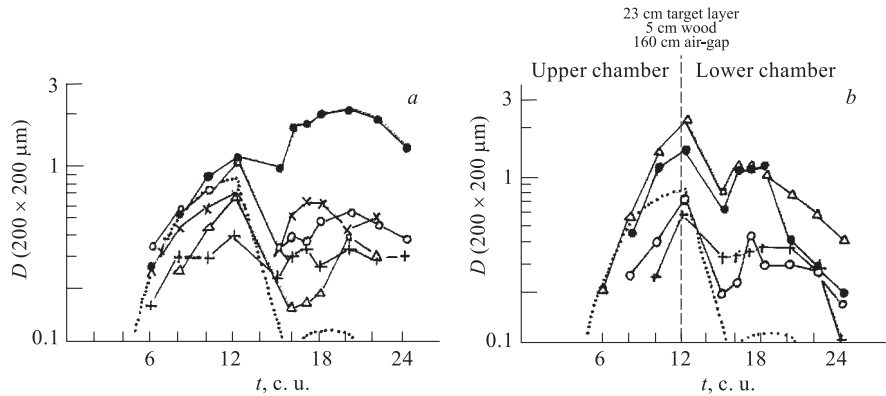


Fig. 10. Examples of transition curves of cascades from Chiron type families [33]. *a*) Mini-clusters: ● — No. S-1 in family 150-90I; ○ — No. S-1 in family 131S-109I; △ — No. S-2 in family 181S-139I; + — No. S-2 in family 131S-109I; × — No. S-10 in family 198S-154I. *b*) Single cascades: ● — No. S-1 in family 155S-136I; ○ — No. S-3-3 in family 131S-109I; + — No. S-2 in family 123S-90I; △ — No. S-1 in family 198S-154I

curves of individual cascades from various Chiron events. Figure 11 shows the average transition curves of high energy showers, with $\Sigma E(\gamma) \geq 10$ TeV, from Chiron-type families. For comparison, the average calculated transition curve was shown by dotted line. In calculations it was assumed that 100 γ rays of energy greater than 10 TeV enter into the chamber from the atmosphere. The power index of an integral spectrum, $\gamma = -1.3$, the same form as observed in the experiment was assumed. One finds that experimental showers demonstrate far stronger penetrating power than that expected in the case of electromagnetic particle incidence. A possibility of the showers being γ rays from the ordinary type of meson production has been made implausible both from the argument on their penetration and from isolation and absence of accompanied air showers. If they would be γ rays, we should expect accompanied air cascades from neutral pions associated with them.

- *Very wide lateral spread.* It seems that the high-energy showers from Chiron-type events *are also not usual hadrons* produced through the ordinary multiple meson production, high in the atmosphere. Assumption of $p_T(\pi) \sim 400$ MeV/c for such pions and $k_\gamma \sim 0.3$ for their secondary interactions gives heights $H \sim 4-8$ km (i. e., 3-5 nuclear mean free paths) for typical $\langle E(\gamma)R \rangle$ measured in Chiron-type families. Some hadrons could survive such distances, by chance escaping the secondary interactions, but not their majority. Besides that, hadrons produced at such altitudes should be accompanied by air cascades from neutral pions associated with them, what is not observed.

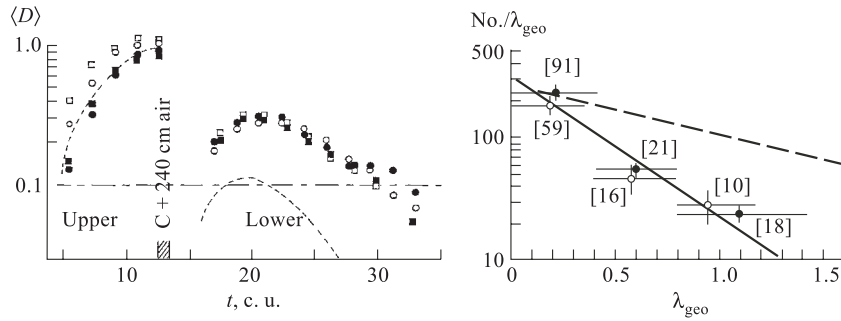


Fig. 11. Average transition curves of high energy showers of $\Sigma E_{vis} \geq 10$ TeV from Chiron-type families [26]: Ch. No. 21: ■ — single [33]; □ — cluster [52]; Ch. No. 22: ● — single [59]; ○ — cluster [45]

Fig. 12. Distribution of shower starting positions of high energy showers, measured by λ_{geo} [26]: ○ — Ch. No. 19; ● — Ch. No. 21, 22

• *Rapid attenuation (large interaction cross section).* Another surprising observation is a rapid attenuation of both single high-energy «hadrons» and mini-clusters. Majority of them start the shower development just after entering the chamber and their collision mean free path turns to be much smaller than the geometrical value. It is illustrated in Fig. 12 which gives the distribution of shower starting position in Chacaltaya two-storey chambers, No. 19, 21, and 22. 222 hadronic showers of $E_{vis} \geq 10$ TeV were selected from 82 Chiron-type families of $\Sigma E_{vis} \geq 100$ TeV. The dotted line in the figure shows the attenuation expected by assumption of geometrical mean free path in the chamber materials. The experimental results indicate the collision mean free path as small as $\sim 1/2-1/3$ of the geometrical value.

It is worth to note that a similar surprising behaviour has been also found in the study of shower development of the high energy cascades from 17 superfamilies of visible energy greater than 700 TeV detected in homogenous-type lead chambers [60] which have fair advantage for the study of overall transition behaviour of shower development. The high-energy hadrons in super families showed shorter attenuation length than ordinary single arrived cosmic-ray hadrons [26,60]. It was reported [60] $\lambda_{att} = 170_{-26}^{+47}$ g/cm² for 143 hadrons of $E_{\gamma} \geq 10$ TeV, and $\lambda_{att} = 137_{-26}^{+57}$ g/cm² for 68 hadrons of $E_{\gamma} \geq 20$ TeV for hadrons in superfamilies in comparison with $\lambda_{att} = 252 \pm 30$ g/cm² obtained for single-arrived ordinary cosmic-ray hadrons detected in thick lead chambers. This result seems to be especially surprising if one supposes that high energy hadrons in superfamilies are dominantly pions. Then their attenuation length should be larger than that

for ordinary cosmic-ray hadrons which are mainly protons [60]. The experiment gives the opposite result and one can estimate that λ_{coll} of high energy hadrons in superfamilies is about one half of that the one of ordinary cosmic-ray hadrons.

It should be noted, however, that up to now the unexpectedly short mean free path of hadrons was observed only in very high-energy superfamilies. Preliminary results [64] of the analysis of showers from 58 families with the visible energy greater than 100 TeV, detected in the Pamir thick lead chamber, gave the value of attenuation mean free path equal to $233 \pm 40 \text{ g/cm}^2$, for hadrons with energy greater than 10 TeV.

Results presented here seem to indicate the existence of «the new state of hadrons» which are emitted in the high-energy Centauro-type interactions. Authors of Ref. 58 suggested, basing on thermodynamical arguments from the fire-ball model, that the secondary particles observed in these exotic events could be some heavy and long-lived particles (with masses $\sim 10 \text{ GeV}$ and lifetimes $\tau_0 \geq 10^{-9} \text{ s}$).

1.4. Penetrating Clusters and Halo. Penetrating component, accompanying the exotic events, has been observed in the form of *strongly penetrating cascades, clusters or «halo»*.

The term *minicluster* [65] is used for strengthening the cluster characteristics which are different from ordinary atmospheric electromagnetic cascade showers, even though the spread of the clusters has a similar dimensions as air cascades. As has been already said in the previous section, miniclusters are very narrow collimated shower clusters (of a lateral spread $\sim 1 \text{ mm}$ or less, $\langle E(\gamma)R \rangle \sim$ a few $\text{TeV} \cdot \text{mm}$, and $p_T \sim 10\text{--}20 \text{ MeV}/c$). At a first glance they look like pure electromagnetic cascade from the atmosphere. The characteristic which distinguishes them from pure electromagnetic cascade is their strongly penetrative power. Miniclusters are observed in the most forward angular region and, assuming the production height of the order of $\sim 1 \text{ km}$, their emission angles turn out to be of the order of $\sim 10^{-6}$ radians. They show a strong concentration of energy in this very forward region. The fraction of cluster energy relative to the total visible energy of the family is substantially large and the essential amount of energy flow is concentrated within a circle of a radius of a few to several millimeters from the cluster axis. This phenomenon has been discovered in Chiron-type families but it appears also in other Centauro-species (e. g., in Mini-Centauro [56]).

Besides the ordinary miniclusters (called sometimes also «uniclusters»), being the isolated single clusters and characterized by relatively small multiplicity, the *giant-miniclusters* (called «*multiclusters*») have been also observed (e. g., giant minicluster in Chiron-type family No. 174S-134I [65], found in Chacaltaya chamber No. 19). These are unusual shower core bundles with exceptionally large multiplicities and they are suggested to be the ensembles of ordinary miniclusters [65]. The analysis [66] of the huge shower cluster spectra suggests its low

original multiplicity. A shower cluster starts from a small number ($\sim 4-5$) of high-energy particles with small primordial transverse momenta. Subsequent enhancement of shower core multiplicity, accompanied by softening of its energy spectrum is the consequence of the passage through the atmosphere. The nature of parent particles is unknown. The study of their penetrating power indicates that they are not of pure electromagnetic origin, even if they show such small spread as expected from electromagnetic processes. On the other hand, it seems that they are also not ordinary hadrons. Majority of these showers start developing as soon as they enter into the lead in the upper chamber.

Some examples of hadron-rich giant miniclusters are shown in Table 8. Among them are:

Table 8. Giant-miniclusters, examples

Event, Ref.	Collab., Chamber		N	E , TeV	Q_h	$\langle ER \rangle$, GeV·m	E_{halo} , TeV	E_{th} , TeV	Remarks
C22-178S-139I [37]	Brasil-Japan 2-storey	γ	43	229	0.70	40*	—	2	Single penetr. cluster
		h	6	533				2	
		tot		762				2	
P3-C4-G454H454 [37]	USSR-Japan Standard carbon	γ	22	326	0.66	97*	—	4	Hadron rich str. penetr. cluster
		h	23	633				4	
		tot		959				4	
C19-11S-021I [37]	Brasil-Japan 2-storey	γ	72	417	0.44	180*	—	2	Penetr. cluster ($\Sigma E_{\text{vis}} = 465$ TeV)
		h	10	321				2	
		tot		737				2	

*Measured by showers of $E(\gamma) \geq 20$ TeV.

C22-178S-139I [37]. It was found in the two-storey Chacaltaya chamber No.22. The shower cores at the cluster area were scanned in nuclear emulsion plates under the microscope. It is a typical example of the family confined in small dimensions of a spread of the order of several millimeters. It is composed of only three very high-energy showers, starting in the upper chamber, about 30 low energy showers near the detection threshold energy and one C-jet located approximately at the position corresponding to the one of high-energy upper-chamber showers. The transition curves of these three high-energy cascades are shown in Fig. 13. In this chamber there is 30 cm of plastic target and 230 cm of air-gap between the upper and lower chambers. Usually, such air-gap strongly disturbs the transition curve, i. e., significantly reduces the numbers of electrons in the

lower chamber, due to the electron scattering through the air-gap. The observed transition curves demonstrate unexpectedly strong penetrating power, indicating that they cannot be of electromagnetic origin. It is also questionable if they could be caused by interactions of usual hadrons. The analysis of longitudinal and lateral spectra allows one to suspect the existence of a new type particle production, characterized by very small transverse momentum, of the order of $p_T(\gamma) \simeq 30$ MeV/c, assuming that the main interaction occurred at about one collision mean free path, i. e., ~ 1200 m at Chacaltaya, above the detector.

P3-C4-G454H454 [37]. Very interesting event with the high-energy hadron-rich cluster (of visible energy ~ 1000 TeV) in the centre of the family was found in the Pamir-joint chamber C4 series P3. One observes more than ten high-energy shower-cores of visible energies greater than 10 TeV, concentrated within a small area of a radius of ~ 3 mm. A striking feature is the strong penetrating power of the cluster which was observed deeply in the H-block. The longitudinal profiles of penetrating showers show similar transition behaviour as that recognizable in Fig. 13. The estimated $p_T(\gamma)$ of high-energy showers inside the cluster is as small as $\simeq 20$ MeV/c if we assume that the interaction height is equal to one collision mean free path at the Pamir altitude.

An unusual penetrative nature of miniclusters has been studied by Chacaltaya, Pamir and also by Chacaltaya–Pamir Collaborations. The results of the study of penetrating component in 17 families with $\Sigma E(\gamma) \geq 100$ TeV, observed in the Chacaltaya chamber No.19 (24 penetrating showers out of 37 ones in total) and in the chamber No.18 (16 penetrating showers out of 30 ones in total) supported the existence of unusual showers with strong penetrating power [66,67]. Similar conclusions have been obtained from the study of penetrating showers registered in the Pamir carbon chamber («Pamir 79/80» with one carbon block of 60 cm thick) where 187 penetrating showers from 37 families with $\Sigma E_{\text{vis}} \geq 100$ TeV were picked up [68]. The detailed analysis of high-energy shower-clusters of visible energy beyond 100 TeV observed in Pamir-joint chambers (analyzed 173 families of $\Sigma E_{\text{vis}} \geq 100$ TeV) is described in [59,69]. The general conclusions from this study as well as the single-core showers and cluster-structure

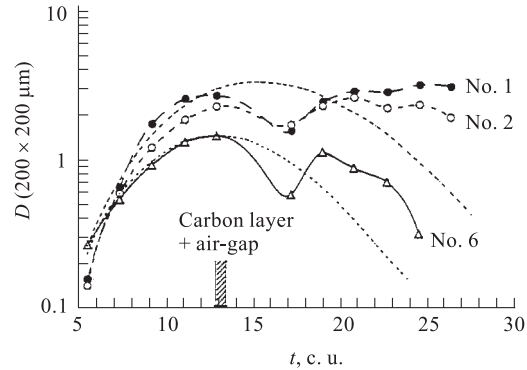


Fig. 13. Transition curves of the three highest energy showers from the hadron-rich minicluster event C22-178S-139I [37]. Dotted curves are simulated electromagnetic cascades

ones, are the same for three experiments. They agree that there exist unusual showers with unexpectedly strong penetrative power. Besides that, two very different components of transverse momentum are observed. Shower inducing secondaries are produced with large p_T ($\langle p_T(\gamma) \rangle \sim 2-3 \text{ GeV}/c$), far beyond that expected from the ordinary type. A low p_T phenomenon, of the order of the electromagnetic one, seems to be responsible for cores generation inside the cluster.

Miniclusters are considered to be the premature stage of other phenomenon called *halo*. Halo is the diffusion dark spot with dimensions $\sim 1-1000 \text{ mm}^2$ observed in the centre of families. Sometimes it consists of several hadron cores, spaced very closely together. The first gigantic halo event named «Andromeda» was discovered in the Chacaltaya chamber No. 14 in 1969. Since that time the statistics of halo events have steadily increased and events with different halo configurations have been found by mountain experiments at Mts. Chacaltaya, Pamir, Fuji, and Kanbala [50]. About 50% of γ -hadron families with energy $\Sigma E_\gamma \geq 500 \text{ TeV}$ are halo events. The examples of cosmic-ray families in which shower spots surrounding the central halo show abundantly hadron rich composition, the same behaviour as seen in cosmic-ray families of Centauro species, were also found. The halos of anomalously strong penetrative nature (e. g., Tatyana [53]) were observed. The five Chacaltaya families: Andromeda, Ursa Maior, M. A. I, M. A. II, and M. A. III [50] are examples of fully analyzed halo events.

Many calculations were performed to understand the mechanism of halo formation and its surprising features such as, for instance, the strong penetration capability. Generally the data show a contradiction between the longitudinal and lateral halo development which cannot be resolved assuming the ordinary cosmic ray composition.

In principle, the nature of superfamilies shows similar characteristics with Centauro species, i. e., unusual hadron rich composition for showers which surround the central halo. There are also strong indications that the relative p_T of hadrons within miniclusters and halos are in $\sim 20-30 \text{ MeV}/c$ range, the same as in Chirons. Such properties as: strong penetrative nature and two different components of the transverse momentum invoke the idea that in the extremely high-energy interactions the strongly collimated bundle of particles is frequently produced. They develop in the «halo» after atmospheric degradation.

The other striking feature of halo events is the existence of many-centre halos and their alignment along a straight line. Parton-parton scattering naturally leads to the alignment of the final state nucleon fragments with two or more parton jets. However, the observed alignment is reported to be significantly greater than that expected from QCD. Fraction of aligned events in superfamilies was claimed to be between 26-43% depending on the type of the chamber (higher for deep Pb chambers) [70]. It has been revealed not only in the Pamir experiment but also in

the Tien-Shan large ionization calorimeter and in the emulsion chamber exposed at the Concorde board in the stratosphere. According to recent calculations [70], the explanation of the abnormal fraction of aligned events needs some mechanism of coplanar production of hadrons as well as *the existence of highly penetrating particles*. Penetrating component could prevent a destruction of the coplanarity during the development of the nuclear cascade in the thick atmospheric target above the emulsion chamber. It has been checked in simulations that assumed mechanism of the coplanar emission is lost in the «normal» process of the nuclear-electromagnetic atmospheric shower development.

There are many other examples of strongly penetrating clusters or halos not listed here. Unfortunately, serious experimental difficulties in measurements and analysis of halo/cluster events occur frequently. They do not allow for reliable identification of electromagnetic and hadronic parts and estimation of the fraction of hadronic component.

1.5. Anomalous Transition Curves. Anomalous cascade transition curves have been firstly noticed during the study of Chiron-type families (see Subsec. 1.3). Later, they have been encountered also in other events [26, 59] (see Subsecs. 1.1, 1.4). Typical examples of long-range cascades (clusters) registered in Chacaltaya two-storey chambers are shown in Fig. 14.

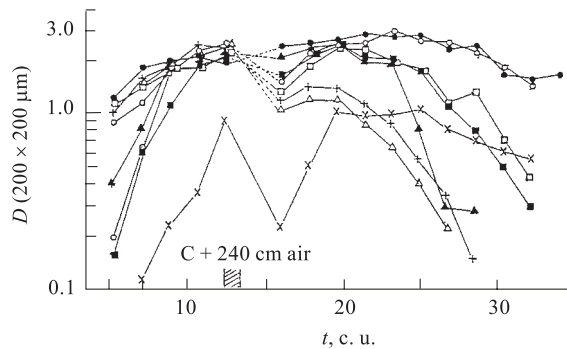


Fig. 14. Examples of anomalous transition curves registered in Chacaltaya two-storey chambers [26]

The common feature for all such showers is that they start their development just after entering the top of the chamber and penetrate through the whole apparatus without significant attenuation. Unfortunately, due to relatively small depth of these chambers and their inhomogenous structure it is impossible to conclude unambiguously about the exotic nature of individual cascades. In many cases the shape of transition curves could be simply explained by consecutive interactions

of the same hadron. Only statistical analysis of groups of showers may indicate that something unusual happens (see Subsec. 1.3). Recently, a penetrating nature of cascade showers observed in the two-storey carbon type chamber was compared with simulated γ -ray-induced and hadron-induced cascade showers. Using QGSJET and modified UA5 model, it was shown [71] that about 34 % of penetrating showers observed in the two-storey chamber No. 19 are neither γ -ray-induced nor hadron-induced showers. A possible explanation is proposed in connection with «miniclusters».

Many-maxima structure of cascades has been also observed in carbon chambers of the Pamir experiment. Although thick multiblock carbon chambers constitute only a small fraction of all exposed apparatus, some interesting events have been also detected there [43, 72]. The example is the family N830 [72] detected in the Pamir 76/77 chamber, consisting of a standard gamma block and four identical sections of hadron blocks (each consisting of 25 cm of rubber and 5 cm of lead with X-ray films as sensitive layers). Among hadron cascades there were observed three high energy ones revealing a multihump structure and traversing tens cascade units through the chamber material.

Homogenous type thick lead chambers are the most appropriate apparatus for the study of penetrability and for looking at anomalies in cascade development. The spectacular examples are exotic cascades detected in the Centauro-like event C-K (see Subsec. 1.1). Unfortunately, up to now, rather small area of these chambers has been exposed and analyzed. Most of experimental material comes from several thick lead chambers installed at the Pamir in the years 1988–1991 by the MSU (Moscow State University) group. Some extremely interesting events have been found there and reported in [26, 60]. The examples are shown in Fig. 15. The presented cascades exhibit surprising features, such as many maxima structure and very slow attenuation. Some of them penetrate through the whole apparatus without noticeable attenuation, sometimes even indicating a growing tendency.

Simulation calculations of transition curves in homogenous thick lead chambers have been performed [13, 73, 74] with the purpose to compare the transition behaviour of ordinary hadrons with the experimental one. Some artificial cascades revealed wave-shaped transition curves, showing the successive maxima separated by the depth corresponding to about one collision mean free path or so (~ 15 cm) in lead. It is, however, much longer distance than experimentally observed one. Generally, the simulated pictures are at the first glance qualitatively different from the experimentally observed curves. More recent simulations, assuming four models of hadron–nucleus interactions (VENUS 4.12, QGSJET, HDPM, and modified UA5, all widely accepted as standard models) confirmed the unusual character of long-penetrating cascades [13, 74]. In particular, the widths of experimentally observed cascades and the distribution of the ratio of energy released in the first peak to the total energy of the cascade disagree with those obtained in simula-

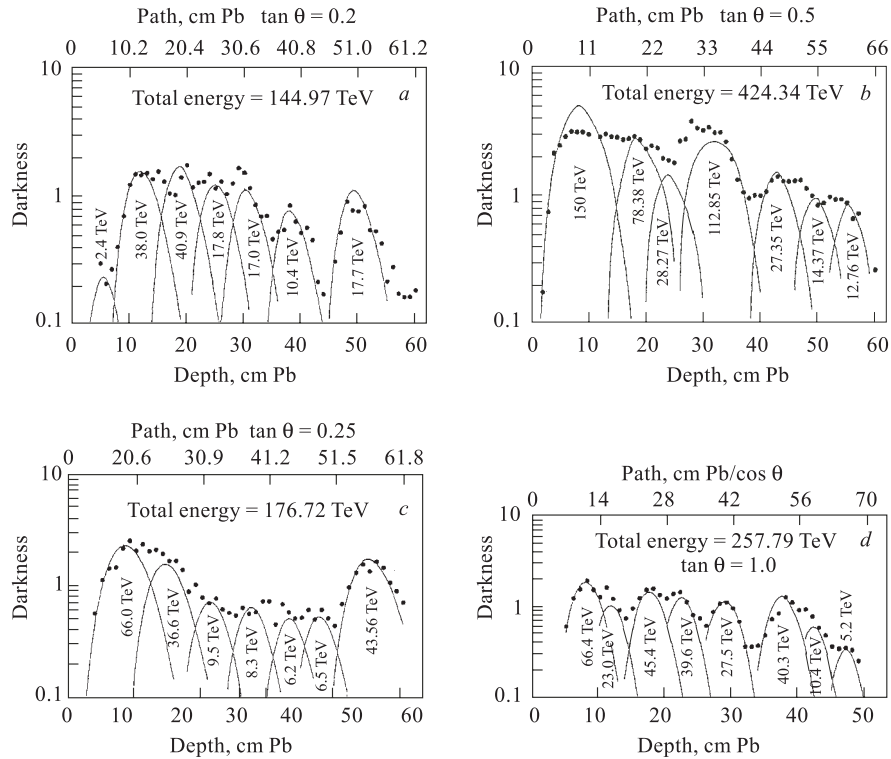


Fig. 15. Examples of anomalous transition curves registered in thick lead chambers [26]: a) Pb73-B15-F12-2; b) Pb69-B8-S152; c) Pb73-B9-F1-H; d) Pb73-B8-S127-100

tions. As an example, the distribution of the widths of 133 cascades detected in the Pamir thick lead chamber in comparison with the simulated one, assuming the QGSJET model, is shown in Fig. 16. It is easily seen that both proton and pion induced simulated cascades are much narrower than the experimental ones.

Investigation of the mechanism of transferring the energy into γ rays, during the passage of the hadron through the chamber, indicates that in simulated events most of energy is released in the first interaction. It again apparently disagrees with experimental observations. Authors of [13, 73, 74] conclude that extensive simulation studies support the existence of exotic long-penetrating cascades. They suggest, as a possible explanation, the extremely collimated hadron bundles, saying, however, nothing about their origin.

It is plausible that the observed strongly penetrating cascades are the same phenomenon as the so-called long-flying component. This effect was firstly no-

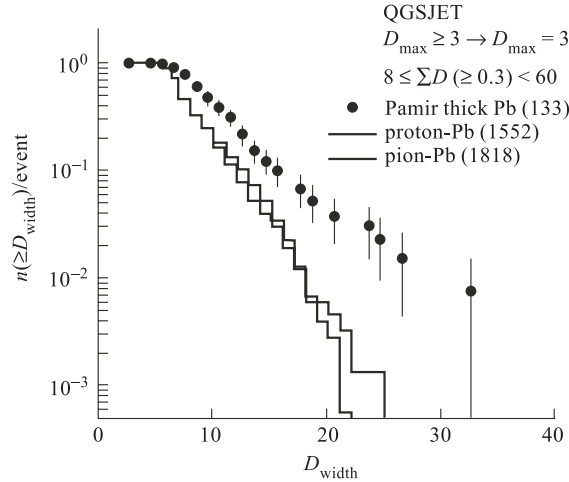


Fig. 16. Distribution of widths of simulated and observed cascades [13]

ticed [18,46] in the Tien-Shan lead calorimeter. It was observed that the attenuation length (extension) of the cascade is almost constant up to calorimeter cascade energies of ~ 10 TeV, increasing twice in the energy interval 10–300 TeV. This observation means a nontrivial hadron energy deposit at larger depths in the lead calorimeter. The effect has been later confirmed by the investigation of attenuation of hadrons in deep lead Pamir chambers [75]. At depths corresponding to 3–6 hadron attenuation paths an excess of cascades, which cannot be explained in the framework of a present knowledge about development of hadron-induced cascades in lead, have been observed. An abundance of cascades detected at large depths (~ 78 –192 c. u.) constitutes $\sim 33\%$ of the total intensity. Distributions of cascade origin points cannot be described as $dN/dt \sim \exp(-t/\lambda)$ with the same slope for all depths: $\lambda_{\text{meas}} = 212 \pm 19$ g/cm² at depths 22–78 c. u., and $\lambda_{\text{meas}} = 310 \pm 36$ g/cm² at depths 78–192 c. u. [75]. There were considered two explanations of the observed phenomenon:

1. *Hypothesis of copious production of leading unstable particles, having relatively long lifetimes.* Generally the phenomenon could be explained by adding to the normal hadron component some particles decaying inside the chamber, at depths somewhere between several tens centimeters and two meters, with energies $E \geq 20$ TeV. They should carry their energy deeply into lead absorber, practically without spending it in nuclear interactions. Particles with heavy quarks (c, b, t) satisfy these criteria. Among them charmed particles were considered the best candidates: their masses are around 2 GeV/c², lifetimes $\sim 10^{-12}$ – 10^{-13} s,

and the inelasticity coefficient in interactions of charmed particles with nuclei is small. However, for obtaining a satisfactory description of experimental data very large charm cross section production must be assumed. This, so-called, «leading charm» hypothesis needs ~ 10 times larger cross section for charm hadroproduction, than resulting from extrapolation of accelerator data, and additionally a small inelasticity coefficient.

2. *Hypothesis of some heavy ($m > 10 \text{ GeV}/c^2$) and long-lived ($\tau_0 \sim 10^{-8}-10^{-6}$) s particles, weakly absorbed in the atmosphere.* Such particles, if consisting of heavy and light quarks, should interact with a cross section approximately similar to that for ordinary hadrons but with a very small inelasticity coefficient.

2. CENTAURO SPECIES STATISTICS

2.1. Mts. Chacaltaya and Pamir Experiments. The basic question is what is the intensity of Centauro species. The well-known numbers, cited in many papers (see, for example, [76]), are intensities measured by Pamir–Chacaltaya Collaboration and claimed to be of the order of $\sim 10^{-2}-10^{-3} \text{ m}^{-2} \cdot \text{y}^{-1}$ for Centauros and $\sim 10^{-1} \text{ m}^{-2} \cdot \text{y}^{-1}$ for Chirons, at the Chacaltaya altitude.

However, it should be mentioned that before giving the statistics of Centauro-type events, the precise definition of such objects should be formulated. If we use very sharp criteria defining such events their numbers will be not very large. Up to now there are reported only two superclean Centauro events, without observed presence of any γ 's, found in the two-storey Chacaltaya chambers, of the total exposure $ST = 3.49 \cdot 10^2 \text{ m}^2 \cdot \text{y}$ (for the sensitive solid angle of the emulsion chamber $\Omega = 0.7$). A question of appearance of superclean Centauros has been considered in [14]. The intensity of cosmic-ray events at energies corresponding to the observed Centauro events was calculated from the formula:

$$I(> \Sigma E_{\text{vis}}) = 0.9(\Sigma E_{\text{vis}}/100 \text{ TeV})^{-1.25 \pm 0.10}/(\text{m}^2 \cdot \text{y} \cdot \text{sr}). \quad (1)$$

Comparing the calculated expected number of cosmic ray events (with $\Sigma E_{\text{vis}} = 100 \sim 3000 \text{ TeV}$) [59] with the total number of observed clean Centauros (i. e., Centauro I and New Centauro) the probability of appearance of such superpure species has been estimated to be $> 10^{-3}$ [14]. Simulations (based on 13714 events) gave probabilities $1.0 \cdot 10^{-5}$ and $2.0 \cdot 10^{-6}$ for Centauro I and New Centauro respectively. The difference between the experimental and simulated probability of observation of such events indicates that Centauro events cannot be produced by a fluctuation in the multiple particle production and/or in collision mean free path. Figure 17 is the diagram of the N_h vs. Q_h for the Chacaltaya families (with $\Sigma E_{\text{vis}} \geq 100 \text{ TeV}$) with the marked contours giving the normalized densities of simulated events.

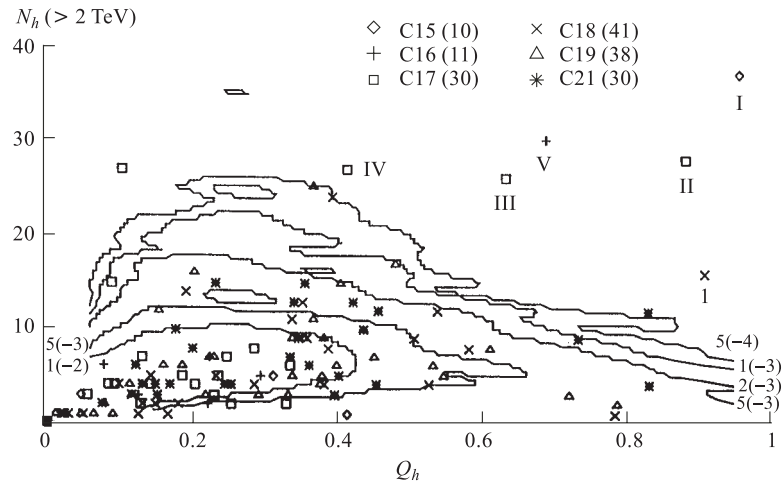


Fig. 17. N_h - Q_h diagram of families and Centauros observed at Mt. Chacaltaya. Contours give the normalized density of the simulated events [14]

Similar events, i. e., characterized by the appearance of a family of showers at the certain apparatus layer, deeply inside the chamber, without accompanied showers in the upper part of the apparatus, have been observed [77] also in the deep lead chamber «Pamir 74/75». Unfortunately, in this case it was impossible to exclude the trivial explanation that the observed phenomenon is simply a «usual» family, reaching the chamber during the time of its assembly.

The sharp definition of Centauro phenomenon can be a little released to include the events in which the observed electromagnetic component is very small. In this case the following numbers as the lower limits of their frequency can be quoted: 7 Centauros, 21 Chirons, and 15 Mini-Centauros found in 305 families with $\Sigma E_\gamma \geq 100$ TeV (from Chacaltaya and Pamir joint chambers) [35].

Further extension of the definition to the objects with anomalously high fraction of hadronic component causes that $\sim 20\%$ of all families with the total visible energy $E_{\text{vis}} \geq 100$ TeV should be recognized as Centauro-species. This question has been studied carefully in [26,59] and it is illustrated in Fig. 18. The analysis was based on the unbiased sample of 429 families from Chacaltaya (open circles), 173 from the Pamir-Joint chambers and 135 from a part of the Pamir chambers of $500 \text{ m}^2 \cdot \text{y}$ (closed circles) with total visible energy greater than 100 TeV. There is shown a scatter diagram of N_h vs. Q_h , where N_h denotes the number of hadrons in a family with visible energy greater than 4 TeV. Figure 18, *b* shows 523 simulated families with the total visible energies greater than 100 TeV.

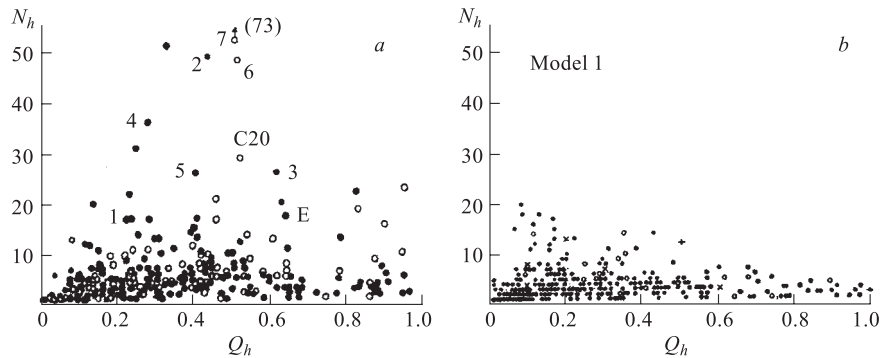


Fig. 18. *a*) N_h - Q_h diagram of families detected in Pamir, Chacaltaya, and Pamir-Joint chambers. *b*) The same for the simulated families. Different marks signify the different primary cosmic-ray nuclei: \bullet — proton; \circ — α ; \diamond — CNO; \times — heavy; $+$ — Fe [59]

In simulations, the structure of the chambers was taken into account and normal chemical composition of primary cosmic-rays has been assumed. Different marks on the plot refer to families due to different primary cosmic-ray nuclei. The basic mechanism of particle interaction was the production of hadronic clusters and their decay with parameters chosen to reproduce the CERN UA-5 experiment results. One sees that in the experimental data there exist abundant families with anomalously rich hadron content, sometimes in both the number and the energy fraction. They are beyond expected fluctuations in the distribution from UA-5 type hadronic interactions. None of the simulated families is found to have $Q_h \geq 0.75$ and $N_h \geq 5$, though the experiment shows the existence of families of much richer hadron composition. Among the families there are events with a very large number of hadrons, expressed by a circle and a number in Fig. 18, *a*. All those are superfamilies with $\Sigma E_{\text{vis}} \geq 1000$ TeV. Among them the family marked as 7 is called Centauro VII, the family marked by C20 is called Centauro VI, both found in the Chacaltaya chambers. Family «Elena» found in the Pamir thick-lead chamber is marked by E. Other events marked 1–6 are superfamilies: P3'-C1-90, P3-C5-505, P2-C96-125, P3-C2-201, P3'-C4-369, found in Pamir-joint chambers, and M. A. III coming from Chacaltaya chamber. Some of them are connected with a strongly penetrative huge halo, what suggests its strong hadronic nature. However, because of the technical problems with measurements of the halo, presented results include only the analysis of the off-halo part. The characteristics of both the off-halo part and estimations of the halo region are published in [37, 59]. The off-halo part of superfamilies shows tendency of hadron-dominant nature in either N_h and Q_h or both, even though

these superfamilies are estimated to have been produced at high altitude. From the study of the off-halo part the large value of p_T can be also concluded.

It is important to note that there are no significant differences among three experiments. Figures 18, *a, b* tell us that such anomalously rich hadron content is neither caused by the incidence of heavy nuclei in the primary cosmic rays, nor by the superposed fluctuations of ordinary-type hadronic interactions. The anomalously hadron-rich families constitute a substantial part of the unbiased observed samples, at least $\sim 20\%$. The effect of the anomalous hadron dominance in families is much enhanced if the analysis is restricted to the events generated at the distances not far from the top of the chamber. It was shown in [59], where the events with rather small lateral spread, i. e., with $\langle E^* R^* \rangle \leq 300 \text{ GeV} \cdot \text{m}$, after applying the «decascading» procedure for γ rays, have been selected.

These conclusions have been supported by the more recent, extensive simulation studies [13] based on four different models of hadron-nucleus interactions (VENUS, QGSJET, HDPM, and modified UA-5) and by using the CORSIKA code for simulation of nuclear-electromagnetic cascade development in the atmosphere. The enhancement of hadron-rich families cannot be explained by widely accepted models of «normal» interactions. The question of abnormal dominance of hadron component has been studied separately also for ultra high energy events. In [37], there has been presented the systematic analysis of 75 families with $\Sigma E_{\text{vis}} \geq 500 \text{ TeV}$ detected in Chacaltaya two-storey chambers ($300 \text{ m}^2 \cdot \text{y}$), Pamir-joint chambers ($\sim 530 \text{ m}^2 \cdot \text{y}$), and in the part of the Pamir exposition ($\sim 500 \text{ m}^2 \cdot \text{y}$). Among presented families, four Centauro-type, two Chiron-type, and ~ 10 other hadron-rich events could be noticed. The families coming from homogenous type lead chambers (110, 60, and 40 cm of Pb thick from a total exposure $\sim 450 \text{ m}^2 \cdot \text{y}$) have been also separately analyzed. The list and characteristics of 17 superfamilies with $\Sigma E_{\text{vis}} \geq 700 \text{ TeV}$ and 40 families with $100 \leq \Sigma E_{\text{vis}} \leq 500 \text{ TeV}$ are shown in [60]. Among them at least three events with $Q_h \geq 0.5$ are present.

2.2. Mts. Kanbala and Fuji Experiments. The Centauro-like event named «Titan» has been reported in 1977 by Mt. Fuji experiment [29, 78]. The authors emphasized its large p_T and hadron-rich character. It was suggested that all secondaries are hadrons. A systematic search for Centauro events has been done later [79] in the thick-type lead chambers* by the China–Japan Collaboration. The total exposure was $\sim 130 \text{ m}^2 \cdot \text{y}$ at Mt. Kanbala (5500 m a. s. l.) and $\sim 380 \text{ m}^2 \cdot \text{y}$ at Mt. Fuji (3750 m a. s. l.). Among 30 hadron families (with the total visible energy greater than 100 TeV) coming from thick lead chambers

*Mts. Kanbala and Fuji groups mostly used Pb and Fe chambers with the total thickness of 10–70 c. u. The flat type chambers which constitute the most part of the exposed apparatus are not suitable for the Centauro problem study.

exposed at Mt. Fuji and 100 families coming from Mt. Kanbala chambers, no candidates of Centauro events have been found. The upper limit of the fraction of such events was estimated to be 3% (95% C.L.) in the hadron families with energy greater than 100 TeV. The puzzle of the nonobservation of Centauro events by these experiments still remains a mystery. Several reasons, such as differences in experimental conditions, in emulsion chamber designs, and data analysis procedure used by different collaborations can be suspected. In particular, the following reasons should be mentioned:

1. *Some differences in hadron identification procedure.* Mt. Kanbala and Mt. Fuji groups classified hadrons and γ rays only statistically by referring to the starting depth of showers. In the Chacaltaya and Pamir experiments additional criteria have been used, based on differences in development (lateral and longitudinal) of hadronic and electromagnetic cascades. Not only showers observed in the lower chambers were regarded as hadrons. Showers from upper chambers have been studied under the microscope and some of them consisting of well-resolved cores or revealing many-maxima structure in the longitudinal development were also identified as hadrons.

2. *Difference in exposure altitude.* Mt. Fuji laboratory, giving the main part of the experimental data to the Centauro problem study, is located at the much lower altitude than Mt. Chacaltaya or Pamir. If Centauro species were born in nucleus-nucleus collisions or if they are the «strongly penetrating objects» produced at the top of the atmosphere or somewhere in the extra-galactic region, then the decrease of their flux with the atmospheric depth is quite plausible.

2.3. JACEE Experiment. The Japanese-American Cooperative Emulsion Chamber Experiment, JACEE, has flown emulsion chambers with balloons near the top of the atmosphere. Despite of a small area and short time of exposure, as compared to Chacaltaya/Pamir experiment, a few events with anomalous $N_\gamma/N_{\text{charged}}$ ratio have been observed by JACEE Collaboration. However, these events differ in some essential points from classical Centauros. The anomalies were noticed at incident energies lower than that estimated for «classical» Centauros and unusual $N_\gamma/N_{\text{charged}}$ ratios were observed only in the limited $(\eta - \phi)$ phase space region. Besides that, an excess of photons (anti-Centauro), in contrary to the hadron excess observed in Centauros, was claimed. The examples are:

1. The 4L-II-27 event [80] of incident energy of 80 TeV has been found among 41 studied events with $E_0 \geq 40$ TeV. 149 charged particles and 120 γ 's have been here observed. Almost all γ quanta were emitted in a limited region of the very forward direction. The $N_\gamma/N_{\text{charged}}$ ratio has been measured to be 2.6 ± 1.1 in the region of pseudorapidity $5.5 \leq \eta \leq 7.5$. It is a significant deviation from the expected ratio of ~ 1 .

2. The event with $\Sigma E_\gamma = 15.4$ TeV, described in [81,82], is one out of a sample of about 70. It was initiated by a singly charged primary. The collision

occurred within the detector. Almost all leading particles were γ quanta. Photons appear to form two clusters. The leading cluster consisted of about 32 γ 's with $\langle p_T \rangle \simeq 200$ MeV/c and only one accompanying charged particle, the second one had three times as many photons as charged hadrons (about 54 photons versus 17 charged).

3. The event presented in [83] is a peripheral collision of Fe nucleus ($E \simeq 9$ TeV/nucleon) in emulsion. 27 γ quanta with $\eta \leq 6$ were observed. As they came from pair conversions at only 0.8 radiation lengths, the authors expect that the total number of photons should be about 50. At the same time, only 6 charged particles (out of 21 charged tracks detected in the whole angular region) fell in the same kinematical range.

In all these events there was observed a tendency to a group emission of π^0 mesons. Such π^0 groups, having similar directions and momenta, could be signs of a formation and a subsequent decay of the chiral condensates. It should be mentioned, however, that these events were found in emulsion by scanning for the leading photon showers, so there was a «trigger bias» in favour of a large neutral fraction. It would be interesting to hear something about anti-Centauros from the mountain-top emulsion chambers. Here, there is, however, even much more stronger «trigger bias» in favour of gamma families, and thus the interpretation of data, from this point of view, is a complicated exercise. It is rather difficult to identify anti-Centauros unambiguously with exception of unusual and rare events in which the interaction vertex is close to the top and clearly resolved in the chamber.

Table 9. Centauro statistics

Laboratory	Altitude, m (g/cm ²)	Chamber	Exposure, m ² ·y	No. of families $E_{vis} \geq 100$ TeV	No. of Centauros	Ref.
Mt. Chacaltaya (Brasil–Japan)	5200 (540)	Two-storey carbon	300	121	~ 8*	[37,59]
Pamir (USSR–Poland)	4300 (600) or 4900	Carbon type	500	135	~ 3*	[37,59]
Pamir (Russia–Japan)	4300	Carbon type or thick Pb	530	173	~ 2*	[37,59]
Mts. Kanbala (China–Japan)	5500 (520)	Thick-Pb	130	30	—	[79]
Mt. Fuji (Fuji Collab.)	3750 (650)	Thick-Pb	380	100	—	[79]

* ~ 20% hadron rich families in the sample.

2.4. Summary of the Centauro Species Statistics. Summarizing results of cosmic ray emulsion chamber experiments, it can be stated that Centauro-type anomalies have been observed by several different experiments and collaborations, working under different experimental conditions and using various types of chambers. Examples of detected unusual events were given in the previous sections. However, the systematic search for Centauros, by using the same criteria, has been made only for the part of the exposure from the three experiments: Chacaltaya Collaboration, Pamir Collaboration and Pamir-Joint Chambers. China–Japan (Mt. Kanbala) and Mt. Fuji Collaborations, in their systematic Centauro search, used different types of chambers and different criteria of data analysis. Table 9 shows the statistics of «unambiguous» Centauros found only in that part of experimental material where systematic and uniform searches were done.

It should be emphasized, however, that extension of the «Centauro» definition to all hadron-rich species causes that about 20% of events among the families with the total visible energy $\Sigma E_{\text{vis}} \geq 100$ TeV can be regarded as Centauro-like anomalies.

3. CENTAURO EXPLANATIONS

The possibility that fluctuated air showers mimic Centauro-type events seem to be the most natural suspicion. This question has been studied by many authors (see, for example, [84, 85]). Recently, very careful analysis of this problem, by using the most modern simulation tools, as CORSIKA code (and four different models of hadron-nucleus interactions: VENUS, HDPM, QGSJET, and modified UA5), has been done by M. Tamada [13]. All considered models fail in describing Centauro species. In particular none of models was able to explain the experimentally observed fluxes of hadron-rich events. They fail also in describing many characteristics of events, such as anomalous hadron-gamma correlations (e. g., N_h vs. Q_h), minicluster, and giant-minicluster structures, etc.

Especially, no one has succeeded in reproducing the Centauro I event. The possibility that a heavy nucleus interacting in the lower part of the atmosphere could give rise to Centauro I-type event was considered for example by Acharaya and Rao [85]. They have shown that, in principle, it would be possible to reproduce the event, though the total number of such events expected in the global data sample is $\sim 2 \cdot 10^{-5}$ what is in apparent discrepancy with the observed flux of Centauros. Similarly, in [14] (see also the previous section) the probability of finding a «clean» Centauro event, like Centauro I or New Centauro, among simulated events was found to be several orders of magnitude smaller than the experimental one.

The suspicion that Centauro-like phenomena would arise from nucleus–nucleus collisions was examined in many works. Keeping in mind that there

is a negligible probability that nucleus would penetrate so deeply into the atmosphere B. Mc Cusker [86] suggested that a small fraction of iron nuclei from a primary cosmic rays would survive passage through several hundred $\text{g} \cdot \text{cm}^{-2}$ of the atmosphere and produce Centauro events. But P. B. Price et al. [87] showed (taking into account various chains of fragmentation) that the flux of surviving heavy nuclei is too low by a factor of $\sim 10^{-10}$ to account for Centauros.

So, it is widely believed that Centauro related phenomena could not be due to any kind of statistical fluctuation in the hadronic content of normal events.

Therefore, new type of interaction or the creation of a new kind of matter is conjectured to be responsible for these extremely unusual phenomena. In the last years many interesting models have been proposed by different authors. It would be difficult to describe or even list all of them. Some of them are amenable to experimental verification in accelerator conditions, the other ones seem to be unamenable. Some of them (e. g., [88]) assume that the exotic objects of unknown origin are present in the primary cosmic ray spectrum and they are seen as Centauros during their penetration through the atmosphere. The other ones assume that the exotic events are produced in extremely high-energy hadron-hadron (e. g., [89]) or nucleus-nucleus (e. g., [23, 24]) interactions. Many of them incorporate the strong penetrability as the main feature of the phenomena. For instance, the problem of very small flux of heavy nuclei at the mountain level was avoided in [24], by conjecturing that the initial collision of the heavy cosmic-ray nucleus does occur very high in the atmosphere. The fireball created in the central collision of a heavy nucleus with air nucleus is a very dense object which penetrates several hundred $\text{g} \cdot \text{cm}^{-2}$ of the air before exploding into fragments.

The widespread opinion that *the likely mechanism for Centauro production is the formation of a quark-gluon plasma* was incorporated in a lot of proposed models. Other exotic attempts, as for example the color-sextet quark model [90], based on Pomeron physics in QCD, were also developed. It needs adding to the Standard Model an additional flavour doublet of color sextet quarks.

All proposed explanations are based on two different believes. In the first case it is assumed that mostly baryons are the products of Centauro-type events. Such picture is incorporated for example in diffractive-type fireball models (see Subsec. 3.2 and [38, 89, 91]) and in scenarios with strange quark matter (see Subsec. 3.3 and [23–25, 76, 88, 92]). In the second case, particles produced by the Centauro mechanism are suppose to be mainly mesons and there are numerous attempts to explain Centauros as different types of isospin fluctuations [93–102]. According to [94, 96] large isospin fluctuations could be due to the Bose nature of the emitted pions, and a laser-like (so-called PASER) mechanism is considered to be responsible for Centauro formation. The other theoretical speculations predict large isospin fluctuations arising from formation

of localized regions of misalignment vacuum which become coherent sources of a classical pion field. In particular, formation of disoriented chiral condensate (DCC) [81, 97, 98, 100, 101] is suggested to be a possible explanation of Centauro-like phenomena (see Subsec. 3.3). It seems, however, that all these attempts have at least one common difficulty. It has been shown in [103] that families produced at mountain altitudes are insensitive to any isospin fluctuations.

In this section some of the models will be shortly described. The most attention will be given to the strange quark matter fireball [23, 24] model which, in our opinion, gives the best chance for simultaneous explanation of different Centauro-related phenomena. It has been used also as the basis for the designing and simulation calculations done for the CASTOR experiment at the LHC.

3.1. Exotic Extraterrestrial Glob of Matter. In [88] it was postulated by Bjorken and Mc Lerran that Centauro could be a metastable glob of highly compressed quark matter present in the primary cosmic ray spectrum. These globs could have radii of several fermi and contain several hundred quarks. Since the mean transverse momenta of the Centauro-decay products are several times larger than the normal value typical of a nucleus it can be expected that the glob would have radii $\sim 3-5$ times smaller than that of an ordinary nucleus and a very high density, $\sim 30-100$ times that of ordinary nuclear matter. If the binding energies of the constituents in the dense nuclear matter are of the same order as the transverse momenta, then the glob should be characterized by both the binding energy much higher than that of conventional nuclear matter and by the reduced geometrical cross section, allowing it to penetrate deeply into the atmosphere. To develop this idea authors of Ref. 88 used the crude liquid-drop model. They formulated the stability condition and described the evolution of the glob during its penetration through the atmosphere.

The energy of the glob is generally a function of its baryonic number N and it was taken to be the sum of the three terms:

- *The volume term*, αN , where α is an extensive parameter, arising from repulsive quark interactions and being for the bag model with no interaction ~ 900 MeV;
- *The surface term*, $\beta N^{2/3}$, which reduces the strength of the repulsive quark interactions owing to the presence of a surface. It destabilizes globs of arbitrary large N and induces a condensation down to globs of finite baryon number;
- $\Delta(N)$ *term*, which summarizes all the finite-size corrections to $E(N)$, not already included in the previous terms

$$E(N) = \alpha N - \beta N^{2/3} + \Delta(N). \quad (2)$$

If $E(N) > Nm_p$, the globs are not absolutely stable with respect to decay into nuclear matter. Thus the stability condition with respect to single-nucleon

emission is:

$$\frac{dE}{dN} < m_p \quad (3)$$

and hence

$$\frac{2}{3}\beta N^{-1/3} - \frac{d\Delta}{dN} > \alpha - m_p. \quad (4)$$

The globs are always unstable for baryon number N greater than some limiting value N_0 . For $N < N_0$ they are stable with respect to nucleon emission unless for some baryon number N_c the term $d\Delta/dN > 2/3\beta N^{-1/3} + m_p - \alpha$. In this case the system would be metastable for $N_c < N$ and $N < N_0$ and would spontaneously decay for $N < N_c$ or $N > N_0$.

Upon entering the atmosphere, the glob collides with air nuclei with the collision length $\sim 30 \text{ g/cm}^2$ (for $R_{\text{glob}} \sim R_{\text{air}}$). Such process heats the glob, and it cools either by radiation of mesons or evaporation of baryons. The boiling of baryons decreases the baryon number, what can remove the glob from the metastability region into a stable or unstable region. In the former case the glob will explode and in the latter one it will collide with air nuclei until it is evaporated. Thus in some cases the glob could be characterized by *a large degree of penetration and short interaction length*, leading to a considerable deposition of energy in the atmosphere. To estimate both the energy transferred to the glob per collision and the evaporation, authors used a simple model of a glob consisting of an ideal degenerate Fermi gas of quarks. Taking the quark-proton cross-section to be $\sigma_{\text{qp}} \sim 12 \text{ mb}$, $k_F \sim 1 \text{ GeV}$ and assuming the collision of the glob of the baryon number $N \sim 100$ with the air nucleus ($N_{\text{air}} \sim 14$), they obtained [88] that the fractional energy loss of a glob $\Delta E/E$ is $\sim 3\%$. For the gamma factor $\sim 10^3\text{--}10^4$, the glob loses somewhere between $10^3\text{--}10^5 \text{ GeV/collision}$ and (omitting the possibility of explosion and assuming a collision length $\sim 30 \text{ g/cm}^2$ as appropriate for $R_{\text{glob}} \simeq R_{\text{air}}$) it could easily penetrate a distance $X \sim 6000\text{--}8000 \text{ g/cm}^2$ in the atmosphere and reach the sea level.

In Ref. 88 were also discussed two other variants: the glob containing an unconfined massive quark or being a fractionally charged hadron with large baryon number. In the former case, the glob would have the quantum numbers of a quark. As the quark in such a model is expected to be a complex object of a relatively large mass and size, its long-range color field should attract nucleons via an induced color dipole moment and help to compress the quark matter to the required high density. Below a certain baryon number, the binding energy per nucleon will monotonically increase, causing that the «stripped glob» consisting of an unconfined quark and a few tightly bound nucleons would penetrate to sea level. There are, in fact, rather serious experimental constraints on this hypothesis as it leads as well to unacceptable flux of quarks at sea level as to an unacceptable rate of horizontal air showers (with zenith angle $> 70^\circ$).

The picture proposed in [88] has the following difficulties:

- problem of the glob origin;
- unacceptably large rates of fractionally charged quarks and/or horizontal air showers at sea level;
- adequate explanation of the absence of pions.

3.2. Diffractive Fireballs. Numerous phenomenological models (e. g., [23, 89]) assume that a fireball plays a role of an intermediate state for Centauro production. They were inspired by some experimental characteristics of exotic events which can be satisfactorily explained by means of the fireball scenario. All of them postulate the production of «exotic» clusters, the differences concern the type of a projectile and the mechanism of evolution and decay of the fireball.

An example is the scenario [38, 89] in which Centauros and Mini-Centauros are proposed to be a result of isotropic decay of «exotic» fireballs coherently produced in a diffractive dissociation process. In this phenomenological model a nucleon–nucleon collision at $\sqrt{s} \sim 1.8$ TeV can create a diffractive superheated fireball with a mass ~ 180 GeV in the forward region centered around pseudorapidity $|\eta_{\text{cms}}| = 2.2$ and with a spread $\Delta\eta = \pm 0.7$. The high p_T reflects the temperature of the phase transition. Within this model, the unusual hadron-electromagnetic asymmetry is assumed to be caused by a phase transition, similar to the DCC hypothesis, due to the superheated fireball conditions (with, however, the identification of the hadrons as nucleons). In principle, there is no explanation why pion emission should be suppressed in the quark-gluon plasma. The cross-section for a diffractive event with this mass was predicted to be ~ 0.33 mb. Full Monte Carlo simulation of Centauro-like events was carried out using this model [38, 91]. The code consists of two parts: *Code Nucleus* + *Exotic Algorithm*. *The Code Nucleus* describes the nucleus–nucleus collisions, using the superposition model. The nucleon–nucleon collision was described by the UA5 algorithm, based on codes for nondiffractive and single diffractive interactions. *The Exotic Algorithm* was a code that included the exotic channel, i. e., a diffractive production of a baryonic fireball and its isotropic decay into baryons. The total inelastic cross section was assumed to be:

$$\sigma_{\text{in}} = \sigma_{\text{norm}} + \sigma_{\text{exot}} \quad (5)$$

with $\sigma_{\text{norm}} = \sigma_{ND} + \sigma_{DD} + \sigma_{SD} \simeq \sigma_{ND} + \sigma_{SD}$, where σ_{ND} , σ_{SD} , σ_{DD} and σ_{exot} are the cross sections for nondiffractive, single diffractive, double diffractive and exotic processes respectively.

The branching ratio of «exotic diffractive channel» (Centauro and Mini-Centauro) was chosen to increase with incident baryon energy as

$$P_{\text{exot}} = 0.333 \log(E_N/100 \text{ TeV}). \quad (6)$$

This model successfully reproduces the kinematics of cosmic ray exotic events. Moreover, it also permits to reproduce the experimental data for electromagnetic

family flux. In opposite to «normal» diffractive events where the majority of secondary particles are pions, in exotic diffractive events the secondary charged particles were assumed to be only nucleons and antinucleons. Multiplicity of nucleons was generated using a Poisson distribution with $\langle N \rangle = 100$ for Centauro and $\langle N \rangle = 15$ for Mini-Centauro. The inclusion of exotic process in nuclear interaction of cosmic ray particles with atmospheric nuclei, reduces the expected electromagnetic family flux, because the production of π^0 's in Centauro-like events is suppressed by some unknown mechanism. It has been shown that in the extremely high energy region ($E_0 \geq 10^5$ TeV) a dominant exotic channel is consistent with experimental data from emulsion chamber experiment. The model allows one to understand the negative search for Centauro events at $Spp\bar{p}S$ CERN collider. It introduces the energy threshold for Centauro production connected with the point of the phase transition ($\sqrt{s}_{\text{th}} \sim 2000 \pm 500$ GeV), which is much higher than energy of $Spp\bar{p}S$ experiments ($\sqrt{s} = 540\text{--}900$ GeV) and comparable to that of the Fermilab collider ($\sqrt{s} = 1.8$ TeV). The negative results for Centauro search in some Tevatron experiments operating in the central rapidity region (e. g., CDF experiment) were also expected from this model [91], as the Centauros are assumed to be produced close to diffractive dissociation region.

3.3. DCC. 3.3.1. Centauros as DCC Manifestation. The QCD phase transition from normal hadronic matter to the Quark-Gluon-Plasma manifests itself in two forms: deconfinement transition and chiral symmetry restoration. One of the interesting consequences of the chiral transition is the formation of a chiral condensate in an extended domain, such that the direction of the condensate is misaligned from the true vacuum direction. The formation of these so-called Disoriented Chiral Condensate (DCC) domains in high energy collisions of both hadrons and heavy ions, has been proposed by many authors [81,97,98,100,101], however, this subject is still a quite speculative one. There is no compelling argument that DCC must exist, but there is no compelling argument that it does not exist.

The important question is: what are the basic signatures of DCC? The main features of that disoriented piece of quark matter result directly from its definition. In both descriptions, the linear and nonlinear sigma models, DCC can be defined as a cluster of pions, coherently produced, with anomalously large fluctuations in the neutral fraction. Pions from a DCC domain will be emitted at low p_T and will have a distinct distribution pattern compared to the normal pion production mechanism without DCC. An important feature of this radiation is coherence, which means that the multiplicity distribution of produced particles should be of Poisson-type, and there will be no Bose–Einstein enhancement. A DCC almost by definition will consist of a cluster of pions with almost identical momenta and in its own rest frame will have approximate spherical symmetry. Assuming some transverse boost for DCC and the internal rela-

tive velocities of the pions within a DCC cluster, smaller than the transverse boost velocity, it should look like in the laboratory frame as a colorless mini-jet.

A convenient quantity to characterize a DCC is the fraction of neutral pions per event

$$f = \frac{N_{\pi^0}}{N_{\pi^0} + N_{\pi^+} + N_{\pi^-}}.$$

In a DCC model the probability of finding a given neutral fraction is

$$P(f) \simeq \frac{1}{2\sqrt{f}} \quad (7)$$

in the limit of large number of pions.

In generic particle production, that is, production by mechanisms other than DCC, production of a pion of any given charge is equally likely to isospin symmetry, so that f is binomially distributed with mean $\langle f \rangle = 1/3$. Hence, a basic signature of DCC production is the presence of very large event-by-event fluctuations in the fraction of produced neutral pions. A significant low p_T enhancement should be also observed.

Other DCC signatures include various effects on pion pair correlation. Searching for DCC is connected with the correlation question, although it is not understood completely what correlation structure of the distribution chiral order parameter is likely to be. Z. Huang and X. Wang [102] found (basing on a linear σ model) that a rapidity interval in which the pion field is correlated in isospin direction could be as large as $\sim 2-3$ rapidity units and the cluster structure of pions radiated from the coherent pion field may occur anywhere in the whole rapidity region. According to [81] the natural correlation length for DCC is of the order of 1–2 units of rapidity. However, this is yet an unsolved theoretical issue. One can imagine, for example, a piece of a DCC centered at rapidity of +1, and another one centered at -1 with a different chiral order parameter and having some small overlap at rapidity 0. The question is how do the two pieces interact? Will there be a tendency to create a common alignment, or will they form independent domains? Such question has been asked in [81] with a suggestion that there is even a remote possibility that the nonlinearities of the linear sigma model are strong enough to promote long-range correlations in rapidity. The formation time and corresponding correlation length have been also estimated in [98] by nonlinear sigma model and quenching approximation. The correlation length was estimated as ~ 8 fm in nuclear collisions at 200 GeV/nucleon (taking WA80 data). This large value reflects the coherence of the source. The ratio of «anomalous» correlation length, related to a DCC mechanism, to the «ordinary» correlation length was estimated as ~ 5.6 [98, 104]. It should be mentioned that some

signs of the existence of the long range correlations have been already reported in 1991, in NA35 data (sulphur–sulphur central collisions at 200 GeV/nucleon), where the so-called coarse grain fluctuations have been studied by using different kinds of multiplicity moments [105] and fractal analysis [106]. The results may indicate the appearance of weak, long-range correlations, with the length $\xi \gg 3$ rapidity units and suggest the appearance of a coherent domain connected with fragmentation region.

To answer the basic question, if a DCC scenario could be able to explain all Centauro related phenomena needs, however, very careful studies. Some doubts can be mentioned at once. At first, it seems that using a DCC scenario it would be rather difficult to explain simultaneously both the large transverse momenta observed in the Centauro species and the existence of a strongly penetrating component. The anomalously high $\langle p_T \rangle$ of the particles produced in Centauro-type events seems to be the main problem. Assuming even that the value of the gamma inelasticity factor, k_γ , is closer to 0.4 than 0.2, as it was taken in cosmic-ray papers, the obtained $\langle p_T \rangle \simeq 0.875 \pm 0.375$ GeV. This value seems to be still too high to be connected with a DCC mechanism. On the other hand, one cannot rule out that the narrow and strongly penetrating clusters, observed in Chiron-type events, are produced by a transversally boosted DCC. It cannot be excluded that the coherently emitted groups of DCC pions may have a net transverse drift velocity, forming the «colorless» jet. J. Bjorken [107] speculates that the relative p_T of the pions in the «colorless» jet may be under 100 MeV, what is very close of that measured for cosmic-ray miniclusters observed in Chiron-type events.

The other question concerns the existence of charged DCC, i. e., the events in which the orientation of the vacuum is orthogonal to the π^0 direction. Bjorken [81] considered this idea, as more speculative than ordinary DCC, however, he did not exclude it. He proposed the scenario where, for example, the positive charge DCC is produced at negative η , and the negative charge DCC is produced at positive η , with a «domain wall» in between. He found that the width of the dipole layer could be about 1–2 units of rapidity. Assuming that charged DCC could be formed, both Centauros and anti-Centauros should be observed in the same experiment. As it has been already mentioned, the experimental situation is surprising. Both extremes are claimed to be seen in cosmic ray data but by two various experiments and in different energy range. There were found some anti-Centauro like events by JACEE Collaboration and no Centauros. There are Centauros and no reported anti-Centauro events in Chacaltaya and Pamir experiments. Figure 18 does not show any excess of γ -rich events when the observed families are compared with the simulated ones. It allows one to doubt if Centauro and DCC are the same phenomenon. On the other hand, it should be mentioned that the analysis of γ -hadron families detected at mountain laboratories from the point of view of disoriented chiral condensates done in [104, 108, 109] does not exclude a small contamination of DCC clusters among normally produced par-

ticles (see the next subsection). However, this result is inconsistent with the conclusion contained in [103] where authors demonstrate that artificial families produced at mountain altitudes are insensitive to any isospin fluctuations. Their simulations showed that all scenarios of isospin fluctuations lead to essentially the same characteristics of families registered at mountain altitudes because the cascading process in the atmosphere «kills» the characteristic features of the main interaction. It suggests that Centauros should originate from strongly penetrating projectiles.

3.3.2. DCC Search in γ -Hadron Families. In 1996, a Brasil emulsion group reported [104] an analysis of several tens cosmic ray events of visible energy greater than 100 TeV from Mt. Chacaltaya. They plotted the number of observed hadrons against the energy fraction of hadronic component (N_h vs. Q_h) and compared the experimental diagrams with the simulated ones. Artificial families were constructed for two different models. The first scenario which does not include an anomalous channel was called «ordinary interaction» model. It was based on two separate algorithms for nondiffractive and single diffractive interactions used by the UA5 group for the description of nucleon–nucleon collision. The second model included an anomalous production (DCC) in the diffractive channel, i. e., a coherent emission of pions from a large domain of disoriented chiral condensates in the *leading particle region*.

It was shown that N_h vs. Q_h distribution does not match Monte Carlo simulation based on UA5 data. Experimental distributions were better simulated by a Monte Carlo which included 24 % of DCC production rate in the leading particle region. On the other hand, a significant discrepancy between the experimental family flux and results of simulations should be mentioned. Even the model including the anomalous channel (DCC) fails in description of such global characteristics as the family flux observed at mountain altitudes. The question of unusual transverse momentum observed in hadron-rich families was not investigated by the authors of [104].

More recently, a more advanced analysis using the robust observables has been done [108, 109]. The robust observables $r_{i,j}$ are constructed through the ratios of normalized bivariate factorial moments $F_{i,j}$.

$$r_{i,j} = F_{i,j}/F_{i+j,0}, \quad (8)$$

where

$$F_{i,j} = \frac{\langle N_{\text{ch}}(N_{\text{ch}} - 1) \cdots (N_{\text{ch}} - i + 1) N_{\gamma}(N_{\gamma} - 1) \cdots (N_{\gamma} - j + 1) \rangle}{\langle N_{\text{ch}} \rangle^i \langle N_{\gamma} \rangle^j}. \quad (9)$$

As has been shown in [110], the robust observables are sensitive to DCC admixtures in multiple production. The basic difference between generic production and DCC production is that in the former case the generating function depends

only upon one variable, while for DCC it depends nontrivially upon two. Thus the factorial cumulants are very convenient tools for distinction between the distributions. If a distribution of ratio of neutral to all pions, f , is governed by a binomial distribution, as it is observed in standard pion production, called generic pion production, then

$$F_{i,j} = F_{(i+j),0}. \quad (10)$$

Therefore many ratios of the $F_{i,j}$ are expected to be unity:

$$r_{i,j}(\text{generic}) = \frac{F_{i,j}}{F_{(i+j),0}} = 1, \quad (11)$$

and particularly for $i \geq 1$ and $j = 1$.

$$r_{i,1}(\text{generic}) = 1. \quad (12)$$

If, on the other hand, a distribution of f is of the form $p(f) = 1/(2\sqrt{f})$, as predicted by a DCC mechanism, then in the semiclassical limit

$$r_{i,1}(\text{DCC}) = 1/(i+1). \quad (13)$$

Thus the values of $r_{i,j}$ below 1 could be the indicators of a DCC formation. The results presented in [108] were based on analysis of 59 γ -hadron families, with $\Sigma E_{\text{vis}} > 100$ TeV, detected in thick lead chambers, of $57 \text{ m}^2 \cdot \text{y}$ exposure. The robust observables have been calculated for real and simulated families and compared one to the other. It was concluded that there are peculiar clusters of pions with large asymmetries in the neutral pion fraction distribution, absent in the artificial families.

Similar conclusion has been obtained in [109] where 139 γ -hadron families with energies $100 < \Sigma E_{\text{vis}} < 700$ TeV, from Pamir experimental data, have been analyzed. Here the behaviour of robust observables as a function of the visible energy of a leading jet, obtained after decascading procedure, was studied. The authors of Refs. 108, 109 explain the observed deviation from the simulated characteristics as a copious production of pions from a DCC domain, formed in the far-forward angular region. It should be noted, however, that the production rate of DCC, estimated in [104] as 21–24% for the leading particle region, is not sufficient to explain the global characteristics, such as the energy spectra of families. For the whole inelastic channel this value was estimated to be less than 5%.

The analysis [104, 108, 109] has been done in the whole region of the experimentally accessible phase space. More information could be achieved from the study of robust observables in pseudorapidity and/or azimuthal angle bins of different sizes. Some hints can be taken from the earlier studies of multiplicity

fluctuations in pseudorapidity bins [111]. The analysis has been done for several events, coming from the similar type thick lead chamber of the Pamir experiments. Strong fluctuations have been revealed in the high-energy ($\Sigma E_{\text{vis}} > 100$ TeV) photon and hadron families. Here, the multiplicity fluctuations have been studied, by means of scaled factorial moments, separately for photonic and hadronic component. Such result, however, may also indicate on fluctuations of the ratio of photon to hadron multiplicity in the analyzed bins (DCC domains). Some difficulties in interpretation of experimental data are connected with discrepancies between various simulation studies. Authors of [104, 108] conclude about the existence of nonstatistical fluctuations in the neutral fraction. This conclusion is based on disaccordance of experimental and simulated characteristics, based on the «normal» model production and Monte-Carlo calculations of the cascade processes through the whole atmosphere. On the other hand, authors of [112] claimed that strong fluctuations observed in atmospheric families are primarily determined by fluctuations in the atmospheric cascades themselves, and there is no need for changing the act of elementary production. The problem needs further investigation.

3.4. Strange Quark Matter. Colour single states observed so far consist of three quarks (baryons), three antiquarks (antibaryons) or quark–antiquark pairs (mesons). Such objects are described by the Standard Model which does not forbid the existence of colour single states in a bag containing an integer multiple of three quarks. In such quark matter bags all the quarks are free within the hadron’s boundary, so such states are inherently different from nuclear ones that are composed of a conglomerate of $A = 1$ baryons. Quark matter states composed of only u and d quarks are known to be less stable than normal nuclei of the same baryon number A and charge Z since they do not decay into quark matter. The strange quark matter (SQM) is a matter with strangeness per baryon of the order of unity, thus containing a comparable fraction of up, down, and strange quarks. If it ever exists, may be a stable ground state of a QCD instead of the nuclear matter. The fact that SQM is absolutely stable does not contradict the ordinary experience that matter is, for the most part, made of ordinary nuclear matter. The reason is that changing the ordinary matter to SQM one, a large number of u and d quarks need to convert to s quarks, which would require a very high order weak interaction and therefore it is highly improbable [113]. On the other hand, the existence of ordinary nuclear matter shows that quark matter consisting of only u and d quarks is unstable. Adding a third flavour introduces another Fermi well and thus reduces the energy relative to a two-flavour system what can make the system stable. The most stable configurations would have roughly equal numbers of up, down, and strange quarks with charges of $+2/3e$, $-1/3e$, and $-1/3e$, respectively, therefore minimizing the surface and Coulomb energies. A major destabilizing factor is the large mass of the strange quark. The anticipated mass range for this kind of matter may lie between the masses of light nuclei and that

of neutron stars of $A \simeq 10^{57}$. Some astrophysical mechanisms can convert very large stars into strange stars. Strange matter being the part of the cosmic radiation is called sometimes strange quark *nuggets* or *nuclearities*. Smaller amounts of strange quark matter are usually called *droplets* of strange quark matter, or simply *strangelets*. The existence of stable SQM was postulated by Witten [113]. He also suggested the possibility of production of small lumps of SQM, strangelets with $10^2 < A < 10^6$, in today's universe by quark(neutron) stars, which could convert to more stable SQM stars. They could permeate the Galaxy and reach the Earth. SQM could have important cosmological consequences for today's universe which arise from the possibility that the early universe has undergone a first-order phase transition from SQM to nuclear matter.

Many authors investigated conditions for SQM stability (see, for example, [114–116]). The practical measure of stability of a strangelet is provided by the so-called separation energy dE/dA , i. e., the energy which is required to remove a single baryon from a strangelet. If $dE/dA > m_N$, then strangelet can evaporate neutrons from its surface. Contrary to normal nuclei, SQM stability increases with A and the threshold of its stability is close to $A_{\text{crit}} \sim 300$. Some calculations, based on QCD and the phenomenological bag model [116, 117] (up to the baryon number $A = 40$), suggest that strange quark matter may be metastable or even completely stable for a wide range of bag model parameters values ($B^{1/4} \sim 150\text{--}170$ MeV). Generally, for higher bag parameter values there are less long-lived strangelets and they are shifted towards higher values of baryon number A and strangeness factor f_s . There are also predictions that quite small strangelets might gain stability due to shell effects [118, 119]. They are called «magic strangelets». However, due to the lack of theoretical constraints on bag model parameters and difficulties in calculating colour magnetic interactions and finite size effects, experiments are necessary to help to answer the question of the stability of strangelets. The properties of some forms of hypothetical strange matter, as small lumps of strange quark matter (strangelets) or hyperon matter (metastable multihypernuclear objects MEMO's) have been discussed by many authors (see, for example, [115–117, 120]) with special emphasis on their relevance to the present and future heavy ion experiments. Different aspects of strange quark matter physics are described in the reviews [22, 121, 122].

Searches for SQM have been made on terrestrial matter [123], cosmic rays, and astrophysical objects [124]. The searches resulted in low limits for strangelets in terrestrial matter, but on the other hand, some data could be understood by assuming the presence of strangelets in cosmic rays [24, 25, 76, 92, 125–127] (see the next section). Two seismic events have been recently postulated to be good candidates for big strange quark matter globs [128]. Several strangelet candidates have been reported in cosmic ray experiments [129–131]. According to the picture proposed in [24, 25] strangelets could be remnants of the decay of slightly-strange quark matter fireball, produced in central collisions of primary cosmic ray nuclei.

There are a lot of experiments looking for strange quark matter in heavy ion collisions. They are mostly based on such discerning property of strangelets as an unusual charge to a mass ratio ($Z/A \ll 1$). The strange counterparts of ordinary nuclei are searched for in high-energy collisions at Brookhaven [132] and at CERN [133]. To date no experiment has published results indicating a clear positive signal for strangelets. Although experiments were able to set upper limits on the existence of strangelets in the range of sensitivity of the experiments, they were not able to answer the question concerning their existence. There are several definite reasons for this. The main ones are that the experiments are sensitive only to metastable strangelets with proper lifetimes greater than $\sim 5 \cdot 10^{-8}$ s and they look for strangelets in the midrapidity region. Most of experiments (except the E814) used focusing spectrometers which, for a given magnetic field setting, have a good acceptance only for a fixed momentum and charge of the produced particle. Therefore, the production limits obtained in these experiments are strongly dependent upon the production model assumed for lumps of strange quark matter. The present status of strange quark matter searches, both in cosmic ray and in accelerator experiments, is presented by R. Klingenberg in his review [134].

3.4.1. Extraterrestrial Strangelets. Strangelets have been discussed, in the context of Centauros, by several authors [24, 76, 92, 103]. However, in contrary to the picture [24], where they are postulated to be produced in nucleus–nucleus collisions, some authors have considered the possibility that *strangelets are a component of primary cosmic rays*. After penetration deeply into the atmosphere they could decay, evaporating nucleons and producing Centauro-type events. In principle, the ideas presented in [76, 92, 103] are very close to the old picture of Bjorken and McLerran [88]. The main difference is the proposed Centauro-fireball (strangelet) cross section.

S. B. Shaulov in [76] has presented a rather qualitative discussion of the presence of strangelets in the primary cosmic rays. Similarly as in [88], the evaporation of neutrons was assumed to be the main channel of strangelet energy loss, and the energy fraction evaporated in a single act of collision was estimated in similar way. It was obtained that in one act of a collision several neutrons can be evaporated and a strangelet loses energy of several GeV (in its own rest frame). In this work it was postulated that the new penetrating component, carrying a large part of energy through the atmosphere, could qualitatively explain a chain of anomalous phenomena. Extensive Air Shower (EAS) spectrum «knee» naturally originates if the strangelet spectrum has the maximum at the energy higher than 3 PeV, and the strangelet intensity in the maximum is similar to the nuclear one. Large variety of anomalies observed in individual events, such as: Centauro, Chiron, Geminion, halo, penetrating component, etc., could be natural manifestation of the strangelet evaporation during its passage through the atmosphere. Also miniclusters frequently observed in Chirons could be a

consequence of small p_T evaporation processes. Within this scenario, however, it is hard to understand the appearance of high transverse momenta secondaries in such events. For consistency of this picture the beginning of strangelet spectrum near $E_0 \sim 10$ PeV with the power index ≥ 3 should be assumed.

G. Wilk and Z. Włodarczyk presented in [92, 103] the picture of propagation of lumps of Strange Quark Matter through the atmosphere, similar to the one described in [76, 88]. In opposite to [24] and [88] they argue, however, that strangelets are of almost normal nuclear sizes. This statement results from the value of the strangelet quark chemical potential assumed by authors of [92] to be $\mu_q \sim 300$ MeV. Such value disagrees with that estimated in [23], from Centauro experimental characteristics, and being $\mu_q \sim 600$ MeV. According to Refs. 92, 103 the strong penetrability of strangelets is not caused by their small geometrical radii. Strangelets penetrating deeply into the atmosphere are formed in many consecutive interactions with air nuclei, when the mass number of the incident, very heavy lump of SQM is successively diminished. Big primary strangelets can penetrate very deeply into the atmosphere until their baryon number A_{str} exceeds some critical value $A_{\text{crit}} \sim 300\text{--}400$. Below this value they simply disintegrate into nucleons. Such decay could imitate Centauros. According to [92] Centauro events observed at the mountain altitudes would require a primary strangelet of $A_0 \simeq 1000\text{--}2000$. For the mass spectrum of the form $N(A_0^{\text{str}}) \sim \exp(-A_0^{\text{str}}/130)$ the model explains the smaller number of Centauros detected at Pamir altitude (~ 600 g/cm²) than at Chacaltaya (540 g/cm²). Simultaneously, as it was already mentioned, the authors of [103] claimed that their simulations indicate the insensitivity of families detected at mountain altitudes to any isospin fluctuations. It could mean that the explanation of Centauros needs the presence of some very strongly penetrative projectiles in primary cosmic rays. The model passes over in silence the question of high p_T of Centauro-like phenomena.

It is important to note that the proposed pictures of the strangelet penetration through the matter and its successive destruction in the consecutive collision acts should be connected with the observation of the large cloud of the low energy nucleons from the destroyed target nuclei. Interesting, the extremely long delay (> 0.5 ms) neutrons have been recently observed [125] in large Extensive Air Showers ($N_e > 10^6$) by the neutron monitor working in conjunction with EAS instalation «Hadron». This phenomenon appears at primary energies higher than $3 \cdot 10^{15}$ eV and it is observed close to the EAS axis. As the tentative explanation of this phenomenon one can propose the arrival of a new type of primary cosmic ray particles, like strangelets, with gradual dispersion of their energy along the whole atmosphere.

Also muon bundles of extremely high multiplicity observed by ALEPH detector (in the dedicated cosmic-ray run) could originate from strangelets collisions with the atmosphere [126] and two seismic events [128] are interesting candidates.

The old experimental observations of anomalous massive ($A = 75-1000$) and relatively low charged objects ($Z = 14-46$), which could be interpreted as strangelets, should be recalling. These are:

- Two anomalous events, observed in primary cosmic ray by T. Saito et al. [129] in the counter experiment with the balloon (at the depth $\sim 9 \text{ g/cm}^2$).
- The so-called Price's event [130] (detected at the depth $\sim 3-5 \text{ g/cm}^2$).
- The so-called Exotic Track event [131], which was observed in the emulsion chamber, exposed to cosmic rays with the balloon at the atmospheric depth of only 11.7 g/cm^2 at zenith angle of 87.4° . It means that the projectile causing that event traversed $\sim 200 \text{ g/cm}^2$ of the atmosphere. If the Centauro-like events are really caused by strangelets, then the Exotic Track event could be an argument supporting their strongly penetrative power. It is rather impossible for normal nuclei of $A \sim 460$ to traverse $\sim 200 \text{ g/cm}^2$ of matter without fragmentation.

The Exotic Track event motivated the balloon JACEE [135] and the Concorde aircraft [136] experiments intended to search for strangelets with long mean free paths. The list and description of these strangelet candidates can be found in [127].

3.4.2. Strangelets Formed in the Centauro Fireball. At present, several types of models are used to describe the strangelet production in heavy ion collisions [120, 137, 138]. They can be classified into two categories: strangelet production by coalescence of hyperons or by production following a quark-gluon plasma creation. In a very popular coalescence model, an ensemble of quarks, which are products of nucleus-nucleus collisions, form a composite state which fuses to form a strangelet [137]. The formation of a quark-gluon plasma is not needed in this scenario, as hyperons coalesce during the late stage of the collision forming a doorway state for strangelet production. Such scenario favours the production of low mass strangelets in the midrapidity region, formation of strangelets with $A \geq 10$ is rather unlikely. Thermal models further assume that chemical and thermal equilibrium are achieved prior to final particle production [138]. Coalescence and thermal models usually predict lower strangelet cross section than models postulating a formation of a QGP state. Greiner et al. [120] suggest that once a QGP droplet is formed, almost every QGP state evolves into a strangelet by means of the strangeness distillation mechanism. Distillation process provides a possibility for producing more stable large strangelets since the QGP would lose energy by meson emission possibly resulting in a strangelet of approximately the same A as the QGP droplet.

The model of Centauro production in nucleus-nucleus collisions has been proposed in [23] and it has been developed in [24]. The formation of the incident quark-matter fireball, in collisions of the primary cosmic ray nuclei with air nuclei, at the top of the atmosphere, and its subsequent transformation into relatively long-lived strange quark-matter droplet, were postulated. In order to survive passage from the upper atmosphere downward to the Chacaltaya (Pamir) altitude, the Centauro fireball should have a large mean free path ($\lambda \geq 150 \text{ g/cm}^2$)

and/or lifetime $\tau_0 \sim 10^{-9}$ s. Then the hadronization of the Centauro fireball will occur close to the detector. The picture [24,25] is based on models involving an intermediate quark-gluon plasma state and the distillation process as separation mechanism of strangeness and antistrangeness, as described for heavy ion collisions in [120]. The baryon-rich environment is considered. The model avoids the problem of the very small flux of cosmic ray nuclei at the mountain top level and additionally contains very exciting suggestion of the simultaneous interpretation of both Centauros and long-flying component. The strongly penetrating component could be the sign of the passage of strangelets, formed at the last stage of the Centauro fireball evolution, through the matter. This hypothesis has been studied in [25]. The model explains most features of Centauro events. It could likely explain also the observed low family flux. Such features of the exotic fireball, as its strong penetrating power and its decay predominantly into baryons could cause a decrease of the electromagnetic family flux.

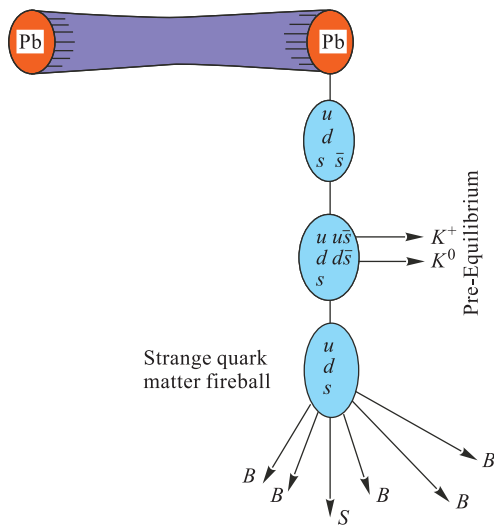


Fig. 19. Centauro fireball evolution scheme [139]

Characteristics and time evolution of Centauro fireball. The main stages of the development in time of the Centauro fireball (see Fig. 19) are the following:

1. *Formation of a quark-matter fireball.* The fireball is created in central collisions of ultrarelativistic ($E_{\text{lab}} \sim 1740$ TeV) medium-heavy cosmic-ray nuclei with air nuclei. At the moment of creation it consists of u , d quarks and gluons only. It has very high matter density, hence high binding energy. As the fireball is formed in the baryon-rich, projectile fragmentation region, the high baryochemical potential prohibits the creation of $u\bar{u}$ and $d\bar{d}$ quarks, resulting in gluon fragmentation $g \rightarrow s\bar{s}$ mainly.

2. *Chemical equilibrium.* The state of (partial) chemical equilibrium may be approached in a time interval $\Delta\tau > 10^{-23}$ s, the relaxation time for $g \rightarrow s\bar{s}$. The larger amount of up and down quarks with respect to the antiquarks results in a higher chance for a \bar{s} quark to find u or d quark and form a K^+ or K^0 than for s quark to form the antiparticle counterparts. Emitted kaons can carry away all strange antiquarks and positive charge, lowering somewhat the initial temperature and entropy.

3. *Strange quark-matter state.* After emitting kaons the *initial quark-matter fireball* is transformed into a *lightly strange quark-matter state* (with the value of strangeness to the baryon ratio $\rho_s/\rho_b \sim 0.06$). The fireball is a mixture of u , d , and s quarks and it is still characterized by very large density, the low temperature, and the value of charge to mass ratio ($Z/A \sim 0.4$) less than that of the original quark-matter fireball. The fireball has a finite excess of s quarks and due to their stabilizing effects [113,120] it could become a *long-lived state* capable to reach the mountain top level before decaying.

4. *Hadronization.* The mechanism of strangeness distillation [120] can cause the strange quark content of the Centauro fireball to form low-mass strangelet(s). The total energy per baryon can be lowered assembling the nonstrange quarks into pure nucleonic degrees of freedom and leaving the strange quarks in a strange matter droplet, its strangeness fraction being enriched to $f_s \simeq 1$. Such state would be a mixture of two phases: pure nucleonic matter and strange quark-matter cluster. The Centauro fireball finally could decay into nonstrange baryons ($\langle N_h \rangle \sim 75$) and strangelet(s) having very high strangeness-to-baryon ratio ($f_s = N_s/A \sim 1$), very low charge-to-baryon ratio ($Z/A \sim 0$), and a small mass number ($A_{\text{str}} \sim 10-15$).

This scenario is based on the experimental Centauro characteristics derived from five «classical Chacaltaya Centauros» (see Subsec.1.1, Tables 1 and 2). Using these characteristics, the *thermodynamic quantities* have been estimated in [23], assuming an ideal two-flavour QGP. Estimated main features of both the Centauro fireball and the strangelet are summarized in Table 10.

More realistic analysis, introducing *three flavours (u,d,s) interacting quarks*, realistic *strangeness equilibration factor* and using the full equation for $\varepsilon(T, \mu_q, \alpha_s, \gamma_s)$, was done in [24]. The energy density has been calculated from the formula [141,142]:

$$\begin{aligned} \varepsilon_{qgp} = & \left(\frac{37}{30} - \frac{11a_s}{3\pi} \right) \pi^2 T^4 + \left(1 - \frac{2a_s}{\pi} \right) 3\mu_q^2 T^2 + \frac{3}{2\pi^2} \left(1 - \frac{2a_s}{\pi} \right) \mu_q^4 + \\ & + \gamma_s \left(\frac{18T^4}{\pi^2} \right) \left(\frac{m_s}{T} \right)^2 K_2 + 6 \left(\frac{m_s T}{\pi} \right)^2 \left(\frac{m_s}{T} K_1 \right). \end{aligned} \quad (14)$$

The entropy per baryon

$$S_b = S/\rho_b, \quad (15)$$

where the baryon density

$$\rho_b = \frac{2}{3} \left(1 - \frac{2a_s}{\pi} \right) \left(\mu_q T^2 + \frac{\mu_q^3}{\pi^2} \right), \quad (16)$$

Table 10. Summary of estimated quantities characteristic of the cosmic-ray Centauro events [23,24]

«Centauro» fireball	
Mass of fireball, GeV	$M_{\text{fb}} = 180 \pm 60$
Volume of fireball, fm ³	$V_{\text{fb}} \leq 75-100^*$
Energy density of fireball, GeV/fm ⁻³	$\varepsilon_{\text{fb}} \geq 2.4 \pm 1^*$
Baryochemical potential of fireball, GeV	$\mu_b = 1.8 \pm 0.3$
Temperature of fireball, MeV	$T_{\text{fb}} = 130 \pm 6$
Quark density of fireball, fm ⁻³	$\langle \rho_q \rangle = 8 \pm 3$
Baryon density of fireball, fm ⁻³	$\langle \rho_b \rangle = 2.7 \pm 1$
Strange quark density, fm ⁻³	$\rho_s \sim 0.14$
Antiquark density, fm ⁻³	$\rho_{\bar{q}} \sim 3.6 \cdot 10^{-3}$
Gluon density, fm ⁻³	$\rho_g \sim 0.6$
Entropy density, fm ⁻³	$S \sim 16.4$
Entropy/baryon density	$S/\rho_b \sim 6$
Strangeness/baryon density	$\rho_s/\rho_b \sim 0.06$
Final charge/baryon	$(Z/A)_f \sim 0.4$
Net strangeness	$N_s - N_{\bar{s}} \sim 14$
Predicted particle ratio	$N(\text{pion})/N(\text{nucleon}) \simeq 7 \cdot 10^{-6}$
«Centauro» strangelet	
Mass	$A \sim 10-15$
Charge/baryon	$Z/A \sim 0$
Strangeness/baryon	$f_s \sim 1$
*According to [140] $V_{\text{fb}} = 27 \pm 16 \text{ fm}^3$ and $\varepsilon_{\text{fb}} = 6.7 \pm 3.6 \text{ GeV/fm}^3$.	

and the entropy

$$S = \frac{1}{3} \frac{\partial \varepsilon}{\partial T} = \left(\frac{74}{45} - \frac{44a_s}{9\pi} \right) \pi^2 T^3 + 2 \left(1 - \frac{2a_s}{\pi} \right) \mu_q^2 T + \gamma_s \left(\frac{3m_s^3}{\pi^2} K_3 + \frac{12m_s^2}{\pi^2} T K_2 + \frac{m_s^4}{\pi^2 T} K_2 + \frac{5m_s^3}{\pi^2} K_1 + \frac{m_s^4}{\pi^2 T} K_0 \right), \quad (17)$$

where $K_i(m_s/T)$ are i -order modified Bessel functions and γ_s is the strangeness equilibration factor.

Using these formulas, it has been shown in [24] that the Centauro fireball with values of the temperature, chemical potential of quark, and energy density estimated previously to be $T = 130 \text{ MeV}$, $\mu_q = 600 \text{ MeV}$, and $\varepsilon = 2.4 \text{ GeV/fm}^3$, is not the ideal QGP fireball because the strangeness equilibration factor is estimated to be less than unity and strong coupling constant is expected to be

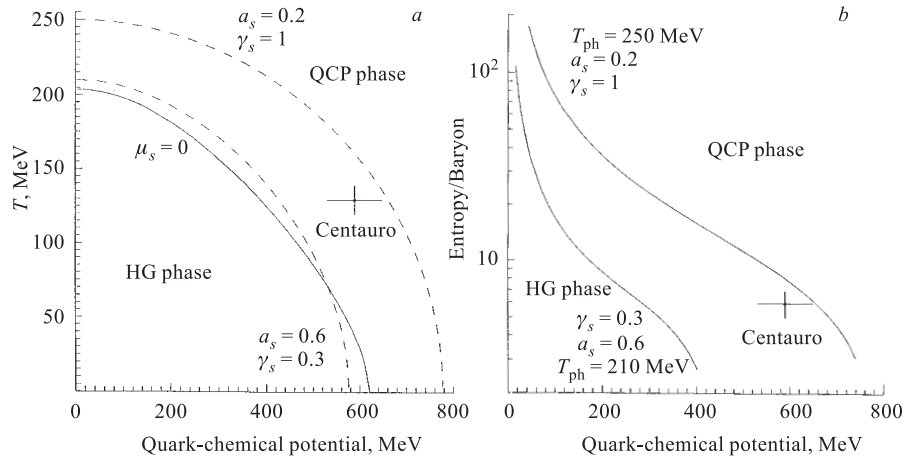


Fig. 20. *a*) Location of the Centauro point (T, μ_q) on the phase diagram for two temperatures: $T(\mu_q = 0) = 250$ and 210 MeV (dashed curves). Solid curve is for $\mu_s = 0$ in the hadron gas. *b*) Entropy per baryon versus chemical potential of quark, for two phase curves [142]

greater than zero. Taking for this quark-matter state the strong coupling constant $\alpha_s \simeq 0.5-0.6$ and $\gamma_s \simeq 0.4$, one obtains the Centauro point located at the phase diagram close to the QGP phase, at the in-between region of the ideal QGP phase connected with chiral phase transition and the Hadron Gas Phase as it is shown in Fig. 20.

Penetrability question. According to this model, Centauro events are produced in central collisions of ultrarelativistic cosmic-ray nuclei with air nuclei. A collision of the medium-heavy cosmic-ray nuclei occurs at the top of the atmosphere. Thus the Centauro fireball must possess features allowing it to reach the mountain-top altitudes (~ 500 g/cm²) without interaction with air nuclei or spontaneous decay during its flightpath of about 15 km. This requirement creates the following questions:

- What is the magnitude of the interaction length λ and the lifetime τ of the Centauro fireball, resulting from the existing experimental data?
 - Do they not contradict the requirement of traversing of about 15 km before the fireball decays?
 - What are the theoretical reasons which could allow such long flightpath?
- These questions have been considered in [24] and the stability question has been studied separately in [140].

Experimental constraints on λ or τ . An estimate of the value of the interaction length of the Centauro fireball can be obtained from the comparison of the observed rate of Centauro events, detected at the mountain top level, after Centauro fireballs decaying, with the results of experiments looking for heavy penetrating particles, assuming that Centauro fireballs before their decays may be identified with such objects. On the one hand, it seems that the large flux of Centauro events detected in Chacaltaya and Pamir emulsion chambers suggests a long interaction length of the Centauro fireball, allowing it to reach the mountain top level. On the other hand, the negative results of the experiments looking for heavy penetrating particles at White Mountains and Mt. Norikura by means of CR-39 films could be explained by assuming a short interaction length of Centauro fireball, allowing for its decay before reaching the mountain top altitude [143]. However, the careful analysis of that seeming contradiction [24] shows that the interaction length of the Centauro fireball, λ_{Cent} larger than 150 g/cm^2 , is in accordance with the results of both kinds of experiments.

The long interaction length of the Centauro fireball could be connected with the very high binding energy and the reduced geometrical cross section (the estimated volume of the fireball [24] is more than six times smaller than that of the ordinary nucleus with $A = 75$). If the Centauro fireball is an unstable state spontaneously decaying with the probability $P(x)$ after travelling a distance $x \approx 15 \text{ km}$, then the lifetime τ_0 , in its own frame, assuming $P(x) \sim 10\text{--}50\%$, is obtained to be of the order of 10^{-9} s . This means that the fireball could decay via weak interactions, since strong decays occur within $\sim 10^{-23}\text{--}10^{-24} \text{ s}$. Even so, the lifetime of 10^{-9} s is unrealistically long for a nonstrange, normal quark matter state.

Theoretical justifications of the long flightpath, i. e., stability question. It was estimated in [24] that the interaction length of the Centauro fireball in the atmosphere $\lambda_{\text{Cent}} \geq 150 \text{ g/cm}^2$ is in accordance with different experimental observations. This is an extremely long interaction length. It is about 1.6 times larger than that of a nucleon and about 35 times larger than that of a normal nucleus of a comparable mass number. The long lifetime and small cross section could be attributed to its very high binding energy and much reduced geometrical volume. The very high baryochemical potential and the transformation of the initial quark-matter state into a partially-strange quark-matter one, with increased spatial concentration of quarks due to the extra fermion flavour, result in an increase of the binding energy. Extremely large density and binding energy and the small volume may result in the formation of a (meta)stable state. However, the problem is open and according to our present knowledge rather far from satisfactory and quantitative solving. The main questions are:

1. *Radius (and volume) question.*

- The long penetration length of the Centauro fireball through the atmosphere suggests the small geometrical cross section of that object, i. e., the very small ra-

dus. Comparing the values of the average interaction mean free path of nucleons in the air with that for the Centauro fireball one can expect that $R_{\text{Cent}} \sim 0.9$ fm and $r_0^{\text{Cent}} \sim 0.22$ fm (for $A = 75$). Thus, the Centauro fireball radius could be about 5.5 times smaller than that of a normal nucleus of corresponding A .

- The other estimate of the Centauro fireball radius can be done by using its volume value, $V_{\text{Cent}} \simeq 75 \text{ fm}^3$ as obtained in [23]. Assuming the spherical shape of the fireball one gets $R_{\text{Cent}} = 2.6$ fm and $r_0^{\text{Cent}} = 0.62$ fm. These values seem to be overestimated in comparison with the previous ones.

- Another estimate taken from [140] gives $R_{\text{Cent}} = 1.86 \pm 0.36$ fm and $r_0^{\text{Cent}} = 0.44 \pm 0.08$ fm. Different estimates locate the Centauro fireball radius in the wide range: $R_{\text{Cent}} \sim 0.9\text{--}2.6$ fm and $r_0^{\text{Cent}} \sim 0.22\text{--}0.62$ fm.

2. *Stability curves.* The main question is if extreme conditions, such as a very high chemical potential of a quark and reduced volume, can cause the (meta)stability of the object. A general condition for DQM (Deconfined Quark Matter) bag stability comes from the equalization of the internal (quark-gluon) and external (bag) pressure. The formulas for thermodynamical quantities of strangelets being in mechanical equilibrium can be found for example in [121]. They have been derived assuming the massless u, d , and s quarks of equal chemical potentials μ , and $\alpha_s = 0$. Strangelets are in mechanical equilibrium at fixed temperature T and baryon number A when

$$BV = \left(\frac{19\pi^2}{36} T^4 + \frac{3}{2} \mu^2 T^2 + \frac{3}{4\pi^2} \mu^4 \right) V - \left(\frac{41}{216} T^2 + \frac{1}{8\pi^2} \mu^2 \right) C, \quad (18)$$

where extrinsic curvature $C = \oint (1/R_1 + 1/R_2) dS$ ($C = 8\pi R$ for a sphere), and V and B are the volume and bag model value constant, respectively. In this case

$$A = \left(\mu T^2 + \frac{1}{\pi^2} \mu^3 \right) V - \frac{\mu}{4\pi^2} C. \quad (19)$$

The stability curves obtained from this formula are shown in Fig. 21. There is plotted the temperature T as a function of the radius R for three values of quark chemical potential ($\mu = 300, 500, 700$ MeV) and baryon number $A = 75$. There is drawn also the experimentally estimated Centauro fireball radius limit. It is well inside the «stability region» for the Centauro fireball with parameters close to experimentally obtained values, i. e., $T = 130$ MeV and $\mu = 600$ MeV.

According to the model [23, 24] the Centauro fireball is supposed to be, however, only the slightly strange quark matter glob. It has been concluded in [140] that Centauro fireball quantities, such as $T = 130$ MeV, $\mu_q = 600$ MeV, and $R_{\text{Cent}} = 1.86 \pm 0.36$ fm are within one standard deviation from the stability conditions, thus it might be possible that the Centauro fireball is a metastable state.

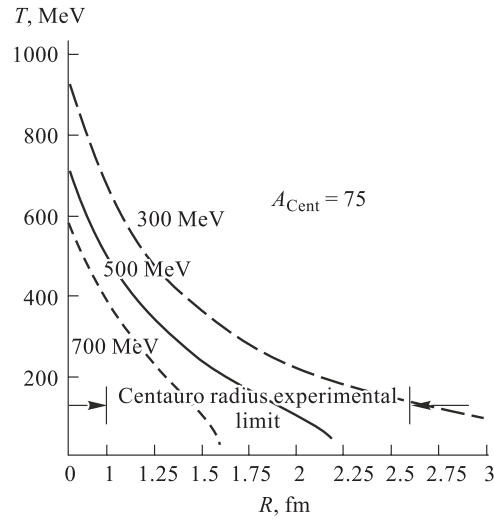


Fig. 21. Stability curves plotted as T versus R for fixed $\mu_q = 300, 500, 700$ MeV for a strangelet with $A = 75$

In the context of discussing the Centauro fireball stability it should be stressed that there are also some predictions concerning the possibility of the existence of stable collapsed nuclei [144]. A collapsed nucleus is a highly dense nuclear matter state, the nucleon density being more than 20 times larger than that corresponding to a normal nucleus, with binding energy per nucleon of hundred MeV and even up to the nucleon mass (for $T = 0$). In this condition, a collapsed nucleus is a cold deconfined quark matter state, with the radius r_0 estimated to be 0.4 fm, which is close to that of the Centauro fireball. It should be mentioned, however, that these attempts need about two times larger bag pressure than the value required for stability of a strangelet at $T = 0$. For instance, $B^{1/4} \sim 375$ MeV is needed for the stabilization of the quark-gluon plasma bag with $T = 130$ MeV, $\mu_q = 600$ MeV, $A = 75$, and $R = 1.62$ fm [140].

Strangelets from the Centauro-Fireball. At the last stage of the Centauro fireball evolution, due to the strangeness distillation mechanism a strangelet can be formed. The characteristic features of such quark-matter nuggets can be estimated by using the above-mentioned quark-gluon plasma model describing the experimental Centauro characteristics. On the other hand, they can be derived independently from the analysis of the strongly penetrating cascades, assuming that they are due to a strangelet passage through the apparatus.

The excess of strange quarks in the Centauro fireball is mainly caused by the preequilibrium emission of the K^+ and K^0 mesons which carry \bar{s} quarks away.

One can assume that the total number of $s\bar{s}$ pairs created in the Centauro fireball volume V approximately equals the number of emitted K^+ , K^0 mesons and it can be estimated from the formula:

$$N_{K^++K^0} \simeq N_{s\bar{s}} = \rho_{\bar{s}}V, \quad (20)$$

where $\rho_{\bar{s}}$ is the s -antiquark density and depends on the temperature by the relation [145]:

$$\rho_{\bar{s}} \simeq 0.178 \left(\frac{T}{200 \text{ MeV}} \right) K_2 \left(\frac{150 \text{ MeV}}{T} \right). \quad (21)$$

For $T = 130 \text{ MeV}$ which is the temperature for cosmic-ray Centauros, $\rho_{\bar{s}} \simeq 0.14 \text{ fm}^{-3}$. Taking a volume of the Centauro fireball $V \sim O(100 \text{ fm}^3)$, the number of created $s\bar{s}$ pairs (and thus emitted kaons) will be ~ 14 . After the pre-equilibrium emission of kaons, a strange quark matter metastable object with a small Z/A ratio is formed. The change of Z/A ratio, because of kaon emission, can be calculated from the formula

$$\left(\frac{Z}{A} \right)_f = \left(\frac{Z}{A} \right)_i - \frac{\Delta Q}{A}, \quad (22)$$

where the net change of the charge

$$\Delta Q = N_{s\bar{s}}((Q_u + Q_d)/2 + Q_{\bar{s}}). \quad (23)$$

Assuming the quark charges $Q_u = 2/3$, $Q_d = Q_s = -1/3$, $(Z/A)_i \simeq 0.5$ and the temperature $T \sim 130 \text{ MeV}$, it was evaluated $(Z/A)_f \simeq 0.4$. In the extreme case when all produced strange quarks became constituents of the strangelet and $N_s/A_{\text{str}} \simeq 1$, the final explosion of the Centauro fireball into nonstrange baryons and accompanied *emission of a small strangelet characterized by $A_{\text{str}} \sim 10-16$* can be expected. Its very high strangeness-to-baryon ratio implies also very low charge-to-baryon ratio ($Z/A \sim 0$).

Strongly Penetrating Cascades as Signs of Strangelets. The hypothesis, that the strongly penetrating cascades can be produced by strangelets, announced in [24], was developed in [25], where the possible connection between the very penetrating component, frequently accompanying the cosmic ray exotic phenomena, and the hypothesis of the formation of strangelets in the process of strangeness distillation was studied. Several possible decay [113, 115, 116, 120, 146] and interaction [92] modes of a small strangelet were considered and its travelling through the homogenous-type thick lead chamber was simulated.

Unstable Strangelets. Objects decaying via strong interactions in the time-scales typical for strong processes ($\tau_0 \lesssim 10^{-20} \text{ s}$) were called unstable strangelets.

Although a variety of such processes is expected [113, 115, 116], the most important one is a *strong neutron emission* $S \rightarrow S' + n$ in which a strangelet S emits a neutron, yielding a daughter strangelet S' with parameters changed by $\Delta A = -1$, $\Delta Y = -1$, $\Delta Z = 0$.

Unstable strangelets decay very fast, practically at the point of their formation. For strangelets with $\tau_0 \sim 10^{-20}$ s and a Lorentz factor $\gamma \sim 10^4 - 10^5$ the estimated length of the decay path will be of the order of $\sim 10^{-5} - 10^{-6}$ cm, what is very small in comparison with the estimated heights of the Centauro fireball explosion ($H \sim 100 - 1000$ m above the chamber). Thus the considered picture resolves into a simple case of a bundle of nucleons entering the chamber. If all nucleons are evaporated with momenta close one to the other, a bundle of strongly collimated nucleons is obtained. If the relative transverse momenta of neutrons are of the same order as those observed in miniclusters, i. e., $p_T(\gamma) \sim 10$ MeV/c, then the average lateral distances between neutrons, at the chamber level, are estimated to be of the order $\sim 100 - 1000$ μm . Thus, depending on the formation height and the energy, a decaying strangelet will produce in the chamber the picture resembling a minicluster or one single long-range cascade (if the relative distances between the decay products are smaller than the lateral resolution of the used detectors). The development of nuclear-electromagnetic cascades, caused by such neutron bundles, in the typical homogenous lead chamber with detection layers placed every 1 cm of the lead absorber was simulated. It has been found that the bundle of several (~ 7) neutrons generates the many-maxima long-range cascades, very similar to the long-flying component observed in cosmic-ray experiments. A typical simulated event is shown in Fig. 22.

The impression of the strong similarity between the simulated and observed transition curves has been confirmed by investigation of the relative distances and the distribution of energy contained in the successive humps [25].

Metastable strangelets. Metastable strangelets are commonly assumed to decay with a lifetime $\tau_0 \lesssim 10^{-4}$ s. They decay via weak interaction processes, of which the most important is *the weak neutron decay*. As it involves a weak interaction flavour-changing process, $s + u \leftrightarrow u + d$, it should be much slower than a strong neutron decay. Generally, however, lifetimes of small metastable strangelets are not predicted precisely at present and they are still a matter of debate [120, 146]. Thus, in principle, a wide range of possible lifetimes of metastable strangelets should be taken into account. In the extreme situation, i. e., sufficiently long(short) strangelet lifetime, the problem simply reduces to the stable(unstable) strangelet scenario. In the intermediate case a strangelet penetrating through the chamber can successively evaporate neutrons. Neutrons interact with nuclei of the lead absorber producing the many-maxima cascades in which the distances between the successive humps are strongly correlated with the time interval between the successive evaporation acts. An assumption of a strangelet lifetime $\tau_0 \sim 10^{-15}$ s leads to the formation of the long-range many-

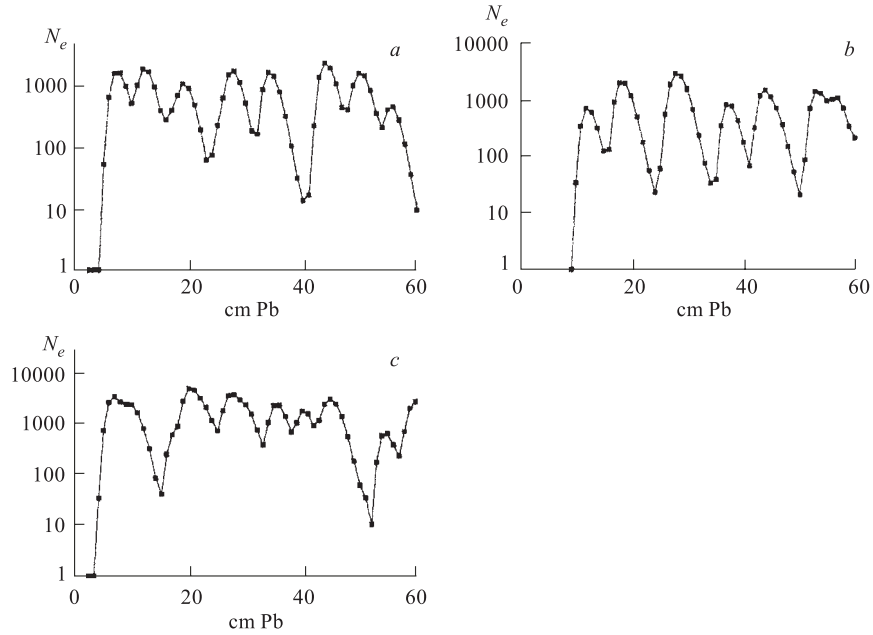


Fig. 22. Examples of simulated transition curves recorded in the lead chamber and produced by various strangelets. Numbers of electrons N_e are counted within the radius of $50 \mu\text{m}$. *a*) Unstable stranglet decaying into a bundle of 7 neutrons ($E_n \simeq E_{\text{str}}/A_{\text{str}} \simeq 200 \text{ TeV}$). *b*) Metastable strangelet ($A_{\text{str}} = 15$, $E_{\text{str}} = 200 A \cdot \text{TeV}$, $\tau \sim 10^{-15} \text{ s}$). *c*) Long-lived strangelet ($A_{\text{str}} = 15$, $\mu_q = 600 \text{ MeV}$)

maxima cascades similar to these observed in the experiment. An example of the transition curve, obtained under the assumption of the evaporation of neutrons from a metastable strangelet with $A_{\text{str}} = 15$, passing through the lead chamber, is shown in Fig. 22.

This hypothesis involves, however, some hardly acceptable points:

- Required lifetime $\tau_0 \sim 10^{-15} \text{ s}$ seems to be too short for the weak neutron decay process (much shorter than for example the lifetimes of both weak semileptonic and weak nonleptonic decays, estimated in [147] on the basis of the Berger–Jaffe mass formula [115] for strangelets of $A_{\text{str}} = 15$).

- The picture assumes that a strangelet decays successively inside the chamber. Thus, it concerns objects produced at a very small distance from the chamber or just inside it. In the case of strangelets produced in typical cosmic-ray families (at heights $H \sim 100\text{--}1000 \text{ m}$ above the chamber) it seems unclear why they do not decay in the air layer, above the apparatus.

Stable Strangelets. The weak radiative decays ($u + d \leftrightarrow s + u + \gamma$) and weak leptonic decays ($d \leftrightarrow u + e^- + \bar{\nu}_e$, $s \leftrightarrow u + e^- + \bar{\nu}_e$) are expected to be slower than a weak neutron emission. The rate of the radiative decays is inhibited by the electromagnetic coupling constant and all β decays by the three-body phase space. Additionally, the strangeness changing β process is suppressed by the Cabibbo factor. Such long-lived objects, called «stable» strangelets, if produced in the high energy cosmic-ray families should pass without decay through the apparatus. The simplified picture of their possible interaction in the chamber matter was assumed.

The strangelet is considered as an object with the radius

$$R = r_0 A_{\text{str}}^{1/3},$$

where the rescaled radius

$$r_0 = \left(\frac{3\pi}{2(1 - 2\alpha_c/\pi)[\mu^3 + (\mu^2 - m^2)^{3/2}]} \right)^{1/3}, \quad (24)$$

μ and m are the chemical potential and the mass of the strange quark, respectively and α_c is the QCD coupling constant.

The mean interaction path of strangelets in the lead absorber

$$\lambda_{s-\text{Pb}} = \frac{A_{\text{Pb}} m_N}{\pi(1.12 A_{\text{Pb}}^{1/3} + r_0 A_{\text{str}}^{1/3})^2}. \quad (25)$$

Penetrating through the chamber a strangelet collides with lead nuclei. In each act of a collision, the «spectator» part of a strangelet survives continuing the passage through the chamber and the «wounded» part is destroyed. Particles, generated at the consecutive collision points, interact with lead nuclei in a usual way, resulting in the electromagnetic-nuclear cascade, developing in the chamber matter.

Penetration of a strangelet with mass number $A_{\text{str}} = 15$ through the chamber, assuming two different values of the chemical potential: $\mu = 300$ and 600 MeV was simulated. In both cases, many maxima cascades can be produced. The example of the transition curve obtained in the process of successive interactions of a strangelet in the chamber matter is shown in Fig. 22.

Calculations done in [25] showed that the long-range cascades observed in the thick homogenous lead/emulsion chambers could be the result of a strangelet penetration through the apparatus. Their strong penetrating power can be connected both with the small interaction cross section (in comparison with a nucleus of comparable A) of the strangelet and with the big concentration of its energy in a narrow region of phase space. This energy could be liberated into a conventional particle production in many consecutive evaporation or interaction acts. In this context, the Centauro-like event with abnormally long cascades found

among its secondaries, described in [42, 43], could be regarded as an event, in which strangelets were generated as remnants of the strange quark matter fireball. It seems that also numerous hadron-rich families accompanied by highly penetrating cascades, clusters or halo could be explained by assuming the same mechanism of the formation of a strange quark matter fireball and its successive decay into predominantly baryons and strangelet(s). In principle, three possible pictures of a strangelet passage through the chamber, which give the long-range many-maxima cascades similar to these observed in the cosmic-ray experiments, exist. The most plausible are scenarios assuming a penetration of a short-lived (unstable or metastable ones) or a long-lived («stable») strangelet. However, to distinguish between these two scenarios a more precise detector and higher event statistics are necessary.

4. SEARCH FOR CENTAUROS IN ACCELERATOR EXPERIMENTS

Centauros and/or related phenomena have attracted a lot of attention since the early 1980s. Several accelerator experiments have been already performed to search for such unusual events. Also some current and future experiments are going to look for them.

4.1. Past Experiments at CERN SPS Collider. The first accelerator searches for the Centauro phenomenon have been performed many years ago (in 1981–1986) at the SPS CERN $p\bar{p}$ collider by the UA1 experiment [148] (at energy $\sqrt{s} = 630$ GeV) and by the UA5 Collaboration [149] (at energy $\sqrt{s} = 546$ and 900 GeV). Both experiments looked for Centauros in the central rapidity region (UA1 at $|\eta| \leq 3$ region and UA5 in wider pseudorapidity interval). The UA5 detector consisted of two streamer chambers, placed on opposite sides of the beam pipe. Charged particles left there tracks which were photographed for analysis. Photons were detected through conversions in a lead-glass plate, placed between the beam pipe and the upper streamer chamber. In the last search the UA5 detector was significantly improved. The geometrical acceptance of the large streamer chambers was about 95 % for $|\eta| \leq 3$, falling to zero at $|\eta| = 5$. The lead-iron-scintillator calorimeter was situated at 90° and covered the interval $|\eta| \leq 0.9$ and azimuthal angle $\Delta\phi \simeq 30^\circ$. In the latest analysis upper limits of 0.1–0.5 % at 95 % C. L. have been placed on Centauro production. No indication of Centauro production was observed.

The negative results of UA1 and UA5 experiments have several possible alternative explanations:

- The energy threshold for the production of such objects is higher than $\sqrt{s} = 900$ GeV, what corresponds to the incident energy in the laboratory frame E_{lab} higher than 431 TeV, when assuming a nucleon projectile. This explanation seems to be especially convincing, as the average incident energy of cosmic-ray

Centaurus has been estimated to be ~ 1740 TeV. The separate question concerns Mini-Centauro species which, in fact, have been observed in cosmic ray experiments in a lower energy region. In this case the reason of their nonobservation by UA1 and UA5 experiments may be the existence of «genetic relations» between different exotic phenomena (see, e. g., [56]).

- Centaurus are produced in the projectile fragmentation region, thus the above mentioned experiments, limited to the central region, were unable to find them.

- Centaurus cannot be born in nucleon–nucleon collisions. This would support the hypothesis of the formation of Centaurus in a nucleus–nucleus collision [23] or its exotic (extra-galactic) origin [88].

4.2. Current Experiments at Tevatron and CERN SPS. 4.2.1. Experiments at Fermilab ($p\bar{p}$ Tevatron at $\sqrt{s} = 1.8$ TeV). At Tevatron energy the situation is delicate because the expected energy threshold for Centauro production is roughly consistent with $p - \bar{p}$ collider energy, when assuming the Centauro formation in nucleon–nucleon collisions ($\sqrt{s} = 1.8$ TeV is equivalent to about $1.7 \cdot 10^{14}$ eV in laboratory frame for nucleon–nucleon collisions). However, if Centaurus were produced in nucleus–nucleus collisions, the situation will be different, as the total interaction energy of the average cosmic-ray Centauro in «60 + 14» c. m. s. is $\sqrt{s} \simeq 6.8$ TeV.

The other question, mentioned already in the case of CERN SPS experiments, is the different kinematical range for cosmic ray experiments and accelerator ones. Cosmic ray experiments are primarily sensitive to an energy flow, and generally detect particles from the fragmentation rapidity region whereas the accelerator studies are mainly focused on the central region of phase space in the c. m. s. [82].

In some Fermilab experiments the Centauro phenomenon is (or is going to be) searched in nucleon–nucleon collisions. These are:

Mini-Max (T-864). This is a small experiment situated at the C0 interaction region of the Tevatron, with the primary goal to search for DCC and possibly related exotic phenomena such as Centauro, in the forward region. It has been designed to measure the ratio of charged-to-neutral pions produced at $\eta \simeq 4.1$. The detector was designed as a telescope of multiwire proportional chambers (MWPC's) together with scintillation counters along the beam pipe, and the lead converter inside the telescope. Charged particles can be observed in the chambers before and after the converter, and photon conversions in the chamber behind the converter. The electromagnetic calorimeter is placed behind the MWPC telescope. Mini-Max is able to observe both charged particles and photons in the region $3.4 < \eta < 4.2$ and it is sensitive to low- p_T particles. The distribution of photons to charged particles ratio is expected to be different for the generic binomial and DCC particle production models (see Subsec.3.3). The main problem of the experiment is the background from the for both γ 's from π^0 (acceptance covers a circle of radius ~ 0.75 units in (η, ϕ) at $\eta = 4.1$). The combined ratios of the factorial moments, which result in experimentally robust variables

(independent of an acceptance and various efficiency factors), were used in the analysis. A comparison of ratios of measured robust variables and those expected from various models showed that data are consistent with the generic production mechanism [110, 150]. Limits on DCC production in various models are claimed to be at the $\sim 5\text{--}20\%$ level.

The C0 group has also designed the Zero Degree proposal for studying far forward physics. Unfortunately this proposal was not approved.

CDF. Also this experiment [151] reports preliminarily a negative search for Centauros in the central rapidity region. According to [152] the CDF Collaboration has put an upper limit of 10 mb on the production of Centauros in $1.3 < \eta < 4.1$. Within each event particles were detected and identified as either hadronic requiring $E_T > 0.4$ GeV, or electromagnetic requiring $E_T \leq 0.2$ GeV, using calorimeter towers out to $|\eta| < 4.2$. The search for Centauro-like events was based primarily on their unique particle kinematics: particle multiplicities $N \sim 75$, $\langle p_T \rangle \sim 1.7$ GeV/c and $\langle \eta \rangle$ of hadrons centered around 2.2 with $\sigma_\eta \sim 0.7$ accordingly to the phenomenological interpretation of Centauros as diffractive fireballs [38, 89]. In addition, search for Centauro candidates with an unusual hadronic-to-electromagnetic asymmetry, as predicted by DCC hypothesis, was done. This analysis, however, does not consider the possibility that Centauros decay to protons and neutrons what can be the additional reason of the negative result.

D0 Detector. The main purpose of D0 detector [153] is the study of high mass states, large p_T phenomena, and the rapidity gap fraction. It basically consists of three elements: the central detector, the liquid argon-uranium calorimeter, and the outer muon detector. It has charged-particle tracking capability up to 3.2 units of pseudorapidity. The uranium-liquid argon calorimeters have full coverage for the pseudorapidity range of $|\eta| < 4.1$. The calorimeters are azimuthally symmetric and have electromagnetic and hadronic resolution of $15\%/\sqrt{E}$ and $50\%/\sqrt{E}$, respectively. The transverse segmentation of the calorimeter towers is typically $\Delta\eta \times \Delta\phi = 0.1 \times 0.1$. Thus the detector is well suited to search for Centauro-type events. The strategy of the search for Centauro events in the D0 detector depends on the interpretation of the event. Assuming the isotropic decay of a fireball with the mass ~ 180 GeV/c into baryons, a large deposit in the hadron calorimeter with no energy in the EM calorimeter is expected. Monte Carlo study shows that the detector is suitable for the Centauro phenomenon investigation.

4.2.2. Fixed Target Experiments at CERN SPS. Some CERN SPS experiments searched for Centauro-like phenomena in heavy ion collisions at the energy $158 A \cdot \text{GeV}$ are presented. Among them:

WA98. The WA98 [154] experiment emphasizes on a high precision, simultaneous measurement of both hadrons and photons. The experimental set-up consists of large acceptance hadron and photon spectrometers, detectors for charged particles and photon multiplicity measurements, and calorimeters for transverse

and forward energy measurements. Among these detectors there are two which are well suited for the DCC search. One can measure charged particle multiplicities with a Silicon Pad Multiplicity Detector ($2.35 < \eta < 3.75$) and photons with a Photon Multiplicity Detector covering $3.0 < \eta < 4.2$. WA98 uses various methods of DCC analysis, such as:

- Global event characteristics, i. e., the total number of photons and charged particles over the entire phase space covered by the photon and charged particle detectors;

- Methods for DCC domains, when the available phase space is divided into several $\eta-\phi$ bins. Among them the wavelet analysis (multiresolution scanning the entire phase space, no averaging over events or $\eta-\phi$ space), various moments and their combinations, i. e., «robust observables» were calculated from the distribution of photons and charged particles in each bin [154].

The measured results were compared to those from simulations and to those from various types of mixed events to isolate the source of nonstatistical fluctuations [155]. The comparison indicates the presence of nonstatistical fluctuations in both charged particle and photon multiplicities in limited azimuthal regions, however, no correlated charged-neutral fluctuations are observed [155]. To date they have observed no events with a large charge-to-neutral fluctuation from among 200 K events, and reported no significant DCC signal in Pb + Pb collisions. Within the context of simple DCC model, upper limits on the presence of localized nonstatistical DCC-like fluctuations of the order $\sim 10^{-2}-10^{-3}$ were extracted.

NA49. The experiment NA49 [156] is a large acceptance hadron detector at the CERN SPS. Four large volume time projection chambers (TPC) record the trajectories of particles. Two of them (VTPC1,2) are placed inside two superconducting magnets and two are placed further downstream and symmetrically on both sides of the beam line. The VTPC2 and MTPC acceptances complement each other around the midrapidity and the combination of both detectors covers a major fraction of the available phase-space. The set-up also includes four time-of-flight (TOF) walls and a set of calorimeters for triggering and E_T measurements. Among many topics which are investigated in the experiment, also a statistically significant determination of momentum space distributions and particle ratios can be performed for single events, allowing for a study of event-by-event fluctuations. The first results of the analysis of fluctuations in the average transverse momentum of individually measured charged particles from event to event, done in a region of $0.005 < p_T < 1.5$ GeV/c and rapidity $4 < y_\pi < 5.5$, have been published in [157]. DCC models suggest that pions emitted from DCC domains will be preferentially produced at low transverse momenta. This provides for a translation of the number fluctuations predicted by the DCC models into p_T fluctuations. The isospin fluctuations of pions production from DCCs lead to multiplicity fluctuations of charged pions at low transverse momenta and therefore to

nonstatistical fluctuations in the distribution of the mean transverse momentum. Using the model in which the DCC production is characterized by the probability to form a single DCC domain in the event and the fraction ξ of pions coming from the DCC it was concluded that assuming DCC's occurring in every event the fluctuations observed in the data rule out DCC sizes of $\xi > 3.5\%$.

EMU16. It is a Magnetic-Interferometric Emulsion Chamber where it is possible to study isospin fluctuations (DCC) at small $y \leq 2$.

Negative results of the Centauro search at collider energies (CERN and Fermilab) allows one to suspect that either the investigated energy region is below the threshold for such events formation, or the methods of looking for Centauro events are not fully adequate because of some misunderstanding the experimental observation (different rapidity regions should be explored, different types of produced particles should be looked for, different projectiles should be used, etc.). If Centauro fireballs are created in nucleus–nucleus collisions, as it is suggested in [23, 24], then in the future collider experiments, at RHIC and LHC, the appropriate conditions for formation of these objects are expected.

4.3. Current and Future Experiments at RHIC and LHC. The relativistic Heavy Ion Collider (RHIC) at Brookhaven has started in June 2000. During Run I the maximum energy was 130 GeV per nucleon pair. In the nearest future the collisions of relativistic heavy ions (i. e., Au-Au) with a centre-of-mass energy of $200 A \cdot \text{GeV}$ are expected to be investigated. Few years later (in 2006), it is planned to start the Large Hadron Collider (LHC) at CERN, with the Pb + Pb beams, carrying the centre-of-mass energy of about $5.5 A \cdot \text{TeV}$. Majority of the experiments has a wide program with the main purpose to find the quark-gluon plasma by looking at many different observables. Among them some exotic signatures related to Centauro phenomena are planned to be used in the following experiments at RHIC:

PHOBOS. PHOBOS detector [1] consists of two parts. The first one is a silicon multiplicity detector covering almost the entire pseudorapidity range of the produced particles and measuring the total charged multiplicity only, $dN/d\eta$. The second one is a two-arm spectrometer at midrapidity. The PHOBOS configuration is that it will give fairly subtle measurements in the midrapidity ($0 < \eta < 2$) and low p_T region. It will be able to look for DCC, produced in the central rapidity region, by signatures such as the anomalies (unusual fluctuations) in the pseudorapidity distribution of charged particles. (No direct comparison between the electromagnetic and hadronic component will be possible.)

STAR. STAR [1] (Solenoidal Tracker at RHIC) consists of high resolution tracking detectors, trigger detectors, and partial coverage of electromagnetic calorimetry inside a 0.5 T solenoid. The measurements will be carried out at midrapidity, over a large pseudorapidity range ($|\eta| < 4$) with full azimuthal coverage ($|\Delta(\phi)| = 2\pi$). The tracking detectors are a silicon vertex tracker covering $|\eta| < 1.7$ and a forward radial-drift TPC covering $2.5 < |\eta| < 4$. In addition

to the tracking detectors, the electromagnetic calorimeter will measure the transverse energy of events, and trigger on and measure high transverse momentum photons. The STAR detector system will simultaneously measure many experimental observables to study signatures of the QGP phase transition as well as the space-time evolution of the collision process.

A highly granular photon multiplicity detector is being planned for the STAR, which in combination with charged particle detectors and forward TPC, will be quite adequate for DCC search, in event-by-event mode. Here one would be able to select on the low- p_T particles, characteristic of DCC pions, and to study π^{+-} spectra at low- p_T .

PHENIX. The physics goals of PHENIX [1, 8] (Pioneering High Energy Interaction eXperiment) are to measure as many potential signatures of the QGP as possible. PHENIX will measure lepton pairs, photons and hadrons, being sensitive to very small cross section processes, as the production of the J/ψ , ψ' and high- p_T spectra. The PHENIX detector consists of three spectrometers: two muon spectrometers covering the full azimuth for $1.1 < |\eta| < 2.4$ and a central spectrometer consisting of two arms each subtending 90° in azimuth and with $|\eta| < 0.35$. DCC search in PHENIX will be possible by correlating signals from charged particle detectors and photons from the electromagnetic calorimeter. Global event characterization is achieved via a silicon multiplicity-vertex detector covering $|\eta| < 2.5$ around midrapidity.

BRAHMS. Small experiment [1] with a forward and midrapidity hadron spectrometer. The detectors used include TPC's, wire chambers, Cerenkov counters, and a time-of-flight system. Their experimental emphasis is a particle identification over a broad rapidity range, covering nearly 12 units of rapidity, well beyond the other experiments capabilities. This may allow one to explore the more baryon dense matter at forward and backward rapidities. BRAHMS experiment is considered to add a photon arm to look for DCC.

Among the experiments planned for LHC there was *FELIX* (Forward ELastic and Inelastic eXperiment) [158]. It was a proposal for a full-acceptance detector and experimental program for the LHC dedicated to study QCD in all its aspects, hard and soft, perturbative and nonperturbative, particularly to investigate also exotic phenomena. Unfortunately it was rejected.

The other one is *CASTOR* [17, 139]. It is a dedicated detector for Centauro and strangelet search in the very forward rapidity region, in nucleus–nucleus collisions. Initially it has been proposed as a part of the ALICE experiment [159]. More recently it has been incorporated into the CMS detector system [160] where the heavy ion program is presently intensively developed, as the complement to pp physics [161].

Generally, different strategies of searching for Centauro related phenomena are proposed by different experiments, dependently on the preferred model. The present and future experiments prefer mostly the DCC mechanism, where the large

imbalance in the production of charged-to-neutral pions could be the result of the approximate restoration of the chiral symmetry. Sophisticated analysis methods are being developed to disentangle DCC events out of the large background of events with conventionally produced particles.

5. CASTOR: A DETECTOR FOR CENTAURO AND STRANGE OBJECT RESEARCH

Heavy ion experiments at CERN LHC will be mainly concentrated in a limited angular region around midrapidity, for example ALICE will be fully instrumented for the hadron and photon identification only in a limited angular region covering the pseudorapidity interval $|\eta| \leq 1$. It constitutes only a small part of the available phase space which, at the beam energy of $2.75 A \cdot \text{TeV}$ for Pb ions at LHC, extends to $|\eta| = 8.7$. Therefore, in addition to the main detector system some smaller detectors covering more forward rapidity region are also foreseen (see, for example, [162–164]).

Already at the early stages of the preparation of the physical motivation for the heavy ion studies at the LHC it was pointed out [165] that the interesting physics beyond midrapidity should be the additional subject of the investigations. From these considerations the idea of the CASTOR detector evolved. CASTOR is dedicated to study the novel phenomena expected to appear in the high baryochemical potential environment produced in Pb + Pb collisions at LHC energies, in particular the formation of Deconfined Quark Matter (DQM), which could exist, e. g., in the core of neutron stars, with characteristics different from those expected in the much higher temperature baryon-free region around midrapidity. Its signatures could be Centauro species, strongly penetrating objects, DCC, etc. [166]. Some theoretical considerations suggest [167] that the phase diagram features a critical endpoint at which the line of the first order phase transition ends. Passing close enough to this critical endpoint should have characteristic experimental consequences, such as a nonmonotonic dependence of the control parameters. Other theoretical ideas attracting a lot of attention are the possibilities of formation of states with different kinds of quark condensates (e. g., colour superconductivity) and the phase transitions between them [168].

In addition, the wide program concerning pp physics at the forward rapidity region is intensively developed for the CASTOR detector.

CASTOR will cover the very forward rapidity region ($\sim 5.6 < \eta < 7.2$) and it was originally proposed to consist of a silicon charged particle multiplicity detector, a silicon photon multiplicity detector, and a quartz fibre tungsten calorimeter with electromagnetic and hadronic sections. The scheme of the apparatus is shown in Fig. 23.

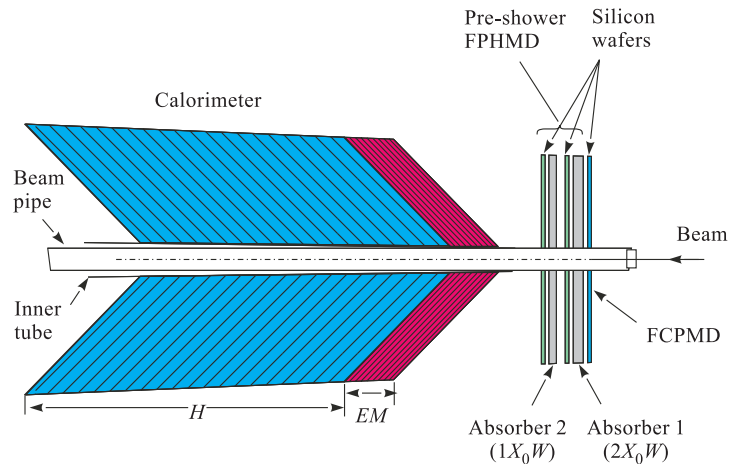


Fig. 23. Schem of the CASTOR detector

The LHC, with an energy equivalent to $\sim 10^{17}$ eV for a moving proton impinging on one at rest, will be the first accelerator to effectively probe the highest cosmic energy domain. From Fig. 2 it is seen that CASTOR is located at the region of a maximum baryon number, high energy flow, and low multiplicity, similarly as majority of cosmic-ray experiments.

The basic experimental aim of CASTOR is to identify events with characteristics similar to those of the exotic cosmic-ray events, in an event-by-event mode. It will look for:

- extreme imbalance between the hadronic and photonic components, both in terms of the particle multiplicity and the energy content of the event;
- nonuniform (in azimuthal angle ϕ) deposition of a large amount of energy;
- highly penetrating objects, far beyond the range of normal hadrons;
- abnormal shapes and structures seen in the transition cascade curves in the calorimeter.

The project is motivated by the experimental evidence of exotic cosmic-ray events on the one side and by theoretical expectations on the other hand [24, 169]. The model of [23, 24] was used to simulate the detector system performance.

5.1. The Design of the CASTOR Calorimeter. At the first stage of the project realization the building of only the calorimeter is planned. The idea of building of the second calorimeter POLLUX, at the opposite side of the interaction point, and additional silicon detectors for measurements of the photon and hadron multiplicity is also considered. Here will be presented the basic version of the

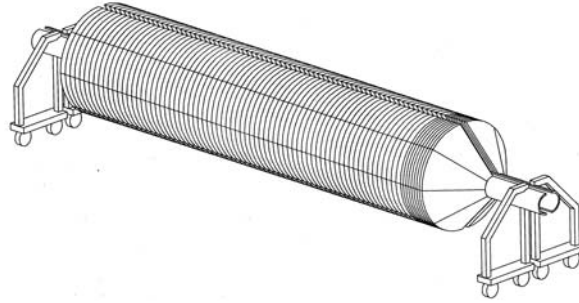


Fig. 24. View of the CASTOR calorimeter

calorimeter. Some further refinements of this design are being considered, but these are not expected to alter its response in an essential way. The general view of the CASTOR calorimeter is shown in Fig. 24.

The calorimeter will be made of layers of active medium sandwiched between tungsten absorber plates. The active medium consists of planes of silica fibres, and the signal will be the Cherenkov light produced as they are traversed by charged particles from the shower. The fibres are inclined at 45 degrees relative to the incoming particles to maximize light output. The calorimeter is azimuthally divided into 8 octants. Each octant is longitudinally segmented into 80 layers, the first 8 ($\simeq 14.7X_0$) comprising the electromagnetic section; and the remaining

Table 11. CASTOR calorimeter specifications

	Electromagnetic	Hadronic
Material	Tungsten + Quartz Fibre	Tungsten + Quartz Fibre
dimensions, mm	$\langle R_{in} \rangle = 26,$ $\langle R_{out} \rangle = 129$	$\langle R_{in} \rangle = 27,$ $\langle R_{out} \rangle = 134$
Absorber plates at 45° , mm	Thickness = 5 Eff. thickness = 7.07	Thickness = 10 Eff. thickness = 14.1
No. of layers	8	72
Eff. length	$56.6 \simeq 14.7X_0 \simeq 0.53\lambda_I$	$1018.1 \simeq 9.47\lambda_I$
Quartz fibre, mm	~ 0.45	~ 0.45
No. of QF planes	2 per sampling	4 per sampling
Sampling	$\simeq 1.84X_0$	$\simeq 0.13\lambda_I$
Reading	Coupling of 4 samplings	Coupling of 4 samplings
No. of readings	2	18
No. of channels	$2 \times 8 = 16$	$18 \times 8 = 144$
QF/W vol., %	10	10

72 ($\simeq 9.47\lambda_I$), the hadronic section. The light output from groups of 4 consecutive active layers is proposed to be coupled into the same light guide, giving a total of 20 readout channels along each octant. Such a calorimeter works as a «shower core» detector, sampling essentially only the part of the shower which lies within a narrow cone around the direction of the particle. Thus the energy of a hadronic shower can be reliably measured also very close to the calorimeter's edge. The transverse width of the hadron shower is about 7 mm (at 200 GeV). The calorimeter is planned to be located at a distance of ~ 1740 cm from the beam interaction point.

The detailed specifications of the basic version of the calorimeter are given in Table 11.

5.2. Probes and Observables of LHC Centauros and Strangelets. According to this model, Centauros are formed in central collisions of ultrarelativistic nuclei. Thus the future collider experiments with heavy-ion beams seem to be appropriate to look for them. Some predictions concerning Centauros which could be produced at RHIC have been given in [23]. The kinematical conditions accessible at RHIC will be very close to these at which cosmic ray Centauros are produced. Almost the same value of energy per nucleon ($\sqrt{s^{\text{RHIC}}} = 200 A \cdot \text{GeV}$ in comparison with $\sqrt{s_{\text{cos.ray}}^{\text{Cent}}} = 233 A \cdot \text{GeV}$) allows one in an easy way to predict the typical features of Centauros expected to be produced at RHIC. In particular, the assumption that transverse momentum of the fireball decay products will be roughly the same for cosmic ray and RHIC Centauros seems to be reasonable. The question is, however, the existence of the baryon rich environment. The first measurements of the ratio of antiprotons to protons [8] indicate that the central region, which is mostly explored by all four RHIC experiments, is meson-dominated. At the LHC the situation will be different, although the crucial conditions for the Centauro events production seem to be well fulfilled. The energy accessible in Pb + Pb central collisions at the LHC ($\sqrt{s^{\text{LHC}}} \simeq 5.5 A \cdot \text{TeV}$, i. e., $\sqrt{s_{\text{tot}}^{\text{LHC}}} \simeq 1150 \text{ TeV}$) will be much higher than the threshold energy for Centauro species production. At the LHC, a region of vanishing baryon density is expected at midrapidity and the pronounced baryon-rich region with maximum baryon density at rapidity between 5–7 (see Fig. 2). Thus the *existence of baryon-rich environment*, which is the essential requirement for the Centauro species production, is also expected. The baryon rich environment is expected to be placed at LHC in the forward rapidity region, what is consistent with the observation of cosmic ray Centauros in the projectile fragmentation range (see Table 2).

5.2.1. Rate of Centauros in CASTOR. The important point is how many Centauros can be produced and detected in CASTOR. The evaluation of the possible rate of Centauros N_{Cent} can be obtained from the formula:

$$N_{\text{Cent}} \simeq N_{\text{coll}}^{\text{centr}} \times P_{\text{Cent}}^{\text{prod}} \times P_{\text{Cent}}^{\text{decay}}, \quad (26)$$

where $N_{\text{coll}}^{\text{centr}}$ is the number of central Pb + Pb collisions during one year of the experiment run; $P_{\text{Cent}}^{\text{prod}}$ is a probability of producing Centauro event in such collision; and $P_{\text{Cent}}^{\text{decay}}$ is a probability of Centauro fireball decay before the CASTOR detection system. To observe the distinct Centauro characteristics in the calorimeter, a decay of the fireball at a distance shorter than 1 m from the interaction point is required. Then

$$P_{\text{Cent}}^{\text{decay}} = 1 - \exp(-1m/(c\tau_0\gamma)). \quad (27)$$

Assuming the Centauro fireball gamma factor $\gamma \simeq 300$ and its lifetime $\tau_0 = 10^{-9}$ s, one obtains that a probability of a Centauro decay at the path shorter than 1 m is greater than 1%. In the opposite case, it could be possible to observe a very big amount of energy released somewhere in the calorimeter and concentrated within very narrow angular cone. Conservatively, we estimated $\sim 0.1\%$ rate of the produced and detected Centauros among the central collisions.

5.2.2. Average Characteristics Estimates. The main features of Centauros and strangelets produced at the LHC can be evaluated by extrapolating the characteristics of these objects registered in cosmic-ray energy range or by doing analytical calculations based on the model. More detailed characteristics and the distributions of the characteristic quantities can be predicted by using Monte Carlo methods (see the next section).

In particular, keeping in mind that shapes of the angular and energy fraction spectra of Centauro secondaries are consistent with isotropic emission of particles from a fireball, we can expect a Gaussian-type pseudorapidity distribution for decay products of «LHC» Centauros. The centre of the distribution, being the function of both the nuclear stopping power Δy_{stop} and a rapidity shift caused by a transverse momentum of emitted particles Δy_{PT} , is generally expected to be placed close to the maximum of the baryon number distribution, i. e.,

$$\langle y \rangle_{\text{Cent}}^{\text{LHC}} \simeq y_{\text{beam}} - \Delta y_{\text{stop}} - \Delta y_{\text{PT}} \simeq 8.7 - 2.0 - 0.9 \simeq 5.8. \quad (28)$$

The first rough evaluation of the optimal position and size of the CASTOR detector and the estimation of its geometrical acceptance [139,170] were done in this way.

Evaluation of other characteristic quantities, as for example the types and multiplicities of produced particles, needs, however, some additional assumptions. The expected multiplicities of kaons $N_{K^++K^0}$, nonstrange baryons N_h , the total number of nuclear active particles N_n , and the baryon number of a strangelet A_{str} emitted from the decay of a Centauro fireball produced in central Pb + Pb collisions at LHC energies were estimated in [170] for two different, extreme scenarios:

1. *Lower limit of the energy density (and temperature).* In the most conservative case it can be assumed that the transverse momentum of the decay

products of LHC Centauro fireball is the same as for cosmic-ray Centauros, i. e., $\langle p_T \rangle \sim 1.7$ GeV/c. Then the average Centauro fireball mass can be estimated from the relation:

$$\langle M_{\text{fb}} \rangle = \langle N_n \rangle \langle E_n \rangle, \quad (29)$$

where $\langle N_n \rangle$ is the mean number of nuclear active particles emitted from the Centauro fireball and $\langle E_n \rangle$ is the mean particle energy in the fireball rest system. One can assume that $\langle N_n \rangle$ equals the number of participating projectile nucleons $\langle N_p \rangle$, i. e., it is in the range of 150–207 for central Pb + Pb collisions and

$$\langle E_n \rangle = \sqrt{((4/\pi)p_T)^2 + M_N^2} \simeq 2.4 \text{ GeV}, \quad (30)$$

where M_N is the nucleon mass.

The volume V_{fb} of the fireball and the number of participating nucleons N_p can be evaluated from simple geometrical considerations. For the volume $V_{\text{fb}} \sim 117 \text{ fm}^3$, corresponding to a central collision with the number of participating nucleons $N_p \sim 150$ ($b \leq 5 \text{ fm}$) [23], these assumptions lead to $M_{\text{fb}} \simeq 350 \text{ GeV}$ and to energy density of LHC quark matter fireball

$$\varepsilon_{\text{fb}} = M_{\text{fb}}/V_{\text{fb}} \simeq 3 \text{ GeV/fm}^3, \quad (31)$$

which is close to that reached in cosmic-ray Centauro events. Using the phase curve given by Eq. (14) with the reasonable strangeness equilibration factor ($\gamma_s \sim 0.4$) one can find that such energy density corresponds to the temperature $T \sim 130 \text{ MeV}$ and to the chemical potential of quark $\mu_q \sim 590 \text{ MeV}$, and the average characteristics of LHC Centauros could be close to those observed in cosmic ray experiments. In particular, the maximal number of emitted K^+ and K^0 for $T = 130 \text{ MeV}$ and the volume corresponding to the numbers of participating nucleons in the range of $N_p \sim 150$ –207 is estimated to be $N_{K^++K^0} \sim 16$ –20 (from equations (20) and (21)). The maximal baryon number of a strangelet will be reached when in the process of strangeness distillation all s quarks will be absorbed in the strangelet, and then $A_{\text{str}} \simeq 16$ –20. Consequently the number of emitted nonstrange baryons

$$N_h \simeq N_n - N_{K^++K^0} \simeq 134$$
–187. (32)

In general, assumption of constancy of $\langle p_T \rangle$ allows one to expect that the values of characteristic quantities (N_h , M_{fb} , ε , T , μ) for Centauros possibly produced at RHIC (Au + Au) and at LHC (Pb + Pb) should be similar one to the other. These values should not also be very different from those found for cosmic-ray Centauros.

2. *Upper limit of the energy density (and temperature).* Assumption of the same $\langle p_T \rangle$ of decay products of cosmic-ray and RHIC Centauros seems to

be reasonable because $\sqrt{s_{NN}^{\text{RHIC}}} \simeq \sqrt{s_{NN}^{\text{cos.ray}}}$. However, it could be no longer valid for LHC because $\sqrt{s_{NN}^{\text{LHC}}} \gg \sqrt{s_{NN}^{\text{cos.ray}}}$. We can expect $\varepsilon_{\text{Cent}}^{\text{LHC}} \gg \varepsilon_{\text{Cent}}^{\text{cos.ray}}$. J. Schukraft quoted in [171] the values of $\varepsilon^{\text{LHC}} \sim 8 - 27 \text{ GeV/fm}^3$ (averaged over different papers) as expected at Pb + Pb central collisions. K. Geiger [172] claimed even $31(17) \text{ GeV/fm}^3$ as the upper limit of the energy density, averaged over the whole central volume, at Au + Au (S + S) central collisions. In such a case the assumption of constancy of the mean transverse momentum can be unjustified. In connection with it, much higher values of the temperature and chemical potential of quark can be reached. It would probably allow one to reach the region of the *ideal QGP*, however, it is not easy to predict the quantitative features of Centauros at these conditions. Estimates of the ranges of characteristic quantities and indications of the most typical signatures of «LHC» Centauros were presented in [17, 139, 170]. Generally, much higher numbers of produced strange quarks ($\rho_{\bar{s}} \gg 0.14 \text{ fm}^{-3}$, e. g., $\rho_{\bar{s}} \simeq 0.5 \text{ fm}^{-3}$ for $T = 190 \text{ MeV}$), and hence higher multiplicities of produced kaons and bigger strangelets can be expected. At the temperature $T \sim 190 \text{ MeV}$ the number of emitted kaons could be $N_{K^+ + K^0} \sim 55-68$, the number of nonstrange baryons $N_h \sim 95-139$, and strangelets with baryon numbers as large as $A_{\text{str}} \sim 55-68$ could be formed.

5.2.3. Expected Signatures. From the above considerations it is clear that «LHC» Centauros should be characterized by signatures dramatically different from other «normal» events. The most typical signatures will be the following:

1. *Abnormal photonic to hadronic ratio.* It is expected that both:

- hadronic to photonic energy ratio E_h/E_γ ,
- hadron to photon multiplicity ratio N_h/N_γ should be much bigger than in «normal» hadronic interactions.

2. *Very low total multiplicity.* The total multiplicity of «LHC» Centauro decay products is expected to be extremely small in comparison with enormous total multiplicity of particles predicted to be produced in «usual» events in Pb + Pb central collisions at LHC energies [171].

3. *Very specific picture of the time development connected with the abnormal particle composition.* The following products of time evolution of the «LHC» Centauro (at projectile fragmentation rapidity) could in principle be observed:

- *Particles K^+ and K^0 .* K^+ and K^0 are expected to be the firstly emitted particles from the long-lived Centauro fireball. Regardless of the long lifetime ($\tau_0 \simeq 10^{-9} \text{ s}$) of the fireball these pre-equilibrium particles will be emitted within very short time interval ($\Delta\tau \simeq 10^{-22} \text{ s}$) and could be observed in detectors much earlier than other decay products of Centauro*. The total number of emitted K^+

*They are emitted practically at the point of interaction; $l = c\gamma\Delta\tau = c\cos\theta\Delta\tau \simeq (0.6-0.9) \cdot 10^{-11} \text{ cm}$, when assuming $\gamma = \cos\theta = 200-300$.

and K^0 can be maximally equal to the number of $s\bar{s}$ pairs created in the volume V_{fb} of the Centauro fireball and several tens of kaons could be produced.

- *Strange quark matter metastable object with small Z/A ratio.* This state is formed after the pre-equilibrium emission of kaons. Then the fireball is a mixture of u , d , and s quarks and experimentally it can be identified by its Z/A ratio less than that of the ordinary nuclear matter. The change of Z/A ratio, because of a kaon emission can be calculated from formulas (22) and (23). Assuming $(Z/A)_i \simeq 0.5$ and the temperature in the range $\sim 130\text{--}190$ MeV one evaluates $(Z/A)_f \simeq 0.45\text{--}0.3$. This slightly strange quark-matter fireball decays after a relatively long time $\tau_0 \sim 10^{-9}$ s. Taking into account consequences of the collider kinematics, which decreases the lab-frame decay lengths, and assuming $\gamma \sim 200\text{--}300$, the object will decay after traveling the path of the order $\sim 60\text{--}90$ m.

- *Nonstrange baryons and highly penetrating strangelet(s).* They should be observed at the last stage of the «Centauro» evolution as the result of the decay of the strange quark matter state after the process of strangeness separation.

Table 12. Average characteristics of Centauro events and Strangelets produced in cosmic rays and at the LHC [17]

Centauro	Cosmic Rays	LHC
Interaction	«Fe + N»	Pb + Pb
\sqrt{s}	≥ 6.76 TeV	$5.5 A \cdot \text{TeV}$
Fireball mass, GeV	≥ 180	~ 500
y_{proj}	≥ 11	8.67
γ	$\geq 10^4$	$\simeq 300$
η_{Cent}	9.9	$\sim 5\text{--}7$
$\langle p_T \rangle$, GeV	1.75	1.75 *
Life-time, s	10^{-9}	10^{-9} *
Decay prob., %	10 ($x \geq 10$ km)	1 ($x \leq 1$ m)
Strangeness	14	60–80
$f_s(S/A)$	$\simeq 0.2$	$\sim 0.1\text{--}0.4$
Z/A	$\simeq 0.4$	$\sim 0.3\text{--}0.4$
Event rate, %	≥ 1	$\simeq 0.1$ central coll.
«Strangelet»	Cosmic Rays	LHC
Mass, GeV	$\simeq 7\text{--}15$	10–80
Z	$\simeq 0$	$\simeq 0$
f_s	$\simeq 1$	$\simeq 1$
η_{str}	$\eta_{\text{Cent}} + 1.2$	$\eta_{\text{Cent}} + 1.2$
* Assumed.		

Assuming that all strange quarks are absorbed in the strangelet and $N_s/A_{\text{str}} \sim 1$, the formation of small strangelets characterized by the baryon numbers of several tens should be expected (see the previous section). In principle, the formation of one bigger or several smaller strange droplets could be possible. The number of emitted nonstrange baryons depends on the size of the strangelet and was estimated to be in the range $\sim 70\text{--}190$. Some average characteristic quantities of Centauros and Strangelets produced in cosmic rays and expected at the LHC are compared in Table 12.

The events of such type may be easily observed in detectors with particle identification, such as silicon detectors, TPC, etc. (the most important is to distinguish between kaons, baryons, and pions). What regards strangelets, if the hypothesis that the cosmic-ray long-flying component is a result of passing of strangelets through the apparatus is true, we could look for them using the deep forward calorimeters. Penetrating through calorimeters they could produce (via their weak decays or by interactions with absorber nuclei) successive maxima seen in their transition curves. Observation of anomalous transition curves needs sufficiently deep calorimeters (above 120 c.u.) with granularity good enough for watching individual cascade development, and detection layers placed every 2–3 c.u. One could consider also the idea of using simple and unexpensive CR-39 plastic detectors which could look for both the high Z quark matter fireballs and for accompanying strangelets.

The important questions, concerning the sensitivity of the CASTOR detector for these signatures and the influence of the background on the distinction of the signals, have been answered by means of the Centauro and Strangelets generators described in the next section.

6. CENTAURO AND/OR STRANGELET SIMULATIONS

6.1. Generator for Centauros. The Monte Carlo generator of Centauro events is based on the phenomenological model of [23,24] and it was described in detail in [173]. The model is formulated in terms of the impact parameter b of the ion collisions, two thermodynamical parameters, baryochemical potential μ_b and temperature T , and the nuclear stopping power Δy_{stop} . The generator calculates the Centauro fireball parameters and produces a full event configuration according to the fireball evolution scenario.

According to the model, the Centauro events occur in the projectile fragmentation region when the projectile nucleus penetrating through the target nucleus transforms its kinetic energy into heat and forms hot quark matter (Centauro fireball) with the high baryochemical potential. The produced glob of deconfined quark matter initially contains u , d quarks, and gluons only, and it is characterized by temperature T and the baryochemical potential μ_b . Its energy density ε and

other thermodynamical quantities, such as baryon/quark number density n_q , are calculated from equations (14) and (16) respectively. The number of quarks N_q in the Centauro fireball is defined from the collision geometry as $N_q = 3N_b$. The baryon number of the fireball, N_b , is calculated from the relation:

$$N_b = 0.9V_{\text{ovr}}(A_1/V_1). \quad (33)$$

The factor 0.9 stands for the central part of the overlapping region V_{ovr} of colliding nuclei with the atomic numbers A_1 and A_2 . Hence one can obtain the volume V_{fb} as well as the mass M_{fb} of the fireball

$$V_{\text{fb}} = N_q/n_q, \quad M_{\text{fb}} = \varepsilon V_{\text{fb}}. \quad (34)$$

At the second stage of the Centauro fireball evolution a partial chemical equilibrium is achieved by coupling \bar{s} quarks with u and d quarks and emission of K^+ and K^0 mesons, what decreases the temperature and entropy. The number of $s\bar{s}$ pairs inside the fireball and hence the number of emitted kaons is calculated from equations (20) and (21).

$$N_s = N_{K^+ + K^0} = n_s V_{\text{fb}}. \quad (35)$$

After emission of $2N_{\bar{s}}$ quarks with kaons, the mass of the remaining strange quark matter (SQM) fireball is defined by the average quark energy and the number of quarks in the Centauro and SQM fireball:

$$M_{\text{SQM}} = M_{\text{fb}}(1 - 2N_{\bar{s}}/n_q). \quad (36)$$

This antistrangeness emission is described as an isotropic decay of the Centauro fireball into $N_{\bar{s}}$ kaons and the SQM fireball with the mass M_{SQM} . At the final stage of the evolution the SQM fireball decays into baryons and strangelets.

6.2. Simulations of Centauro Events. As it was shown in [173] the generator reproduces the main features of Centauro cosmic ray events. Simulations of Centauro events formed in Pb + Pb central collisions at $\sqrt{s} = 5.5 A \cdot \text{TeV}$ have been firstly performed in [173]. New simulations, in an extended range of parameters, were done more recently [174,175]. Different sets, each consisting of 10000 events, were generated. The very central collisions with $0 < b < 1$ fm were studied. Simulations were done for the temperature $T = 130, 200, 250,$ and 300 MeV and baryochemical potential $\mu_b = 1, 1.8,$ and 3 GeV. The nuclear stopping power parameter values were put $\Delta y_{\text{n.s}} = 1.5, 1.0, 0.5$. Keeping in mind the high values of the temperature, and in consequence very high transverse momenta of particles emitted from the fireball, such values of Δy_{stop} lead to the effective stopping bigger than the assumed Δy_{stop} value, at least about one rapidity unit. It gives the position of the maximum of the pseudorapidity distribution

of baryons in accordance with that predicted by HIJING/VENUS generators. The strong coupling constant α_s was taken as 0.3.

The characteristics of simulated Centauro events are apparently different from those obtained from «usual» (e. g., HIJING) generators.

In particular, Centauro events are characterized by almost total absence of a photonic component among secondary particles. The majority of secondary particles are baryons. Some kaons emitted from the primary fireball decay into neutral pions which in turn give photons, but the neutral pion production is suppressed here strongly.

The next surprising feature is a multiplicity of Centauro events which is much smaller than the one predicted by «conventional» generators for nucleus–nucleus

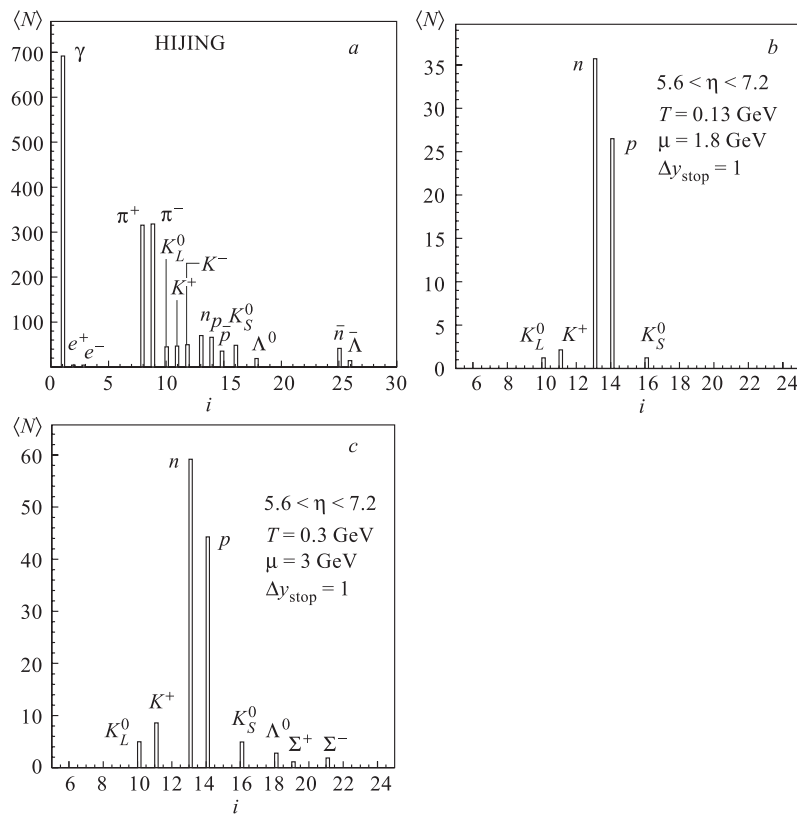


Fig. 25. Average multiplicities of particles produced in a «usual» (HIJING) event (a) and by the Centauro mechanism (b, c). Only particles within CASTOR acceptance are shown

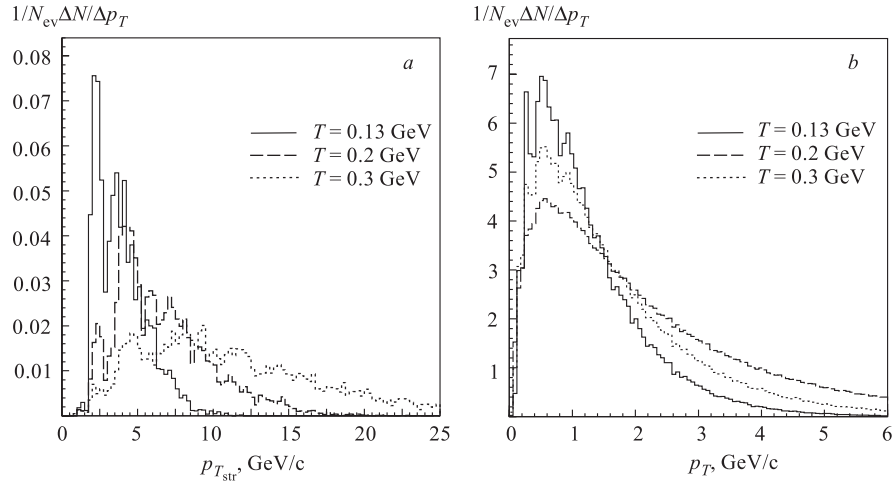


Fig. 26. Transverse momentum distributions of strangelets (a) and hadrons from the Centauro decay (b) ($\mu_b = 1.8$ GeV; $\Delta y_{\text{stop}} = 1$)

collisions at that energy. In Ref. [170] the expected average multiplicities of kaons, nonstrange baryons and the total number of nuclear active particles emitted from a decay of a Centauro fireball, produced in central Pb + Pb collisions at LHC energies, were estimated in analytical way (see Subsec. 5.2.2). The results of the simulations are illustrated in Fig. 25 which shows the average multiplicities of different kinds of particles produced by Centauro mechanism, contained within the geometrical acceptance of the CASTOR, in comparison with the HIJING predictions. The average multiplicities for two sets of events, characterized by $T = 130, 300$ MeV and $\mu_b = 1.8, 3.0$ GeV, are shown as the examples.

Secondary particles in the Centauro events have larger mean transverse momenta in comparison with ordinary hadronic interactions. In usual events, the average transverse momentum of produced particles $\langle p_T \rangle = 0.44$ GeV/c, as predicted by HIJING, which is several times smaller than that of Centauro events. Figure 26 shows distributions of transverse momenta of strangelets and other Centauro decay products for three different temperatures $T = 130, 200,$ and 300 MeV.

The position and shape of rapidity (pseudorapidity) distributions of decay products of the Centauro fireball depend on thermodynamical variables (μ_b and T) and mainly on the nuclear stopping power $\Delta y_{\text{n.s.}}$. Thus the detection probability of Centauro events in the CASTOR detector is also the function of these variables. Figure 27 shows the probability of the production of a strangelet (full line) and other particles (dashed line) from the Centauro fireball decay, as a function of

pseudorapidity η . The region of geometrical acceptance of CASTOR is indicated. Three sets of events with different values of parameters were chosen as examples. It is seen that a strangelet, as it should be expected from cosmic ray observations, always flies in a more forward direction than other particles. The difference is of the order of one pseudorapidity unit. As a consequence, the simultaneous detection of a strangelet and other Centauro decay products will be sometimes excluded. The big chance for detection of both species simultaneously is when

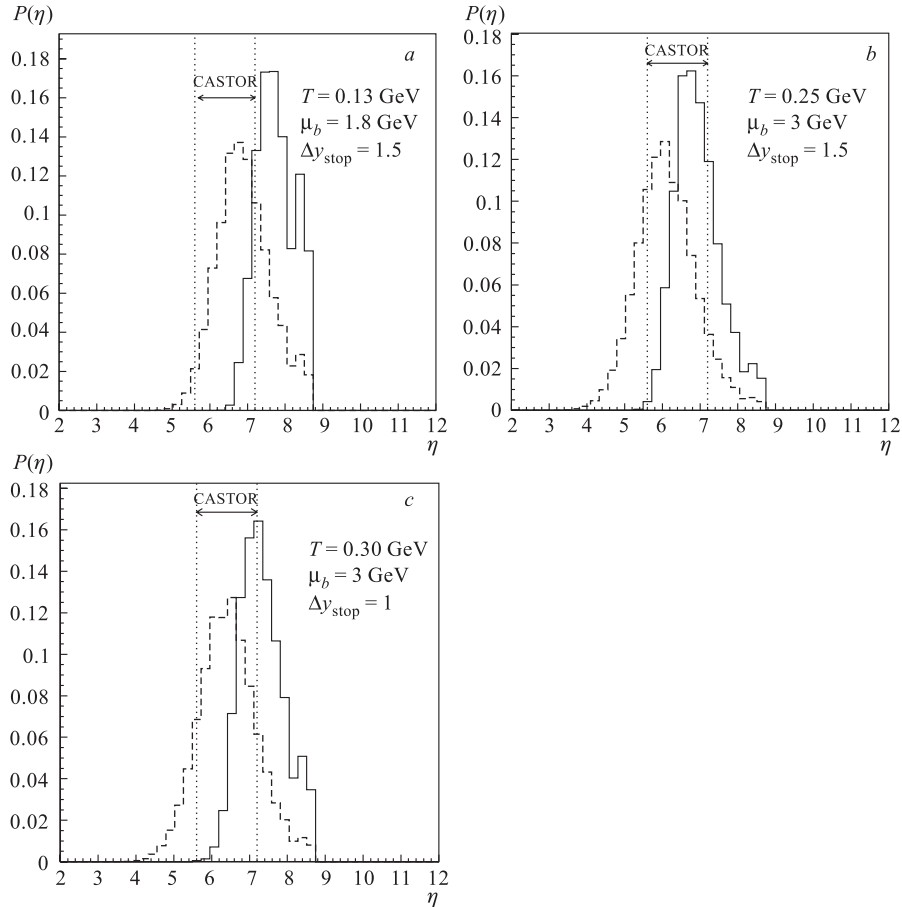


Fig. 27. Probability of a strangelet (full line) and other particles (dashed line) production from the decay of the Centauro fireball as a function of pseudorapidity. The region of the geometrical CASTOR acceptance is indicated with dotted lines

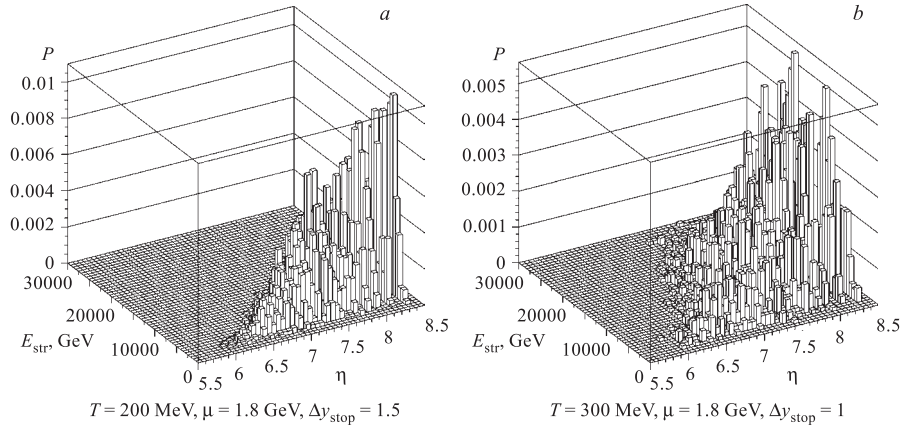


Fig. 28. Probability of a strangelet production as a function of its energy and pseudorapidity

temperature, chemical potential of quark and nuclear stopping power values are close to $T \sim 250$ MeV, $\mu_b \sim 3$ GeV, and $\Delta y_{\text{stop}} \sim 1.5$.

Figure 28 shows two-dimensional lego histograms which illustrate the probability of a strangelet production, as a function of their pseudorapidity and energy.

The question of acceptance has been investigated in analytical way in [170] and later, by simulations, in [173–175]. For the reasonable values of parameters more than 50% of energy (or the number of produced particles) of an event falls into the detector. The maximal degree of containment of Centauro decay products is close to ~ 0.74 .

6.3. Exotic Objects in Deep Calorimeters. Basing on the model of the strangelet formation in the quark-matter (Centauro) fireball, one can expect that at the LHC kinematical conditions the production of a variety of strangelets, characterized by a wide spectrum of the baryon numbers ($A_{\text{str}} \sim$ several tens for the temperature $T \sim 130$ – 190 MeV and quark chemical potential $\mu_q \sim 600$ – 1000 MeV) should be possible (see Sec. 5.2 and Table 12). The important question is what signals will be produced by such exotic objects during their passage through the deep calorimeters, and if these signals can be distinguished from those produced by conventional events. It should be mentioned, however, that properties of CASTOR-type calorimeters differ from those of the deep emulsion chambers used in cosmic ray experiments. The latter have a very fine lateral resolution ($\sim 100 \mu\text{m}$), allowing for the observation of the development of individual cascades through the whole calorimeter depth. In contrast, in the CASTOR-type calorimeter, the signal produced by a strangelet will be detected simultaneously with those generated by other particles entering the same calorimeter octant. Thus,

the additional question is the intensity and the shape of a possible background and an ability to extract an «exotic» signal from it.

Two possible «exotic» scenarios were investigated. In the first one it was assumed that strangelets were born anyway among other conventionally produced particles [25,176] (see Subsec. 6.3.1). In the second case, strangelets produced as remnants of the Centauro fireball explosion, according to the mechanism proposed in [24] (see Subsec. 6.3.2) were considered. In this case the signal will be the sum of a strangelet transition curve and the one produced by nucleons coming from the isotropic decay of the Centauro fireball. This case has been preliminarily investigated in [25] and recently more detailed simulations have been done [175] by GEANT 3.21. In both cases the background was estimated by means of the HIJING generator, assuming that the part of energy going into a conventional particle production equals the difference between the total energy available in the phase space region (and being ~ 150 TeV within the CASTOR acceptance) and the energy taken by a Centauro fireball and/or a strangelet.

6.3.1. Strangelets in the Deep Calorimeter. The scenario, in which strangelets are born together with other conventionally produced particles was investigated in [25,176] for both short-lived and stable strangelets.

Short-Lived Strangelets. Unstable objects which can decay via strong interactions ($\tau_0 \leq 10^{-20}$ s) or the metastable ones decaying via weak nucleonic decays (see Subsec. 3.4.2) were named short-lived strangelets. Generally, however, the lifetimes of small metastable strangelets are not predicted precisely at present [120,146]. If their lifetimes are shorter than $\sim 10^{-10}$ s they could decay before reaching the CASTOR calorimeter and give the same picture as unstable strangelets. In the opposite case the situation is analogous to the case of «stable» strangelets, considered later. The complete decay of a strangelet via strong processes or its fission into a daughter strangelet and an arbitrary number of hadrons is possible. A daughter strangelet will be shifted to a higher strangeness factor f_s . After surviving a strong and possibly also weak nucleonic decay it can reach the region of a very high strangeness factor ($f_s \geq 2.2$) where it is expected to become a long-lived (stable) object [117]. The algorithm of the calculations was the same as used previously for cosmic-ray events (see Subsec. 3.4.2). It was assumed, for simplicity, that a strangelet decays only via neutron emission. Unstable strangelets decay very fast, practically at the point of their formation, thus the considered picture resolves into the simple case of a bundle of neutrons entering the calorimeter.

As has been shown in [25], the scenario in which an unstable or metastable strangelet via strong or weak decays produces a strongly collimated bundle of neutrons, successfully describes the long-range many-maxima cascades observed in the cosmic ray experiments. The successive maxima, seen in the structure of a transition curve, could be the result of interactions of such neutrons in the apparatus.

The general conclusion concerning the signals produced in the CASTOR calorimeter by short-lived strangelets, formed in Pb + Pb interactions at the LHC, is the same as in the study of the cosmic-ray strangelets. Bundles of collimated neutrons can give in the CASTOR calorimeter the unconventional many-maxima signal. Its longitudinal structure and extent depend, of course, on the strangelet energy and on the number of evaporated neutrons N_n . Figure 29 shows three examples of transition curves produced by bundles of 7 and 12 neutrons of energy $E_n \approx 1.2$ TeV and 20 neutrons of energy $E_n \approx 1$ TeV, evaporated by a short-lived strangelet with the baryon number $A_{\text{str}} = 40$. They are compared with the possible background (full line histogram) estimated by HIJING, assuming that the rest of the available energy (i. e., not carried by the strangelet) is going into conventional particle production. For comparison, particles produced in one central Pb + Pb collision were taken.

It was found that a bundle of several neutrons ($N_n > 7$) possessing sufficiently high energies ($E_n > 1$ TeV) produces in the calorimeter a signal which can be distinguished from the conventional event signal. The strangelet signal is higher, has longer longitudinal extent and reveals a many-maxima structure in contrast to the rather smooth background.

Long-Lived Strangelets. «Stable» objects, capable to reach and pass through the apparatus without decay, i. e., having a lifetime $\tau_0 \geq 10^{-8}$ s to traverse the CASTOR calorimeter, were named long-lived strangelets. Similarly, as in the case of cosmic ray strangelets, the simplified picture [25] of the interaction of a stable strangelet in the calorimeter absorber was assumed. Penetrating through the calorimeter a strangelet collides with tungsten nuclei. The mean interaction

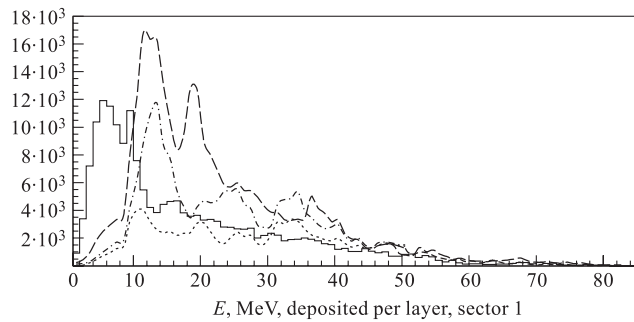


Fig. 29. Transition curves produced by bundles of 7 (dotted-dashed curve) and 10 (dotted curve) neutrons of energy $E_n \approx 1.2$ TeV and 20 (dashed curve) neutrons of energy $E_n \approx 1$ TeV evaporated by a short-lived strangelet of $A_{\text{str}} = 40$. Full line histogram shows the HIJING estimated background. Energy deposit (MeV) in the calorimeter layers, in the octant containing a strangelet, is shown

path of strangelets in the apparatus absorber can be calculated from equation (25). In each act of collision the spectator part of a strangelet survives and continues its passage through the calorimeter and the wounded part is destroyed. Particles generated at the consecutive collision points interact with tungsten nuclei in a usual way, resulting in the electromagnetic-nuclear cascade which develops in the calorimeter.

Penetration of stable strangelets through the calorimeter, assuming $\alpha_s = 0.3$ and several different sets of the initial strangelet parameters was simulated ($\mu_q = 300, 600, 1000$ MeV; $A_{\text{str}} = 15, 20, 40$; $E_{\text{str}} \approx 8\text{--}40$ TeV (or $400\text{--}1000 A \cdot \text{GeV}$). Strangelets characterized by such values of the parameters could be produced at LHC energies [139, 173, 175] according to the picture proposed in [24].

Examples of transition curves produced in the CASTOR calorimeter by various stable strangelets are presented in Fig. 30. Here are mainly shown strangelets with $\mu_q = 600$ MeV, as such value of the quark chemical potential has been estimated from cosmic-ray Centauros. The curves are limited to one calorimeter

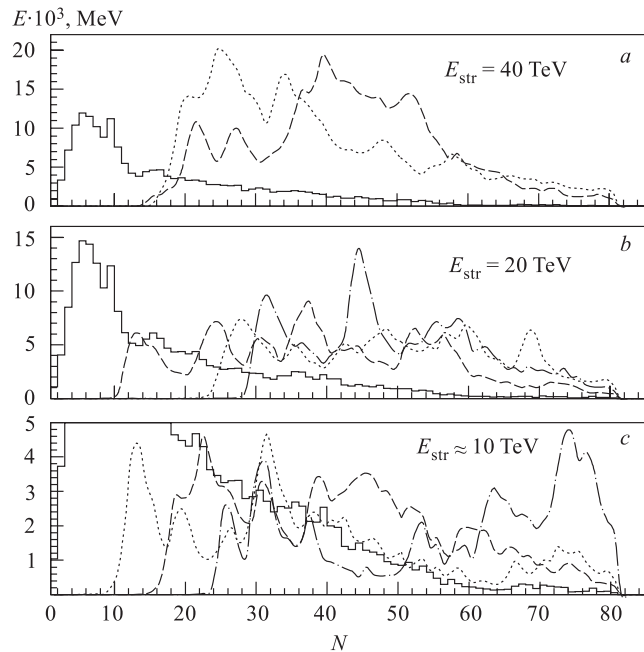


Fig. 30. Transition curves of stable strangelets with energy $E_{\text{str}} = 10\text{--}40$ TeV, baryon number $A_{\text{str}} = 15\text{--}40$, quark chemical potential $\mu_q = 600, 1000$ MeV. Energy deposit (MeV) in the calorimeter layers, in the octant containing a strangelet, is shown. Full line histograms show the HIJING estimated background

octant containing a strangelet. The strangelet cascade profiles are compared with those of the conventional background, produced by particles generated by HIJING (full line histogram), after subtraction of the energy carried by the strangelet.

It has been concluded that:

1. Stable strangelets can produce in the calorimeter long range many-maxima cascades.

2. The strangelet signal is manifestly different from that produced by background from a conventional event, i. e.:

- higher (in the hadronic part of the calorimeter),
- less attenuated,
- farther extended longitudinally (some strangelets give a strong signal even at the very end of the calorimeter, i. e., after penetration of more than 80 cm of tungsten absorber (60 calorimeter layers), where the signal from a conventional event is practically negligible),
- has a different shape (reveals a many-maxima structure in contrast to the smooth background).

3. The penetrating power of the signal increases with the value of the quark chemical potential μ_q (strangelet cross sections decrease with increasing μ_q), and the strangelet baryon number A_{str} .

4. The longitudinal structure of transition curves depends mainly on the strangelet baryon number A_{str} (a many-maxima structure is more pronounced for smaller A_{str}).

The appearance of the many-maxima structure is the consequence of successive collisions of the strangelet with nuclei of the calorimeter material. At each act of collision some part of the strangelet energy is transformed into energy of the secondary particles which in the process of usual interactions initiate nuclear cascades in the calorimeter. Thus the distance between consecutive humps depends both on the value of the mean interaction path of the strangelet in the tungsten absorber λ_{s-W} (hence on μ_q and A_{str}) and on the values of the mean interaction paths of usual particles.

From these simulations it is seen that the deep calorimeter is an appropriate tool for the strangelet detection, independently of the strangelet lifetime. Both stable and unstable strangelets can produce in the calorimeter signals apparently different from the conventional background. The calorimeter will be also able to detect the possible *strangelet evolution* when the strong nucleon emission process transforms a short-lived strangelet into a stable object. Figure 31 shows the transition curve of a short-lived strangelet ($A_{\text{str}} = 23$, $E_{\text{str}} = 23$ TeV) which after evaporation of 7 neutrons, in the strong decay process, becomes a long-lived object.

The probability of strangelet detection in a calorimeter depends both on the strangelet properties and the calorimeter parameters. Generally, such factors as large depth, small longitudinal sampling length, and fine granularity (division

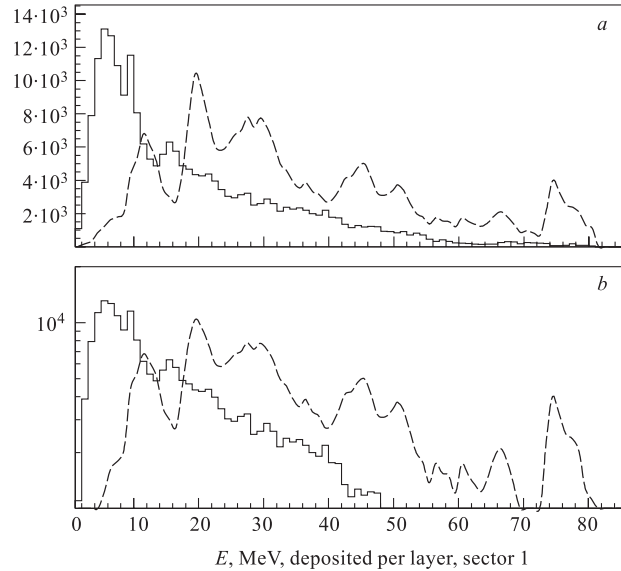


Fig. 31. Unstable strangelet ($A_{\text{str}} = 23$, $E_{\text{str}} \approx 23$ TeV) transformed into a stable one after evaporation of 7 neutrons. Energy deposit (MeV) in the calorimeter layers, in the octant containing a strangelet, is shown

into radial as well as azimuthal sectors) improve the sensitivity to the strangelet detection. The influence of some factors on the sensitivity to the strangelet detection has been studied [176]. It was shown that a deep calorimeter can be sensitive to the detection of strangelets for a wide spectrum of their parameters. For the considered design, stable strangelets with total energy $E_{\text{str}} > 10$ TeV, or energy per baryon number $E_{\text{str}} \geq 500 A \cdot \text{GeV}$ and baryon number $A_{\text{str}} \geq 15$, can be easily identified. Sometimes even less energetic strangelets, because of favourable fluctuations, can produce very deep in the calorimeter a characteristic signal allowing their identification.

In order to identify any unusually penetrating component, the development, intensity (energy content) and propagation of hadronic cascades as a function of calorimeter depth, should be observed. To meet this requirement, the calorimeter must be sampled along its length, with appropriate sampling steps. The simulations presented here have been done for the sampling and reading planes placed every 5 mm ($\sim 1.94X_0$ of effective thickness) in the electromagnetic part and every 10 mm ($\sim 3.88X_0$ of effective thickness) in the hadronic part of the calorimeter. Such sampling is similar to that in the cosmic ray emulsion chambers where the many-maxima long range cascades have been observed and it seems to

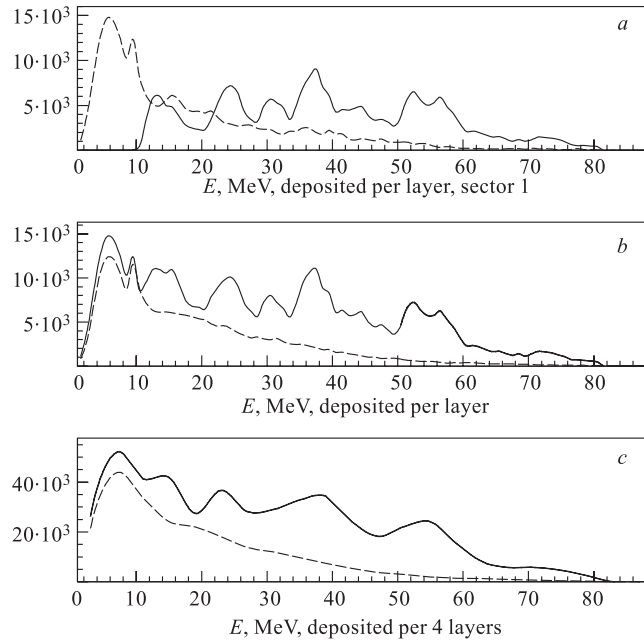


Fig. 32. *a*) Transition curves produced by a stable strangelet (solid curve) ($A_{\text{str}} = 20$, $E_{\text{str}} = 20$ TeV, $\mu_q = 600$ MeV) and by the HIJING background (dashed curve), separately. *b*) Summed signal in the «strangelet» sector (solid curve) in comparison with the average of other sectors (dashed curve) assuming readings of every layer, i. e., every 5 mm in electromagnetic and 10 mm in hadronic sectors; *c*) the same as *b*, but readings of the summed signal from consecutive groups of 4 layers

be also suitable for observation of the many-maxima character of the transition curves produced by strangelets formed at the LHC. It has been also checked that making absorber plates thinner leads only to a small increase of the light output. An important question is how the many-maxima structure changes with the increase of the reading unit thickness. It is illustrated in Fig. 32 where transition curves produced by a typical stable strangelet ($A_{\text{str}} = 20$, $E_{\text{str}} = 20$ TeV, $\mu_q = 600$ MeV) are shown. Figure 32, *a* shows the signals produced by the strangelet and the HIJING background, separately. Figures 32, *b*, *c* show the summed signal in the «strangelet» sector in comparison with the average output from the other sectors. Figures 32, *a*, *b* illustrate the standard sampling and reading step as described above. Figure 32, *c* is the same transition curve obtained for readings of the summed signal from consecutive groups of 4 layers (i. e., every $\sim 16X_0$). As can be expected, with decreasing the number of reading steps, the strangelet signal becomes smoother. The many-maxima structure becomes

rather a wave-like structure but it is still visibly different from the still smoother background.

6.3.2. «Mixed» Events in the Deep Calorimeter. Further questions concern the shape of transition curves produced in the calorimeter by:

- strangelets coming from the Centauro fireball explosion and registered in the apparatus simultaneously with other Centauro decay products;
- Centauro fireball decay products without accompanying strangelets emission (or such case when a strangelet escapes the detection in the calorimeter).

To investigate this topic the exotic events generated by means of the Centauro code were passed through the CASTOR calorimeter, by using GEANT 3.21. For each event the following transition curves were simulated separately:

- a curve produced by the Centauro fireball decay products;
- by the accompanying strangelet;
- and by background of conventionally produced particles, possibly accompanying the Centauro event (estimated by HIJING).

All these three contributions, separately, and also their sum, constituting the so-called «mixed» event, were compared with the «usual» transition curve, produced by HIJING. Analyzed Centauro events were characterized by different values of parameters: temperature ($T = 250, 300$ MeV), chemical potential of quark ($\mu_q = 600, 1000$ MeV), and nuclear stopping power ($\Delta y_{\text{stop}} = 0.5, 1.0, 1.5$ what corresponds to the effective stopping in the range of about $\sim 1.5\text{--}3.0$ pseudorapidity units). In some events strangelets with baryonic numbers $A_{\text{str}} \simeq 20\text{--}40$ and energies $E_{\text{str}} \simeq 8\text{--}20$ TeV were formed, what corresponds to the energy per baryon $E/A_{\text{str}} \simeq 0.3\text{--}1.0$ TeV.

Examples of resulting transition curves are presented in Figs. 33 and 34. Energy deposit in the consecutive calorimeter layers, in the sector containing a strangelet, is shown.

Separate contributions from: Centauro fireball decay products, a strangelet, the HIJING central event and a background from conventionally (HIJING) produced particles are plotted in Fig. 33 showing two Centauro events with unstable and stable strangelets produced among its secondaries. Figures 34 illustrate the signals, expected in the calorimeter, assuming that stable strangelets are formed during the Centauro fireball decay.

This analysis indicates that Centauro events (as well accompanied and not accompanied by a strangelet) can be easily distinguishable from «usual» events. Centauro transition curves in the calorimeter are expected to have apparently different shape and longer extent from those produced by «normal» events. A Centauro produced signal has a maximum at about the 14th calorimeter layer with the average $\langle N_{\text{Cent}} \rangle \simeq 25$. HIJING event produces the maximum of the signal at about the 8th calorimeter layer, with the average at $\langle N_{\text{HIJ}} \rangle \simeq 19$ layer. Generally, Centauro produced signal is stronger in the deeper (hadronic) part of

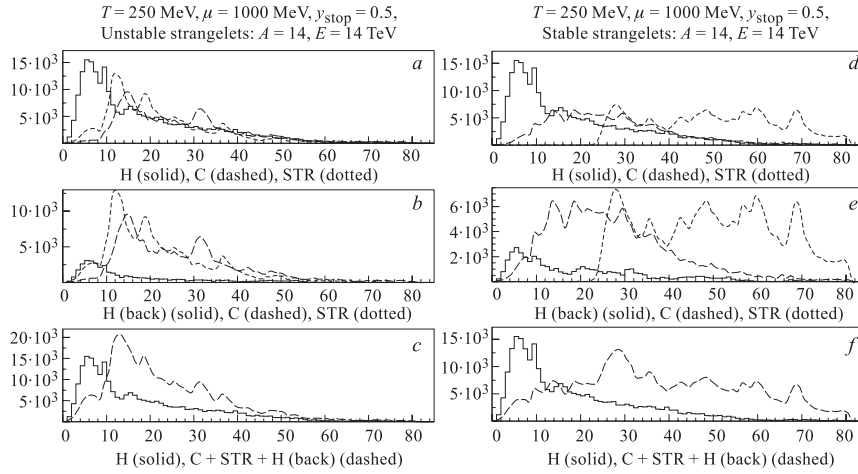


Fig. 33. Transition curves produced by the Centauro event «C» with unstable (*a, b, c*) or stable (*d, e, f*) strangelets «STR», in comparison with HIJING «H». Energy deposit (MeV) in the calorimeter layers, in the octant containing a strangelet, is shown

the calorimeter, in opposite to the HIJING generated one, which is peaked in the electromagnetic section of the calorimeter.

Strangelet transition curves have been analyzed in detail in the previous subsection, with the general conclusion that they are apparently different from those produced by «normal» events and that strangelets produced among other conventional particles should give easily distinguished signal. Here are shown signals, being the sum of Centauro, strangelet and background contributions. These transition curves are again very different from conventionally produced ones. They have much longer extent (they are strongly pronounced in the deep hadronic part of the calorimeter) and many-maxima structure. Their shape depends, of course, on the strangelet and Centauro parameters. The important quantity is the Centauro and strangelet energy falling into the calorimeter acceptance. Generally, higher energy of the exotic species bears smaller conventional background and in consequence gives more pronounced signal. The Centauro fireball energy depends mainly on the value of nuclear stopping power. Figure 34, *b* is the example of the event in which the Centauro fireball energy, covered by the calorimeter equals 158 TeV, exceeding the HIJING predicted value (~ 150 TeV). It results in zero conventional background and hence the summed transition curve is very different from the HIJING predicted one. On the contrary, the event illustrated in Fig. 34, *c* in which the Centauro fireball energy equals 79.5 TeV, carries only about one half of the energy allowed by HIJING in that kinematical region. The remaining energy could go into the conventional particle production. This fact

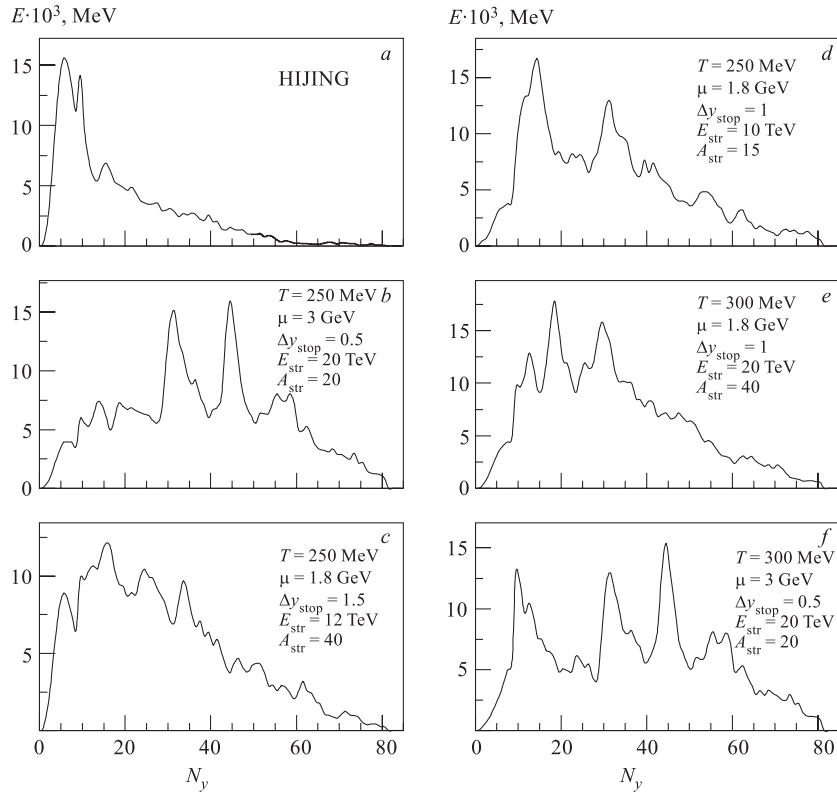


Fig. 34. Examples of resulting transition curves being the sum of Centauro, strangelet, and background contributions, and in comparison with the HIJING event. Energy deposit (MeV) in the calorimeter layers, in the octant containing a strangelet, is shown

in connection with the small strangelet energy causes the expected signals to be weaker than others presented in Fig. 34. But also such events have apparently different characteristics than the «normal» ones and should be easily picked up in the process of analysis of the shape and extent of transition curves in the calorimeter.

Summarizing the results of simulations of exotic objects, it should be stressed that the energy deposit in the deep calorimeters seems to be the new unconventional signature of the quark–gluon plasma. Such objects as Centauro-like events or strongly penetrating/long-lived particles possibly created in the phase transition from the QGP to the hadronic matter, should produce the characteristic long extended signals, during their passage through the calorimeter. This signature should be taken into account in the preparation of the new experiments.

7. SUMMARY

In this work the experimental data from superhigh energy cosmic ray mountain experiments have been reviewed. In spite of many experimental uncertainties and some doubts, it can be concluded that they give a compelling evidence of unusual events which are hardly explained by means of «conventional» models. Among many theoretical attempts to understand these anomalies the more attractive ones are the scenarios with QGP. One of them is the picture assuming the production of a strange quark matter fireball in nucleus–nucleus collisions. At the last stage of the fireball evolution the Centauro-type events and strangelets can be formed. This model allows one to understand many different anomalies, such as the existence of hadron-rich events, a strongly penetrating component, miniclusters, etc. In addition, such picture is consistent with up to now negative results of Centauro search in accelerator experiments and allows one to expect their appearance in future, in heavy ion interactions at RHIC and LHC colliders. The CASTOR, a subsystem of the CMS detector, is proposed to study the baryon-rich environment formed in Pb + Pb collisions at LHC energies and to search for exotic events, such as Centauros and strangelets.

Acknowledgements. I would like to thank all of my colleagues with whom whenever I worked or discussed the topics concerning the cosmic-ray exotic phenomena. In particular, many thanks to Prof. Z. Włodarczyk for our common study of a strangelet question and Dr. A. Angelis for common work in designing the CASTOR detector, his great help in the field of computer calculations and his software being the basis of the codes simulating the passage of the exotic objects through the deep calorimeter. I thank them for the comments and figures included into the paper. I am especially grateful to Prof. J. Bartke for helpful discussions and very carefull and patient reading of the raw version of the manuscript, plenty important remarks and corrections. This work was partly supported by Polish State Committee for Scientific Research grant No. 2P03B 011 18 and SPUB-M/CERN/P03/DZ1/99.

REFERENCES

1. *Harris J.W.* // Lectures at Lake Louise Winter Institute on Quantum Chromodynamics, Lake Louise, Alberta, Canada, 1998 / Ed. by A. Astbury et al. Singapore, 1999. P.99; Preprint YRHI-98-13. 1998.
2. *Bialkowska H.* // Acta Phys. Polonica B. 1997. V. 28. P. 2793.
3. Proc. of the 12th Intern. Conf. on Ultra-Relativistic Nucleus–Nucleus Collisions «Quark Matter'96» // Nucl. Phys. A. 1996. V. 610.
4. Proc. of the 13th Intern. Conf. on Ultra-Relativistic Nucleus–Nucleus Collisions «Quark Matter'97» // Nucl. Phys. A. 1998. V. 638.
5. Proc. of the 14th Intern. Conf. on Ultra-Relativistic Nucleus–Nucleus Collisions «Quark Matter'99» // Nucl. Phys. A. 1999. V. 661.

6. Proc. of the 15th Intern. Conf. on Ultra-Relativistic Nucleus–Nucleus Collisions «Quark Matter'2001».
7. Nagle J.L. Invited talk // Intern. Nuclear Physics Conf. (INPC 2001), Berkeley, California, 2001; nucl-ex/0109016. 2001.
8. Zajc W.A. (*PHENIX Collab.*) nucl-ex/0106001. 2001.
9. Lévai P. et al. nucl-th/0104035. 2001.
10. <http://www.cern.ch/CERN/Anouncements/2000/NewStateMatter>
11. Kharzeev D., Levin E. nucl-th/0108006.
12. Braun M.A., del Moral F., Pajares C. hep-ph/0105263.
13. Tamada M. Talks given at the Intern. Conf. on High Energy Physics, Tampere, Finland, 1999; Intern. Symp. «Chacaltaya–Pamir», Łódź, Poland, 1999; Inst. Cosmic Ray Research, University Tokyo. Report ICRR-454-99-12.
14. Ohsawa A. (*Chacaltaya Emulsion Chamber Collab.*) // Nucl. Phys. B (Proc. Suppl.). 1999. V. 74A. P. 3;
Idem // Proc. of the 26th ICRC, Salt Lake City, USA, 1999.
15. Aguirre C. et al. // Phys. Rev. D. 2000. V. 62. P. 032003.
16. Das Gupta U. et al. // Phys. Rev. D. 1992. V. 45. P. 1459;
MACRO Collab. // 23th ICRC, Calgary, Canada, 1993 / Ed. by R. B. Hicks et al. Singapore, 1994. V. 2. P. 97;
JACEE Collab. // Astrophys. J. 1990. V. 349. P. L25;
Ichimura M. et al. // Phys. Rev. D. 1993. V. 48. P. 1949.
17. Angelis A. L. S. et al. // XXVIII Intern. Symp. on Multiparticle Dynamics, Delphi, Greece, 1998 / Ed. N. G. Antoniou et al. Singapore, 1998. P. 134; hep-ex/9901038.
18. Aseikin V. A. et al. // Proc. of the 14th ICRC, Munich, 1975. V. 7. P. 2462;
Yakovlev V. I., Nikolsky S. I., Pavluchenko V. P. // Proc. of the 15th ICRC, Plovdiv, 1977. V. 7. P. 115;
Yakovlev V. I. et al. // Proc. of the 16th ICRC, Kyoto, Japan, 1979. V. 6. P. 59;
Dremin I. M. et al. // Proc. of the 20th ICRC, Moscow, 1987. V. 6. P. 360;
Bazarov E. V. et al. // Proc. of the 17th ICRC, Paris, 1981. V. 5. P. 32;
Yakovlev V. I. // Proc. of the VII Intern. Symp. on VHECRI, Ann Arbor, 1992 / Ed. L. Jones. 1993. P. 154.
19. Dremin J. M. et al. // Voprosy atomnoy nauki i tekhniki, seria «Tekh. fiz. eksp.». 1985. Vyp. 4(25). P. 3 (in Russian).
20. Altarelli G. et al. // Z. Phys. C. 1989. V. 45. P. 109;
Kurepin A. B. ALICE/95-47, Internal Note/PHY. 1995;
Kurepin A. B. ALICE/93-03, Internal Note/PHY. 1993.
21. Berges J., Rajagopal K. hep-ph/9804233. 1998;
Rapp R. et al. hep-ph/9711396. 1997;
Alford M., Rajagopal K., Wilczek F. hep-ph/9711395. 1997.
22. Weber F. // J. Phys. G: Nucl. Part. Phys. 1999. V. 25. P. R195 (topical review).
23. Panagiotou A. D. et al. // Z. Phys. A. 1989. V. 333. P. 335;
Panagiotou A. D. et al. // Phys. Rev. D. 1992. V. 45. P. 3134.
24. Asprouli M. N., Panagiotou A. D., Gladysz-Dziadus E. // Astropart. Phys. 1994. V. 2. P. 167;
Gladysz-Dziadus E., Panagiotou A. D. // Intern. Symp. on Strangeness and Quark Matter, Krete, 1994. Singapore, 1995. P. 265.

25. Gladysz-Dziaduś E., Włodarczyk Z. ALICE/97-17, Internal Note/CAS. 1997;
for ALICE Internal Notes look at the web: <http://www.cern.ch/ALICE/documents.html>;
Gladysz-Dziaduś E., Włodarczyk Z. // J. Phys. G: Nucl. Part. Phys. 1997. V. 23. P. 2057.
26. Hasegawa S. // Proc. of the VIII Intern. Symp. on VHECRI, Tokyo, 1994. P. 115.
27. Japan–Brasil Collab. // Proc. of the 13th ICRC, Denver, Canada, 1973. V. 4. P. 2671.
28. Barroso S. L. C. et al. // Contr. to 25th ICRC, Durban, 1997;
Chacaltaya Cosmic-Ray Collab. ICRR-Report-390-97-13A.
29. Lattes C. M. G., Fujimoto Y., Hasegawa S. // Phys. Rep. 1980. V. 65. P. 151;
Hasegawa S. (Brasil–Japan Collab.) Talk at FNAL CDF seminar. ICRR Report 151-87-5. 1987.
30. Barroso S. L. C. et al. // Proc. of the VIII Intern. Symp. on VHECRI, Tokyo, 1994. P. 166.
31. Tamada M. // Nuovo Cim. B. 1977. V. 41. P. 245.
32. Chinellato J. A. et al. (Brasil–Japan Collab.) // Proc. of the 5th Intern. Symp. VHECRI, Łódź, Poland, 1988. Łódź, 1988. P. 309.
33. Bellandi J. et al. // Proc. of Workshop Cos. Ray Interactions High Energy Results, La Paz, Rio de Janeiro, 1982 / Ed. by C. M. G. Lattes. P. 42; 102.
34. Funayama Y. // Proc. of Intern. Symp. on Cos. Rays and Particle Physics, Tokyo, 1984 / Ed. by A. Ohsawa, T. Yuda. P. 335.
35. Hasegawa S. (Chacaltaya Collab.) // VI Intern. Symp. on VHECRI, Tarbes, France, 1990 / Ed. by J. N. Capdevielle, P. Gabinski. P. 227.
36. Brasil–Japan Collab. // Proc. of the 21th ICRC, Adelaide, 1990. V. 8. P. 259; 263.
37. Hasegawa S., Tamada M. // Nucl. Phys. B. 1996. V. 474. P. 141.
38. Navia C. E. et al. // Phys. Rev. D. 1994. V. 50. P. 5732.
39. Borisov A. et al. (Pamir and Chacaltaya Collab.) // Phys. Lett. B. 1987. V. 190. P. 226.
40. Pamir and Chacaltaya Collab. // Proc. of the 20th ICRC, Moscow, 1987. V. 5. P. 334.
41. Baradzei L. T. et al. (Pamir Collab.) FIAN Preprint 208. M., 1989.
42. Buja Z. et al. // Proc. of the 17th ICRC, Paris, 1981. V. 11. P. 104.
43. Buja Z. et al. (Pamir Collab.) // Workshop, Cedzyna, Poland, 1980. P. 73.
44. Bayburina S. G. et al. // Nucl. Phys. B. 1981. V. 191. P. 1.
45. Bielyayev A. A. et al. Electromagnetic Cascades in Cosmic Rays of Ultra-High Energy. M., 1980 (in Russian).
46. Yakovlev V. I. // Proc. of Intern. Seminar on Cosmic Ray Cascades, Sofia, 1980. P. 111.
47. Kumano H. // Proc. of the 20th ICRC, Moscow, 1987. V. 5. P. 387.
48. Bielawska H. et al. // Nuovo Cim. C. 1989. V. 2. P. 763;
Tamada M., Tomaszewski A. // Proc. of the 5th Intern. Symp. VHECRI, Łódź, Poland, 1988. Łódź, 1988. P. 330.
49. Borisov A. et al. (Pamir Collab.) // Proc. of the 20th ICRC, Moscow, 1987. V. 5. P. 351.
50. Yamashita S. // J. Phys. Soc. of Japan. 1985. V. 54. P. 529.
51. Amato N. et al. // J. Phys. G: Nucl. Part. Phys. 1994. V. 20. P. 141.
52. Chinellato J. A. et al. // Proc. of the 20th ICRC, Moscow, 1987. V. 5. P. 363;
Yamashita S. et al. // Ibid. P. 367.
53. Pamir Collab. // Pamir Coll. Workshop, Cedzyna, Poland, 1980. P. 94;
Pamir Collab. // Proc. of the 17th ICRC, Paris, 1981. V. 5. P. 291.

54. *Japan-USSR Joint Em. Chamber Exp.* // Proc. of the 19th ICRC, La Jolla, 1985. V. 6. P. 332.
55. *Borisov A. S. et al.* // Proc. of the 20th ICRC, Moscow, 1987. V. 5. P. 383.
56. *Hasegawa S.* // Proc. of Intern. Symp. on Cos. Rays and Particle Physics, Tokyo, 1984 / Ed. by A. Ohsawa, T. Yuda. P. 718.
57. *Borisov A. S. et al.* // Ibid. P. 248; Proc. of Workshop Cosmic Ray Inter. High Energy Results, La Paz, Rio de Janeiro, 1982. P. 445.
58. *Chinellato J. A. et al. (Brasil-Japan Collab.)* // AIP Conf. Proc. No. 85. 1981. P. 500;
Hasegawa S. et al. // Proc. of Intern. Symp. on Cos. Rays and Particle Physics, Tokyo, 1984 / Ed. by A. Ohsawa, T. Yuda. P. 319.
59. *Baradzei L. T.* // Nucl. Phys. B. 1992. V. 370. P. 365.
60. *Arisawa T. et al.* // Nucl. Phys. B. 1994. V. 424. P. 241.
61. *Baradzei L. T. et al.* // Proc. of Workshop Cos. Ray Inter. High Energy Results, La Paz, Rio de Janeiro, 1982. P. 449.
62. *Tamada M., Yokoi K.* // Bulletin of Science and Engin. Research Lab., Waseda Univ. 1986. No. 113. P. 21.
63. *Chacaltaya and Pamir Collab. ICRR-report-295-93-7.* 1993. P. 9 (Contribution to the 23th ICRC, Calgary, 1993).
64. *Kopenkin V., Fujimoto Y.* // Nuovo Cim. 1996. V. 19. P. 1017.
65. *Hasegawa S.* // Proc. of Intern. Symp. on Cos. Rays and Particle Physics, Tokyo, 1984. P. 62;
Tamada M. // Ibid. P. 352.
66. *Hasegawa S. ICR-report-197-89-14.*
67. *Tamada M., Funayama Y.* Report of Sci. and Engin. Res. Lab., Waseda Univ. 1985. No. 85-5;
Funayama Y., Tamada M. Ibid. No. 85-6.
68. *Bielawska H. et al.* // Proc. of Intern. Symp. on Cos. Ray Particle Physics, Tokyo, 1984. P. 374.
69. *Chacaltaya and Pamir Collab.* // Proc. of the 22th ICRC, Dublin, Ireland, 1991. V. 4. P. 101.
70. *Capdevielle J. N., Slavatinsky S. A.* // Nucl. Phys. B (Proc. Suppl.). 1999. V. 75A. P. 12.
71. *Tamada M.* // Nucl. Phys. (Proc. Suppl.). 2001. V. 97. P. 146; 150 (contribution to the XI ISVHECRI, Campinas, Brasil, 2000).
72. *Borisov A. S. et al. (Pamir Collab.)* // Proc. of Intern. Symp. on Cos. Rays and Particle Physics, Tokyo, 1984. P. 3.
73. *Tamada M., Kopenkin V. V.* // Nucl. Phys. B. 1997. V. 494. P. 3;
Tamada M., Kopenkin V. V. // Nucl. Phys. B (Proc. Suppl.). 1997. V. 52. P. 222.
74. *Tamada M., Ohsawa A.* // Proc. of the 26th ICRC, Salt Lake City, USA, 1999. V. 7. P. 11;
Tamada M., Ohsawa A. // Nucl. Phys. B. 2000. V. 581. P. 73.
75. *Hlytchieva V. S. et al.* // IV Intern. Symp. on VHECRI, Tarbes, France, 1990 / Ed. by J.N. Capdevielle, P. Gabinski. Tarbes, 1990. P. 184.
76. *Shaulov S. B.* // Heavy Ion Phys. 1996. V. 4. P. 403.
77. *Gladysz E.* Ph. D. Thesis. Institute of Nuclear Physics, Kraków, 1980.
78. *Akashi M. et al.* // Proc. of the 15th ICRC, Plovdiv, 1977. V. 7. P. 184.
79. *Ren J. R. et al.* // Phys. Rev. D. 1988. V. 38. P. 1417.
80. *Burnett T. H. et al. (JACEE Collab.)* // Proc. of the 20th ICRC, Moscow, 1987. V. 5. P. 185.

81. *Bjorken J. D., Kowalski K. L., Taylor C. C.* SLAC-PUB-6109. 1993;
Bjorken J. D. // *Acta Phys. Polonica B.* 1997. V. 28. P. 2773.
82. *Jones L. W.* // *Proc. of the VIII Intern. Symp. on VHECRI, Tokyo, 1994.* P. 312.
83. *Wilczynski H.* Report INP Krakow 1718/PH. Krakow, 1996;
Wilczynski H. // *Contribution to the 10th Symp. on VHECRI, Gran Sasso, Italy, 1998.*
84. *Acharaya B. S. et al.* // *Proc. of the 16th ICRC, Kyoto, 1979.* V. 6. P. 289;
Dunaevskii A. M. et al. // *Ibid.* V. 7. P. 154;
Shibata M. // *Ibid.* P. 176;
Levina T. G. et al. // *Ibid.* P. 148;
Acharya B. S. et al. // *Nuovo Cim. Lett.* 1981. V. 31. P. 149;
Ellsworth R. W. et al. // *Phys. Rev. D.* 1981. V. 23. P. 771;
Mukhamedshin R. A. // *Proc. of the 17th ICRC, Paris, 1981.* V. 5. P. 343;
Pamir Collab. // *Proc. of the 20th ICRC, Moscow, 1987.* V. 5. P. 334; 351; 383;
Yamashita S., Ohsawa A., Chinellato J. A. // *Proc. of Intern. Symp. Cosmic Rays and Particle Physics, Tokyo, 1984.* P. 30.
85. *Acharya B. S., Rao M. V. S.* // *J. Phys. G: Nucl. Part. Phys.* 1991. V. 17. P. 759.
86. *Mc Cusker B.* // *Proc. of the XVI ICRC, Kyoto, Japan, 1979.*
87. *Price P. B. et al.* // *Proc. Nat. Acad. Sci. USA.* 1980. V. 77. P. 44.
88. *Bjorken J. D., McLerran L. D.* // *Phys. Rev. D.* 1979. V. 20. P. 2353.
89. *Goulianos K.* // *Proc. of the 7th Symp. on Very High Energy Cosmic Ray Interactions (ISVHE-CRI), Ann Arbor MI, USA, 1992.* P. 244; RU92/E-39;
Goulianos K. // *Comments Nucl. Part. Phys.* 1987. V. 17. P. 195.
90. *Kang K., White A.* // *Phys. Rev. D.* 1990. V. 42. P. 835;
White A. R. // *Proc. of the 8th Intern. Symp. on VHECRI, Tokyo, 1994.* P. 468.
91. *Augusto C. R. A. et al.* // *Ibid.* P. 396.
92. *Wilk G., Wlodarczyk Z.* // *J. Phys. G.* 1996. V. 22. P. L105;
Wilk G., Wlodarczyk Z. // *Heavy Ion Phys.* 1996. V. 4. P. 395;
Rybzyński M., Wlodarczyk Z., Wilk G. // *Nuovo Cim. C.* 2001. V. 24. P. 645.
93. *Andreev I. V.* // *JETP Lett.* 1981. V. 33. P. 367.
94. *Lam C. S., Lo S. Y.* // *Phys. Rev. Lett.* 1984. V. 52. P. 1184;
Lam C. S., Lo S. Y. // *Phys. Rev. D.* 1986. V. 33. P. 1336;
Lam C. S., Lo S. Y. // *Intern. J. of Mod. Phys. A.* 1986. V. 1. P. 451.
95. *Greiner C., Gong C., Müller B.* // *Phys. Lett. B.* 1993. V. 316. P. 226.
96. *Pratt S., Zelevinsky V.* // *Phys. Rev. Lett.* 1994. V. 72. P. 816;
Pratt S. // *Phys. Rev. C.* 1994. V. 50. P. 469.
97. *Anselm A. A., Ryskin M. G.* // *Phys. Lett. B.* 1991. V. 266. P. 482.
98. *Blaizot J. P., Krzywicki A.* // *Phys. Rev. D.* 1992. V. 46. P. 246.
99. *Martinis M. et al.* // *Phys. Rev. D.* 1995. V. 51. P. 2482.
100. *Rajagopal K., Wilczek F.* // *Nucl. Phys. B.* 1993. V. 399. P. 395;
Rajagopal K., Wilczek F. // *Nucl. Phys.* 1993. V. 404. P. 577;
Rajagopal K. hep-ph/9703258. 1997; CALT-68-2104.
101. *Gavin S.* // *Nucl. Phys. A.* 1995. V. 590. P. 163c.
102. *Huang Z., Wang X. N.* nucl-th/9312005. 1993.
103. *Wilk G., Wlodarczyk Z.* // *Nucl. Phys. B (Proc. Suppl.).* 1997. V. 52. P. 215.

104. *Navia C. E. et al.* // Phys. Rev. D. 1997. V. 55. P. 5834.
105. *Bartke J., Gladysz-Dziadus E., Stefański P.* // Proc. of the 20th Intern. Symp. on Multiparticle Dynamics, Gut Holmecke, 1990. Singapore, 1991. P. 530;
Bartke J., Gladysz-Dziadus E., Stefański P. (NA35 Collab.) // Quark Matter'91 Conf., Gatlinburg, USA, 1991;
Bartke J., Gladysz-Dziadus E., Stefański P. // Proc. of the 6th Intern. Symp. on Very High Energy Cosmic Ray Interactions (ISVHECRI), Tarbes, France, 1990. P. 207;
Bartke J., Gladysz-Dziadus E., Stefański P. // Proc. of CAMP Workshop, Marburg, 1990. Singapore, 1991. P. 198;
Bartke J., Gladysz-Dziadus E., Stefański P. // Nucl. Phys. A. 1992. V. 545. P. 321c;
Bachler J. et al. (NA35 Collab.) // Z. Phys. C. 1992. V. 56. P. 347.
106. *Bartke J., Gladysz-Dziadus E., Stefański P.* // Quark Matter'91 Conf., Gatlinburg, USA, 1991.
107. *Bjorken J.* SLAC-PUB-6488. 1994.
108. *Augusto C. R. A. et al.* DCC signature on γ -hadron families seen through robust observables. Unpublished.
109. *Augusto C. R. A. et al.* // Nucl. Phys. B (Proc. Suppl.). 1999. V. 75A. P. 206;
Augusto C. R. A. et al. // Phys. Rev. D. 1999. V. 59. P. 54.
110. *Brooks T. C. et al.* // Phys. Rev. D. 1997. V. 55. P. 5667.
111. *Gladysz-Dziadus E.* // Mod. Phys. Lett. A. 1989. V. 4. P. 2553;
Gladysz-Dziadus E. Report No. 1432/PH, Institute of Nuclear Physics. Kraków, 1988.
112. *Wilk G., Wlodarczyk Z.* // J. Phys. G: Nucl. Part. Phys. 1993. V. 19. P. 761.
113. *Witten E.* // Phys. Rev. D. 1984. V. 30. P. 272.
114. *Fahri F., Jaffe R. L.* // Ibid. P. 2379.
115. *Berger M. S., Jaffe R. L.* // Phys. Rev. C. 1987. V. 35. P. 213.
116. *Chin S., Kerman A.* // Phys. Rev. Lett. 1979. V. 43. P. 1292.
117. *Schaffner-Bielich J. et al.* // Phys. Rev. C. 1997. V. 55. P. 3038.
118. *Gilson E., Jaffe R.* // Phys. Rev. Lett. 1993. V. 71. P. 332.
119. *Madsen J.* // Phys. Rev. D. 1994. V. 50. P. 3328.
120. *Greiner C., Koch P., Stoöcker H.* // Phys. Rev. Lett. 1987. V. 58. P. 1825;
Greiner C. et al. // Phys. Rev. D. 1988. V. 38. P. 2797;
Greiner C., Stoöcker H. // Phys. Rev. D. 1991. V. 44. P. 3517.
121. *Madsen J.* Physics and Astrophysics of Strange Quark Matter Hadrons in Dense Matter and Hadrosynthesis, Cape Town, 1998. Lecture Notes in Physics. P. 162; astro-ph/9809032. 1998.
122. *Greiner C., Schaffner-Bielich J.* Physics of Strange Matter in Heavy Elements and Related New Phenomena. Preprint LBNL-41324; nucl-th/9801062. 1998.
123. *Hemmick T. K. et al.* // Phys. Rev. D. 1990. V. 41. P. 2074.
124. *Alcock C., Olinto A.* // Ann. Rev. Nucl. Part. Sci. 1988. V. 38. P. 161.
125. *Aushev V. M. et al.* // Izv. RAS, ser. fiz. 1997. V. 61, No. 3. P. 486;
Antonova V. A. et al. // Nucl. Phys. B (Proc. Suppl.). 1999. V. 75A. P. 333.
126. CosmoLEP Report 1, CERN LEPC 95-5. 1999. CERN-EP/2000-152.
127. *Rybczyński M., Wlodarczyk Z., Wilk G.* // Nucl. Phys. (Proc. Suppl). 2001. V. 97. P. 85;
Rybczyński M., Wlodarczyk Z., Wilk G. // Acta Phys. Polonica B. 2002. V. 33. P. 277.
128. *Anderson D. P. et al.* astro-ph/0205089.

129. *Saito T. et al.* // Phys. Rev. Lett. 1990. V. 65. P. 2094.
130. *Price P. B. et al.* // Phys. Rev. D. 1978. V. 18. P. 1382.
131. *Ichimura M. et al.* // Nuovo Cim. A. 1993. V. 106. P. 843.
132. *Armstrong T. A. et al. (E864 Collab.)* nucl-ex/0010017. 2000;
Xu Z. (E864 Collab.) // J. Phys. G: Nucl. Part. Phys. 1999. V. 25. P. 403;
van Buren G. (E864 Collab.) // Ibid. P. 411;
Munkoz M. K. (E864 Collab.) // Ibid. P. 417;
Barrette J. et al. (E814 Collab.) // Phys. Lett. B. 1990. V. 252. P. 550;
Aoki M. et al. (E858 Collab.) // Phys. Rev. Lett. 1992. V. 69. P. 2345;
Beavis D. et al. (E878 Collab.) // Phys. Rev. Lett. 1995. V. 75. P. 3078;
Rusek A. et al. (E886 Collab.) // Phys. Rev. C. 1996. V. 54. P. R15.
133. *Ambrosini G. et al. (NA52 Collab. (NEWMASS))* // J. Phys. G: Nucl. Part. Phys. 1997. V. 23. P. 2135.
134. *Klingenberg R.* // J. Phys. G: Nucl. Part. Phys. 1999. V. 25. P. R273.
135. *Miyamura O. et al.* // Proc. of the 24th ICRC, Rome, 1995. V. 1. P. 890.
136. *Capdevielle J.N. et al.* // Ibid. P. 910; Nuovo Cim. C. 1996. V. 19. P. 623.
137. *Baltz A. et al.* // Phys. Lett. B. 1994. V. 325. P. 7.
138. *Braun-Munzinger P., Stachel J.* // J. Phys. G: Nucl. Part. Phys. 1995. V. 21. P. L17.
139. *Angelis A. L. S. et al.* // J. Phys. G. 2002. V. 28. P. 1942;
Angelis A. L. S. et al. // Nuovo Cim. C. 2001. V. 24. P. 755;
Angelis A. L. S. et al. // Nucl. Phys. (Proc. Suppl.). 2001. V. 97. P. 227;
Angelis A. L. S. et al. // Nucl. Phys. B (Proc. Suppl.). 1999. V. 75A. P. 203;
Angelis A. et al. CASTOR draft proposal, ALICE/97-07, Internal Note/CAS.
140. *Theodoratou O. P., Panagiotou A. D.* hep-ph/9908210; Astropart. Phys. 2000. V. 13. P. 173.
141. *Müller B.* Preprint DUKE-TH-92-36; hep-th/9211010;
Müller B. NATO ASI Series. Ser. B: Phys. 1992. V. 303. P. 11;
Harris J. W., Müller B. // Ann. Rev. Nucl. Part. Sci. 1996. V. 46. P. 71; Preprint DUKE-TH-96-105; hep-ph/9602235.
142. *Asprouli G., Panagiotou A. D.* // Phys. Rev. D. 1995. V. 51. P. 1086.
143. *Kinoshita K., Price P. B.* // Phys. Rev. D. 1981. V. 24. P. 1707;
Barwick et al. // Phys. Rev. D. 1983. V. 28. P. 2338;
Nakamura S. et al. // Phys. Lett. B. 1991. V. 263. P. 529;
Price P. B. // Phys. Rev. D. 1993. V. 47. P. 5194.
144. *Bodmer F. R.* // Phys. Rev. D. 1971. V. 4. P. 1601.
145. *Biro T. S., Zimányi J.* // Nucl. Phys. A. 1983. V. 395. P. 525;
Zimányi J. NATO ASI series. Ser. B: Phys. 1992. V. 303. P. 243.
146. *Madsen J.* // Intern. Symp. on Strangeness and Quark Matter, Krete, 1994. P. 191.
147. *Crawford H. J., Desai M. S., Shaw G. L.* // Phys. Rev. D. 1992. V. 45. P. 857.
148. *Arnison G. et al. (UA1 Collab.)* // Phys. Lett. B. 1983. V. 122. P. 189.
149. *Alpgard K. et al. (UA5 Collab.)* // Phys. Lett. B. 1982. V. 115. P. 71;
Alner G. J. et al. (UA5 Collab.). Preprint CERN-EP/86-127. 1986.
150. *Streets J. (Mini-Max Collab.)*. hep-ex/9608012. 1996;
Brooks T. C. et al. // Phys. Rev. D. 2000. V. 61. P. 032003.

151. Melese P.L. (CDF Collab.) // Proc. of the 11th Topical Workshop on $\bar{p}p$ Collider Physics (PBARP96), Padova, Italy, 1997. P.360.
152. Jones L.W. // XXVIII Intern. Symp. on Multiparticle Dynamics, Delphi, Greece, 1998. Singapore, 1998. P.501.
153. Rao M.V.S. (D0 Collab.) // Proc. of the VIII Intern. Symp. on VHECRI, Tokyo, 1994. P.299; Abachi S. et al. // Phys. Rev. Lett. 1994. V.72. P.2332.
154. Nayak T.K. (WA98 Collab.) Invited talk at the QM'97, Tsukuba, Japan, 1997. // Nucl. Phys. A. 1998. V.638. P.249c; hep-ex/9802019. 1998; Aggarwal M.M. et al. // Phys. Lett. B. 1998. V.420. P.169; hep-ex/9710015.
155. Aggarwal M.M. et al. // Phys. Rev. C. 2001. V.64. P.011901.
156. Afanasiev S. et al. (NA49 Collab.) // Nucl. Instr. Meth. A. 1999. V.430. P.210.
157. Appelshauser H. et al. (NA49 Collab.) // Phys. Lett. B. 1999. V.459. P.679.
158. FELIX. Lett. of Intent, CERN/LHCC 97-45. 1997.
159. The ALICE Technical proposal. CERN/LHCC/95-71, LHCC/P3. 1995.
160. CMS. The Compact Muon Solenoid. Technical Proposal. CERN/LHCC 94-38, LHCC/P1. 1994.
161. Baur G. et al. Heavy Ion Physics Programme in CMS. CMS Note 2000/060. 2000.
162. The ALICE forward muon spectrometer. CERN/LHCC 96-32; ALICE TDR5 CERN/LHCC 99-12.
163. Viyogi Y.P. Internal Note ALICE/PMD 98-52; ALICE TDR6 CERN/LHCC 99-32.
164. Dellacasa G. et al. Zero Degree Calorimeter ZDC. ALICE TDR3 CERN/LHCC 99-5. 1999.
165. Bartke J. et al. ALICE Internal Note PHYS/93-12.
166. Gladysz-Dziadus E. (CASTOR group) // Proc. of the 21th Intern. Workshop on Nuclear Theory, Rila Mountains, Bulgaria, 2002. To be published; Angelis A. et al. hep-ex/0209008. 2002.
167. Fodor Z., Katz S.D. hep-lat/0106002.
168. Berges J., Rajagopal K. hep-ph/9804233. 1998; Rapp R. et al. hep-ph/9711396. 1997.
169. Gladysz-Dziadus E., Panagiotou A.D. ALICE/95-18 Internal Note/PHY. 1995.
170. Gladysz-Dziadus E., Panagiotou A.D. ALICE/97-16 Internal Note/CAS. 1997.
171. Schukraft J. Preprint CERN-PPE/94-139. 1994.
172. Geiger K. // Phys. Rev. D. 1992. V.46. P.4965; 4986.
173. Gladysz-Dziadus E. et al. // Proc. of the 3rd Intern. Conf. on Physics and Astrophysics of Quark-Gluon Plasma, Jaipur, New Delhi, 1997. 1998. P.554; Angelis A. et al. Preprint IHEP 2002-8. Protvino, 2002; submitted to «Phys. Atom. Nuclei».
174. Sowa M. Master Degree Thesis. Institute of Nuclear Physics. Kraków, 2000.
175. Gladysz-Dziadus E. ALICE-INT-2001-21, Internal Note. 2001.
176. Angelis A.L.S. et al. Report No.1800/PH, Institute of Nuclear Physics. Krakow, 1998; ALICE Internal Note, CAS/98-38. 1988.